Polarimetric Modelling for Anisotropic stars

By

Mohammed Bakheet M. Al-Malki

**Thesis
submitted to the
University of Glasgow
for a degree of
Ph.D.**

Department of Physics and Astronomy,
The University of Glasgow,
Glasgow G12 8QQ.

June 1992

ProQuest Number: 11011478

ProQuest 11011478

PREFACE

In recent years the interest in polarization modelling has grown . Many models have been produced, for most of which the study of the scatterer density distribution has been of central importance.

Previous work on the problem of the scatterer density distribution involved the study of the effects of: envelope shape; finite spherical star; scatterer occultation by a finite spherical star; and the effect of arbitrary scattering mechanisms.

In the above models a gross assumption was made by taking the star as an isotropic point, or finite, source of light. However, stars in general are not isotropic, and in the present work the polarization produced by the light from an anisotropic point source of light, scattered by the Thomson or Rayleigh mechanisms in an envelope of arbitrary shape will be discussed.

The idea for this research occurred when I was analyzing the polarimetric data of Serkowski (1970) for two RV Tauri stars, under the supervision of D. Clarke. Serkowski suggested that the polarization variations in these stars are due to non-radial oscillation. However,

the lack of a suitable model to be used to fit Serkowski's data prompted us to develop one.

The model of J. Simmons (1982) was the most useful one for our problem, since all that we needed to do was extend his technique to the anisotropy of the light as well as the scatterer density distribution function (so easy !!). However, dealing with the spherical harmonics, which J. Simmons introduced in his model was difficult. Many new and interesting problems were realised in the process of improving this model. They caused the research to shift totally to the present theoretical modelling under the supervision of J. Brown who started the generality in the envelope shape in the polarization modelling (Brown and McLean 1977), and the supervision of J. Simmons whose model this thesis generalizes.

Any non-english speaking student, will encounter two major challenges in addition to that of the research itself. These are the language and the gap between the two education systems here and in his own country. I hope this thesis will show some success on both sides.

An introduction and a brief review of previous works and observations are presented in Chapter one. The original work appears in Chapters two, three, and four. Chapter two contains the calculations for an anisotropic

point light source within a spherical envelope, which has been submitted as a paper to A&A. In Chapter three we went one step further to include an arbitrary shape envelope with an anisotropic point light source. The non-uniform photosphere is discussed in Chapter four, with a model for the variation of the areas of the spots on rotating stars. These last two chapters are being prepared to be published as two more papers. The conclusion and suggestions for future work are given in Chapter five. Four appendices are enclosed with this work.

S. Hammid, and ending with Dr. J. Simmons and Prof. J. Brown. Above all the thanks are to Allah (God) for uncountable favors.

SUMMARY

A theoretical description of the polarization of light, generated by an anisotropic point light source and scattered by an arbitrary shape envelope, is developed in this work, the mechanism of scattering being assumed to be either Thomson or Rayleigh scattering. The description is a development of the earlier work of J. F. L. Simmons' (1982) where he expressed the scattering function and scatterer density distribution function as a summation of multipole contributions. Whereas Simmons analysis was based on an isotropic point light source, the present analysis permits a variable flux to represent the anisotropy of the light source. Thomson or Rayleigh scattering is assumed throughout, and in all cases the scattering envelope is taken to be large compared to the light source. This allows the anisotropy to be expressed in terms of projected area. The model has applicability to rotating, pulsating, binary, and active stars with hot extended envelopes.

The thesis is divided into five chapters plus four appendices. Following a review of previous work in Chapter One, together with a discussion of the motivation and interest of stellar polarimetry, in

Chapter Two the theoretical analysis is established for scattering polarization with an anisotropic point light source within a spherical envelope. This analysis is then applied to an ellipsoidal black body star within a spherical envelope, for which we get explicit integral expressions for the Stokes' parameters and an analytical solution for the special case of a star with a circular equator. As examples of ellipsoidal stars the polarization from a single distorted star (due to e.g. the rotation) such as Be stars, X-ray binaries filling its Roche lobe (e.g. Cygnus X-1 and Centaurus X-3), and pulsating stars (pulsating as a series of ellipsoids) is calculated. The latter show a very complicated pattern of qu-loci, which, in principle, fit the polarization behaviour of such types as RV Tau and Omicron Ceti. The maximum polarization of about 20% of the total light is expected from a disk like light source viewed edge on (Galaxies would be good example, since they are very distorted light sources).

In Chapter Three the anisotropic light source theory is generalized to include an arbitrarily shaped envelope. In the harmonic summation which results it is found that approximation up to the second order terms is quite acceptable, when both the light source and the envelope are ellipsoidal. The maximum polarization is enhanced (due to the envelope being ellipsoidal) to

about 35% when a disk of scatterers is perpendicular to the disk like star observed edge on. In general whether the polarization undergoes enhancement or cancellation is dependent on the angle between the rotation axis of the ellipsoidal star and the axis of symmetry of the ellipsoidal envelope. The effects of rotation and pulsation are also calculated.

In Chapter Four the analysis is applied to the case of light source anisotropy arising from a non-uniform photosphere (e.g. hot or cool spot). Calculation of the projected area of the spot as it varies during stellar rotation is done without any of the simplifying assumptions usually made in stellar light curve modelling. Again the approximation of the second order terms of the harmonic summation is acceptable for spots of likely physical size (e.g. of angular extent < 30°). In general the polarization caused by stellar spots is much smaller than that produced by nonsphericity of the star. The analytic expressions for the projected area of a spot simplifies the polarimetric calculations for a fixed spot, for a spot with umbra and penumbra, for a spot varying with time in its size, temperature, and location, and for a star with more than one spot. The results of this Chapter is applicable to solar type stars, late type (giant) stars such as α Ori.

Chapter Five comprises an overview of our conclusions with recommendations for future work. In this chapter we discussed the importance of the approximation of the second order terms of the harmonic summation, the similarity between the polarization produced by isotropic light sources within arbitrary shaped envelopes and anisotropic light sources within spherical envelopes, and results of the application of the theory. This leads to further suggestions for more applications and development of the model. Topics covered by the appendices are :

A) Some analysis of Serkowski's (1970) observations for U Mon, where the period of light variationsis calculated directly from the polarimetric data.

B) The mathematical proof for the projected area of an ellipsoid.

C) Some numerical values for the multipoles of the flux $f_{\ell m}$ and the multipoles of the envelope K_{ℓ},

D) Values of coefficients of the spherical harmonics, rotation matrices and Clebsh-Gordon coefficients.

Contents :

CHAPTER ONE

1. INTRODUCTION

CONTENTS :

§1.1. INTRODUCTION :

Polarimetric studies of the light scattered off circumstellar matter have produced considerable interest in recent years. The first theoretical formulation of stellar polarization was done by Chandrasekhar, using radiative transfer theory for Thomson and Rayleigh scattering, to calculate the linear and elliptical polarization of the radiation field in the stellar atmosphere (Chandrasekhar 1946a&b and 1947, *cf.* Schwarz 1984). Many observations confirmed this theoretical work, but added new astrophysical discoveries and questions. For example V. A. Dombrovskij discovery of large polarization in the Crab Nebula in 1954 (*cf.* Gehrels 1974) – What is the cause ?; four years later many observations showed a strong wavelength dependence in the linear polarization of planets, stars, and nebulae (e.g. Grigoryan 1958) – again Why?; in 1962 N. M. Shakhovskoj observed variable polarization in the early-type eclipsing binary β Lyr. (Shakhovskoj 1962); K. Serkowski found strong intrinsic polarization for Mira stars in 1966 (Serkowski 1966); and finally J. Kemp discovered circular polarization on a white dwarf star in the 1970's (see e.g. Kemp and Wolstencroft 1972). One wonders if all stellar types produce polarization?. That can be answered by further observations.

However, we need theoretical models to explain the cause of the polarization. There was little development in theoretical models until the 1960's, when the results of Chandrasekhar's work above were tabulated in convenient form by Coulson, Dave and Sekera in 1960 (Coulson *et al.* 1960, *cf.* Gehrels 1974), and some more detailed polarimetric models were presented (e.g. Shakhovski 1965 and Collins 1970).Since then many detailed models have been published. Before we discuss any of these models in detail, it is a good idea to show the advantages of polarimetric studies, by asking this question :

§1.1.1. WHAT KIND OF INFORMATION DO WE GET FROM STELLAR POLARIZATION ?

Stellar polarization is affected by the shapes of the star and of any circumstellar envelope, by the brightness distribution on the stellar surface, also by dependence on the scattering particle distribution function and by variation of the scattering mechanisms within the envelope (e.g. Brown and McLean 1977; Simmons 1982; Friend and Cassinelli 1986; Clarke and McGale 1986 and Brown, Carlaw and Cassinelli 1989). Polarization thus serves as a diagnostic of the geometry of circumstellar matter, of the illuminating stars, and

also of their orientation in space.

In particular, by studying the time dependent qu-loci the inclination and orientation of some binary stellar systems can be determined. This result has been shown in the work of Brown, McLean and Emslie (1978), Rudy and Kemp (1978), Simmons (1983), and their application like those by Aspin *et al.* (1981), Simmons *et al.* (1982), and Dolan and Tapia (1989). Even in the case of single stars, some information can be obtained from the geometry dependence of the polarization (Brown and McLean 1977, and Clarke and McGale 1987).

Moreover, stellar polarization often has a wavelength (λ) dependence. It has been proved by many observations (e.g. Serkowski 1970, Shawl 1972, Shawl 1974, and Raveendran, Kameswara Rao, and Anandaram 1989), that the wavelength dependence differs from star to star, but a common feature for late type stas is a fast increase with decreasing wavelength (Gehrels 1974). For *Mie* scattering models the theoretical wavelength dependence of polarization has been shown to be nearly independent of the envelope geometry in the case of an optically thin envelope, uniform in particles' density distribution and with asymmetrical shape (Shawl 1975, Simmons 1982). This wavelength dependence of the observed polarization therefore imposes limitations on physical conditions in the envelope rather than on its

geometry. For an example, if electron scattering was the dominant source of opacity, then the intrinsic polarization should not depend strongly on the wavelength, while if hydrogen absorption dominates, the intrinsic polarization will be very small (Shawl 1974). Fig 1-1 shows the observed wavelength dependence of polarization for early-type stars as presented by Kruszewski (1974).

As a final example, note that from polarization we can derive considerable physical information on magnetic fields. One example is the study of the local solar magnetic field through the polarization of microwaves from flares (Zirin 1988). Secondly, information on solar and stellar magnetic fields can be found through the Zeeman effect which splits spectrum lines into several polarized components. In the simplest case a line is split into three components, the so called Lorentz triplet. The central line is at the rest wavelength in the original, while the other two are polarized and displaced symmetrically to both sides. The size of this displacement is dependent on the strength of the magnetic field. The usefulness of the polarization arises when we observe stars with magnetic fields in different directions. If we observe in a direction parallel to the magnetic field lines, then only the two displaced components will be seen having *circular* polarization in opposite directions, while the central line intensity decreases to zero - the so called
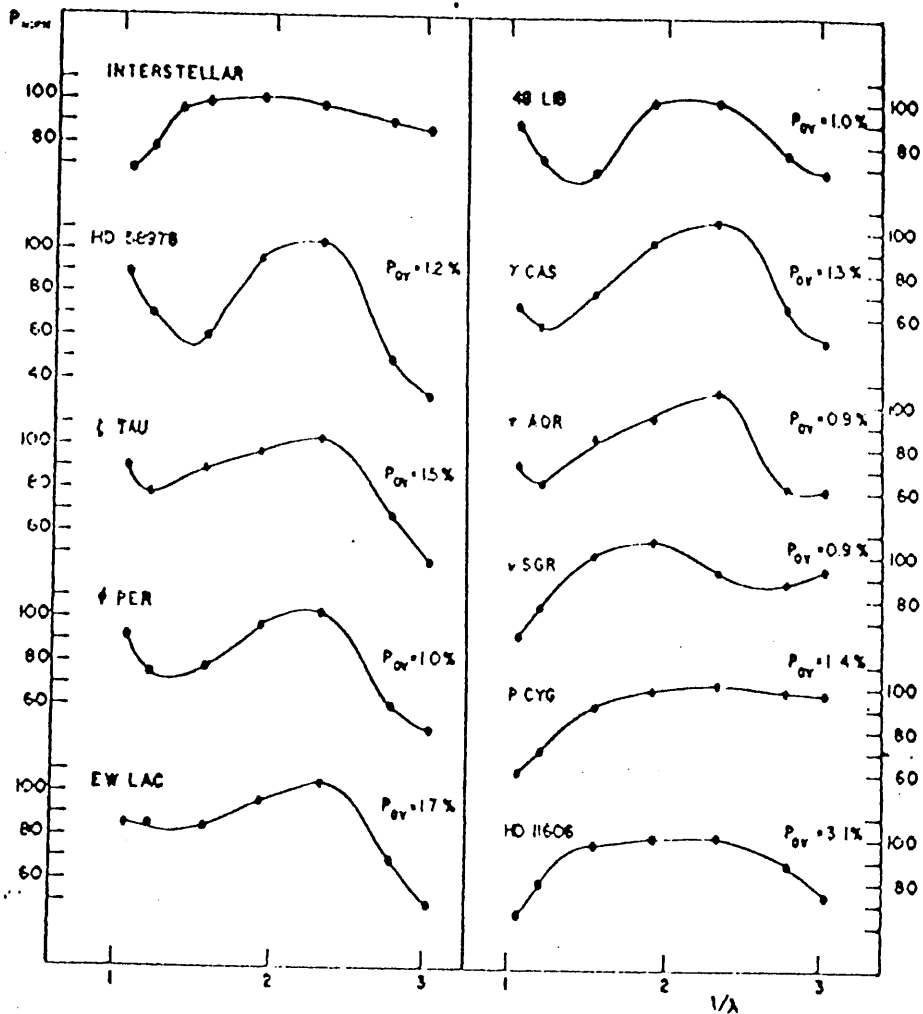
Fig. 1-1. The wavelength (in 1/μ) dependence of polarization for a sample of early-type stars with emission lines. The characteristic interstellar curve is shown for comparison (*from* Kruszewski 1974).

longitudinal Zeeman effect. If we were to observe in the direction perpendicular to the magnetic field, we would observe the so called *transverse Zeeman* effect, when all three components would be seen, the central being twice as strong as each of the displaced components, and all of them *linearly* polarized. The two shifted components are polarized in the direction perpendicular to the magnetic field, while the central one is polarized parallel to the magnetic field (Böhm-Vitense 1989, see Fig. 1-2).

In the case of interstellar matter, the astronomers now routinely use the direction of interstellar polarization as an indicator of the direction of the interstellar magnetic field (Shu 1982).

Obviously, a polarimetric model should relate to as much of those polarimetric informations as possible. Now one may ask this question :

§1.2. HOW CAN WE GATHER THE INFORMATION FROM THE POLARIZATION ?:

We will find part of the answer in the best book ever written in this field " *Planets, Stars and Nebulae studied with Photopolarimetry*" edited by T. Gehrels, where he said in his introduction (Gehrels 1974) :
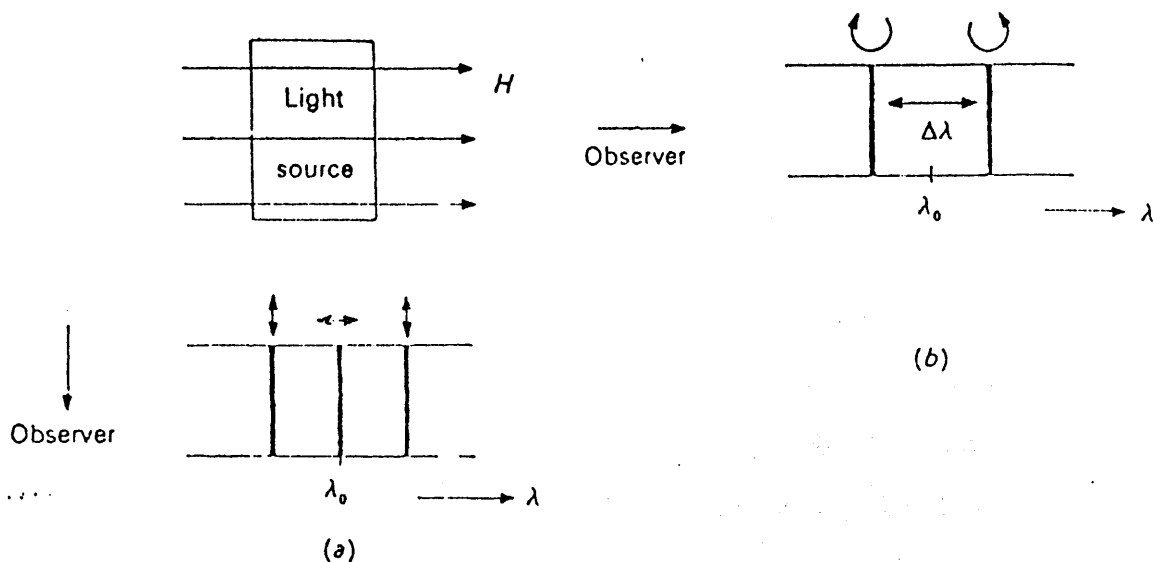
Fig. 1-2. The splitting of a spectral line due to the Zeeman effect is shown : (a) for the case when the observer is in the direction perpendicular to the magnetic field (i.e. the transverse Zeeman effect), (b) for the case when the observer looks at the light source in the direction parallel to the magnetic field (i.e. the longitudinal Zeeman effect). The directions of circular and linear polarization of the emitted light are indicated by the arrows (Böhm-Vitense 1989).

' Three basic methods are used to gather information from the polarization and brightness measurements.

1). The most fundamental is to make comparisons with the scattering theories like the Rayleigh-Chandrasekhar theory of multiple molecular scattering and Mie theory of scattering by small particles. However, a decreasing order of applicability is seen [We assume he means less theoretical models in this field, which is not the case, see (e.g.) Stamford and Watson (1980) and Lefèvre (1992)]. A rigorous solution may be made in the case of multiple scattering in a clear molecular atmosphere overlying a ground that reflects in a prescribed manner. Separately, also the problem of single scattering on a spherical particle of known size and refractive index has a rigorous solution. The study of interstellar grains is already further complicated because the size and refractive indices have distributions, and there are effects of aspect and particle shape to be considered. A molecular atmosphere with aerosols and "ground" effects is highly complex; the cases of the Venus and Jupiter atmospheres may be the ultimate challenge in our work, especially because of non-uniformities in the cloud deck (Coffen and Hansen 1974).

2). A second method that is applicable even when one cannot apply rigorous theory is to compare one observed

object with another. For instance, if it is true that circular polarization observed on the planets has limited usefulness in theoretical analysis (Kemp 1974), there still will be great merit in comparing various planets and observed hemispheres [of the planets].

3). Laboratory results on appropriate samples can help in the understanding of phenomena observed at the telescope. Examples of such work for the study of surface of the moon and the asteroids are given by Pieters (1974) and by Bowell and Zellner (1974).'

The first method is used in the basis of most stellar polarimetric modelling and calculations. In addition to the basic theory of scattering, however, modelling also includes distribution of scatterers over type, size, and in space. It is mainly the last that we consider in this thesis. Such models and calculations of stellar polarization have so far fallen into two limiting categories : that when the polarization is produced by the stellar light scattering in rotationally distorted atmospheres; and scattering in extended envelopes (detached from the star).

§1.2.1. Scattering by rotationally distorted atmospheres

This was modelled in the Chandrasekhar (1946a&b; 1947) formulation of the problem using radiative transfer techniques, the star being treated as a nonpoint source of light. Many results have been calculated for illuminated gray and nongray stellar atmospheres using Thomson and Rayleigh scattering such as in Collins (1970); Collins and Buerger (1974); Cassinelli and Haisch (1974) and Haisch and Cassinelli (1976). Collins' work found the polarization of the light scattered in the photosphere of the star to be much smaller than the polarization observed from early type stars. Cassinelli and Haisch concluded that a highly flattened extended envelope, beyond the normal stellar atmosphere was required to explain the observations (*cf.* Brown and McLean 1977).

Some calculations have been done in particular cases of anisotropic light sources, e.g. Gnedin *et al.* (1976) calculated the polarization for close X-ray binaries using a two dimensional model of an ellipsoidal Roche lobe with and without hot spot. Stamford and Watson (1980) calculated the polarization of a hot nonradial pulsator. They found, for an atmosphere applicable to B type variables, a quite small polarization in the visual range, as expected from the above work of Collins (1970)

and Haisch and Cassinelli (1976). Recently, Lefèvre
(1992) used radiative transfer techniques to calculate
the polarization of a star which departed from the
spherically symmetric case, using as an example a star
with a photospheric hot spot surrounded by a spherical
shell.

§1.2.2. SCATTERING BY EXTENDED ENVELOPES :

Regarding the envelope as an extended tenuous ring-
(or disk-) like cloud detached from the star, was
suggested by Cassinelli and Haisch (1974) (see Sec.
1.2.1). In modelling this situation approximations are
usually made, such as treating the star as a point
source of light and taking the envelope to be optically
thin for scattering and sometimes also for absorption.

The first analysis of this technique was given by
Shakhovski (1965). He considered scattering in a thin
circular ring of electron (Thomson) scatterers lying in
the equatorial plane of the star but with arbitrary
inclination to the earth. Shakhovski concluded that the
polarization of the scattered light only (without the
addition of the direct unpolarized starlight) from any
such plane ring would be of the form :

$$P = \sin^2 i \ / \ (\ 2 + \sin^2 i \ ) \qquad\qquad (1-1)$$

with the maximum value at $i=90°$ (when the star is

observed equator-on) of 1/3. He also deduced that the same result must hold for any plane disk (by subdivision into rings), and that the plane of the polarization (maximum intensity) always lies in the projected polar axis direction (i.e. perpendicular to the scattering plane).

Several extended analyses of this problem followed this one, for both Thomson and non-Thomson scattering e.g. for particular case of $i=90°$ (Capps et. al. 1973), or for particular axisymmetric three-dimensional geometries, such as an ellipsoidal shell (Zellner 1971), or a circular sector rotated in the equatorial plane (Kruszewski et al. 1968). An analysis of Mie scattering polarization was carried out by Shawl (1975), for an arbitrarily shaped envelope, concentrating on the polarization wavelength dependence and the reddening of the scattered light.

The first general analytic treatment for the polarization of starlight from an unpolarized isotropic point light source due to single scattering on the electrons of an axisymmetric circumstellar cloud (Thomson scattering), was given by Brown and McLean (1977). In this paper the above Shakhovski polarization relation of polarization to stellar inclination was developed to include a general shape factor :

$$P = \sin^2 i \; / \; [\; 2\,\alpha + \sin^2 i\;] \tag{1-2}$$

where $\alpha=(1+\gamma)/(1-3\gamma)$ and γ is a *shape factor*, defined by the ratio of two moments (integrals) of the density distribution function in spherical coordinates, and related to the oblateness (or prolateness) of the envelope. The maximum residual polarization P_R (after addition of the unpolarized direct starlight) is about -20% for a polar line envelope ($\gamma=1$), and about +10% for a plane disk envelope ($\gamma=0$), for a mean scattering optical depth $\overline{\tau}=0.1$ (*see* Fig. 1-3). The residual polarization is given by :

$$P_R \simeq \overline{\tau} (1 - 3 \gamma) \sin^2 i \qquad\qquad (1-3)$$

These results will be the same in case of Rayleigh scattering, but with the same wavelength dependence of τ as the Rayleigh cross section (i.e. λ^{-4}). Brown & McLean applied their results to hot (early type) shell stars (e.g. Be stars).

For single cool stars, Simmons (1982) generalized the work of Brown and McLean (1977) to arbitrary Mie scattering in optically thin circumstellar shells of arbitrary shape . He also assumed an isotropic point source of light, approximating the scattered flux and Stokes' parameters as sums of multipole contributions. Each contribution takes the form of a product of two factors, one arising purely from the density distribution function of the scatterers, and the other from the phase function of the scattering mechanism. Simmons concluded quite generally that the form of the
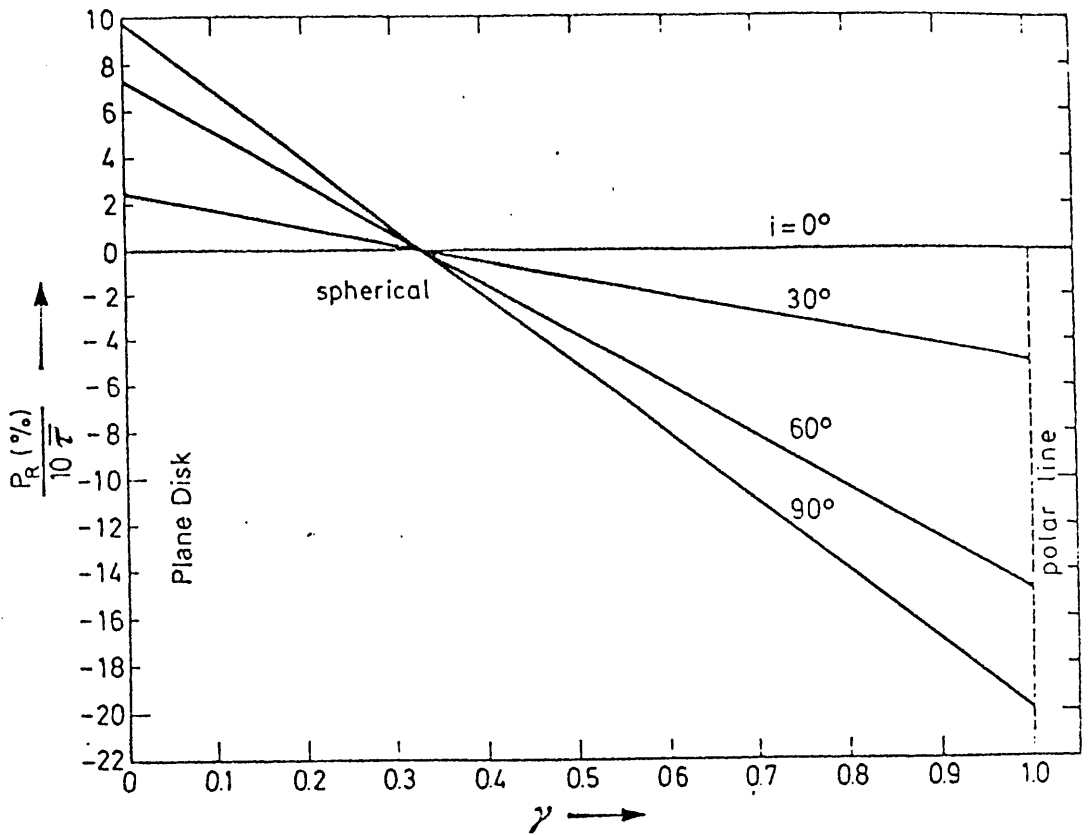
Fig. 1-3. The residual polarization PR (%) (i.e. when the direct starlight is added to the polarized radiation). the ratio PR/$\bar{\tau}$ is shown as a function of γ for various inclinations, where $\bar{\tau}$ is the mean scattering optical depth (Brown and McLean 1977).

polarization versus wavelength (λ) dependence is independent of the specific density distribution of the scatterers in the envelope, and the position angle of the polarization is independent of the specific scattering mechanism.

Brown, McLean, and Emslie (1978), and Rudy, and Kemp (1978) treated the case of multiple light sources in arbitrary shaped envelopes and applied it to rotating binary systems. A generalization to arbitrary Mie scatterers for binary systems is given by Simmons (1983).

Cassinelli, Nordsieck and Murison (1987) derived a factor to correct the Brown & McLean (1977) Thomson and Rayleigh scattering model for a finite size isotropic star, using extended atmosphere radiative transfer theory. This correction (so called depolarization) factor reduced the magnitude of the predicted polarization from a finite stellar disk to less than half of that predicted for the point source for a typical envelope distribution. Two years later, Brown, Carlaw and Cassinelli (1989) rederived this depolarization factor without radiative transfer, obtained the corresponding correction factor for the scattered flux and extended results to limb darkened stars. They also concluded that for the case of non-Rayleigh scattering more complicated correction factors were needed.

Another correction is required for the case in which some of the scattering particles of the envelope are occulted by the star. A series of papers was published on this correction by Milgrom (1979), Brown and Fox (1989), Fox and Brown (1991) and Fox (1991) for Thomson scattering. The general case shows a complicated inclination dependence of the polarization, so any expression of the form of Eq. (1-3) no longer holds.

Most of the previous analytic described work above has treated the light source as isotropic and unpolarized. This not always the case, since stars are in general anisotropic light sources.

§1.3. ANISOTROPIC LIGHT SOURCES :

Collins and Buerger (1974) concluded that a measured polarization in excess of 1-2% for either single or multiple star systems cannot arise by scattering in the atmospheres of the stars, unless the star itself is 'distorted', such as in supergiants where distortion from sphericity can result either by rotation, pulsation, or a large magnetic field. Such 'distortion' of the light sources can mainly be due to two effects :

1- Non-spherical shape.

§1.3.1. ANISOTROPY DUE TO NON-SPHERICAL LIGHT SOURCES:

Non-spherical stellar shapes are produced to a greater or lesser extent by rotation, by pulsation and by a companion star (binary).

Rotating stars in general will be distorted from sphericity. They may take either oblate or prolate shapes, depending on the angular momentum and the strength of the magnetic field. The oblateness can be expressed in terms of Maclaurin spheroids with the circular equatorial cross section radius larger than the polar cross section radius) and the prolateness in terms of Jacobi ellipsoids (both the equator and the polar cross section are ellipses) . For a negligible magnetic field , the Maclaurin spheroids range from a sphere to a flat disk according to the value of the angular momentum. Jacobi ellipsoids range from an axially symmetric configuration to a very long needle shape, but it is found that they represent possible equilibrium states only for angular momenta exceeding a critical value. The dynamically stable shape, from a geometrical point view, starts as a stable Maclaurin spheroid where the equatorial cross section is circular with radius of unity and the polar axis ranges from 1 down to 0.58 (as

rotation increases). At the latter point, to maintain stability the star becomes a Jacobi ellipsoid when the polar axis and one of the equatorial axes shrinks to about 0.1 of the longer axis of the equator. Beyond this the star develops more complicated shapes (Tassoul 1978, see Tables 1-1 and 1-2).

Other reasons for non-sphericity are non-radial oscillations of the star (i.e. pulsator) and the influence of a binary companion, such as the production of a star which fills its Roche lobe (see Tassoul 1978, Sec. 2.4.2.2, and Fig. 1-4a&b).

§1.3.2. Anisotropy due to non-uniform photosphere :

The second main reason for anisotropy of a stellar light source is a non-uniform brightness distribution of the radiating surface. This may be caused by a magnetic field, by spots or by convection cells...etc.

We will discuss, as examples of this anisotropic effect, convection cells and star spots which may be thought of as bright and dark spots, respectively. Bright photospheric spots (where $T_{spot} > T_{star}$, e.g. granules or supergranules) can have temperatures above the stellar photosphere by up to 1000 K (Doherty 1986),

TABLE 1-1
PROPERTIES OF THE MACLAURIN SPHEROIDS

τ	e	a_1	a_3
0.00	0.	1.000000	1.000000
0.02	0.373909	1.025418	0.951039
0.04	0.511028	1.051737	0.904035
0.06	0.605447	1.079070	0.858817
0.08	0.676908	1.107544	0.815227
0.10	0.733413	1.137304	0.773121
0.12	0.779224	1.168520	0.732365
0.14	0.816962	1.201394	0.692834
0.16	0.848380	1.236162	0.654409
0.18	0.874723	1.273107	0.616978
0.20	0.896912	1.312575	0.580433
0.22	0.915652	1.354987	0.544666
0.24	0.931495	1.400870	0.509571
0.26	0.944881	1.450890	0.475041
0.28	0.956167	1.505909	0.440963
0.30	0.965646	1.567062	0.407218
0.32	0.973562	1.635890	0.373673
0.34	0.980120	1.714542	0.340176
0.36	0.985492	1.806147	0.306545
0.38	0.989825	1.915476	0.272550
0.40	0.993246	2.050287	0.237887
0.42	0.995863	2.224338	0.202115
0.44	0.997770	2.465304	0.164535
0.46	0.999049	2.841411	0.123860
0.48	0.999772	3.604033	0.076988
0.50	1.000000	∞	0.

Here τ is the ratio of the rotational kinetic energy K to the gravitational potential energy W (i.e. $\tau = K/|W|$), with a_1, a_2, and a_3 the semi-axes of the ellipsoid (for Maclaurin Spheroid a1=a2), and e is the eccentricity (Tassoul 1978).

TABLE 1-2

PROPERTIES OF THE JACOBI ELLIPSOIDS

τ	a_1	a_2	a_3
0.1375	1.197234	1.197234	$6.976571(-1)$
0.14	1.362619	1.058823	$6.931102(-1)$
0.15	1.623843	$9.128330(-1)$	$6.746283(-1)$
0.16	1.829508	$8.332346(-1)$	$6.559916(-1)$
0.17	2.026971	$7.742668(-1)$	$6.371794(-1)$
0.18	2.228015	$7.260630(-1)$	$6.181695(-1)$
0.19	2.439037	$6.845402(-1)$	$5.989390(-1)$
0.20	2.665006	$6.475539(-1)$	$5.794633(-1)$
0.21	2.910679	$6.138146(-1)$	$5.597169(-1)$
0.22	3.181212	$5.824744(-1)$	$5.396727(-1)$
0.23	3.482603	$5.529374(-1)$	$5.193021(-1)$
0.24	3.822142	$5.247622(-1)$	$4.985752(-1)$
0.25	4.208964	$4.976078(-1)$	$4.774606(-1)$
0.26	4.654786	$4.712008(-1)$	$4.559259(-1)$
0.27	5.174943	$4.453148(-1)$	$4.339376(-1)$
0.28	5.789902	$4.197578(-1)$	$4.114622(-1)$
0.29	6.527538	$3.943635(-1)$	$3.884668(-1)$
0.30	7.426615	$3.689867(-1)$	$3.649206(-1)$
0.31	8.542318	$3.435010(-1)$	$3.407974(-1)$
0.32	9.955242	$3.177994(-1)$	$3.160786(-1)$
0.33	$1.178655(+1)$	$2.917972(-1)$	$2.907582(-1)$
0.34	$1.422451(+1)$	$2.654381(-1)$	$2.648497(-1)$
0.36	$2.234398(+1)$	$2.116265(-1)$	$2.114801(-1)$
0.38	$4.060607(+1)$	$1.569406(-1)$	$1.569183(-1)$
0.40	$9.348701(+1)$	$1.034255(-1)$	$1.034240(-1)$
0.45	$1.387580(+4)$	$8.489281(-3)$	$8.489281(-3)$
0.50	x	$0.$	$0.$
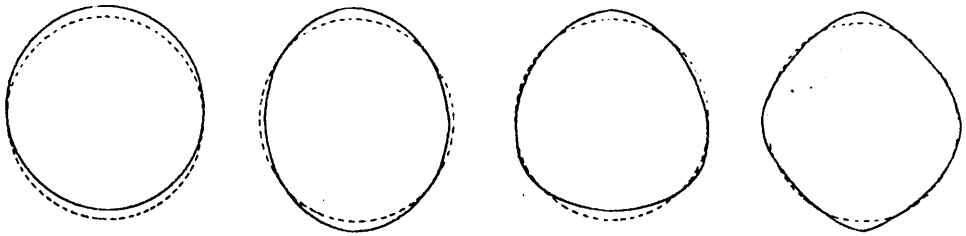
Fig. 1-4a. Distortion of a spherical star (dotted lines) due to pulsation at the lowest spherical harmonics Y_ℓ^0 ($\cos\theta$), with $\ell=1,2,3,4$ (Tassoul 1978p).
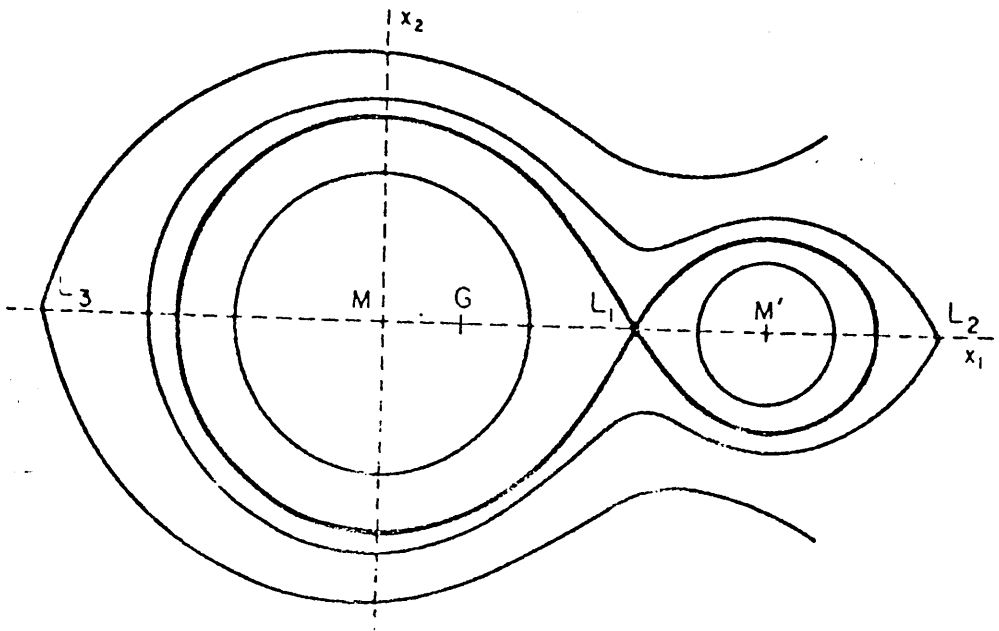
Fig. 1-4b. Level surfaces of Roche model in orbital plane (M'/M=0.215, *from* Tassoul 1978).

and sizes as large as 10% of the stellar surface
(Schwarzschild 1975). They can occur anywhere on the
star and tend to be long-lived in the case of giants.
Dark photospheric spots (where $T_{spot} < T_{star}$, i.e. black
spots) can be cooler than the star by up to 2000 K (Vogt
1981), with sizes up to 15% of the stellar surface.
These occur within $60°$ north and south of the stellar
equator (Bopp and Evans 1973). Virtually any light curve
can be generated by a suitably complex distribution of
spots on a rotating star (Vogt 1981). So far their
polarization effects have not been studied in detail.
Some polarimetric modelling of a hot spot has been
presented by Gnedin *et. al.*(1976), Schwarz and Clarke
(1984) and Doherty (1986), but their analyses are
acceptable only for small spots (e.g. of angular extent
$\psi < 5°$), as we will see in Chapter 4 of this thesis.

These two anisotropic effects will affect both the
light variation and the polarization, and may explain
(with or without counting the effect of arbitrary
envelope shape- see Chapter four) the high polarization
observed in the late-type variable stars of spectral
type K and M (e.g. giants, supergiants, dwarfs) due to
fast rotation, pulsation, and spots (see Collins and
Buerger 1974, Shawl 1975, and Schwarzschild 1975) . Some
early-type stars such as Be stars show polarimetric
variation. Polarization of these stars has been
explained by scattering in an axisymmetric envelope

(Brown and McLean 1977 and Fox 1991), but without the effect of an anisotropic light source. The time dependence of polarization may be explained by such anisotropy, especially for pulsators such as β Cep.. Some of these cases will be discussed in more detail in the following chapters. Next we will present some of the observational results for several stellar-types.

§1.4. POLARIMETRIC OBSERVATIONS :

Luminous stars of spectral type K and M show the largest mean polarization and the biggest changes in polarization (Kruszewski, Gehrels and Serkowski 1968, and Shawl 1975). In a study of the distribution of polarized and unpolarized K and M stars in the HR diagram, Dyck and Jennings (1971) show that nearly all of the supergiants observed show intrinsic polarization, while no giant earlier than M2 was found to be polarized (Fig. 1-5). In general, the hotter the star the greater the luminosity must be for intrinsic polarization to be present (Shawl 1974). So, many late-type stars produce variable polarization, but there are some early-type stars which already show this variability such as β Cep. stars. The wavelength dependence of the polarization has been discussed briefly above (in Sec. 1.1.1). Here we will draw attention to pulsators and spotted stars.
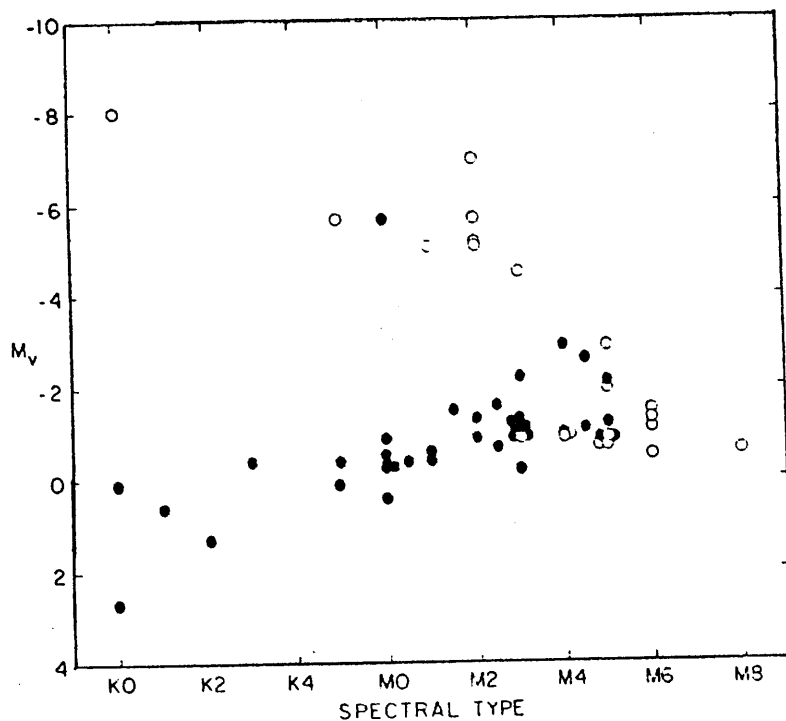
Fig. 1-5. Distribution of polarized (open circle O) and unpolarized (closed circles •) stars in the HR diagram (*from* Dyck and Jennings 1971).

Pulsators show a variable polarization. The first observations of this kind were reported by Serkowski (1970) for RV Tauri stars U Mon. and R Sct., which are late-type stars. Serkowski made of one of the best and longest polarimetric observations for such stars, finding for U Mon a polarization variation from 0% to 1.5%, with large and regular changes in the position angle in the blue region. The position angle remains (in the blue region) close to $0°$ around and before the deep light minima and close to $105°$ about the shallow light minima that occurs halfway between the deep minima. In addition, both position angle changes occur at the phase when the spectral lines are doubled (due to Doppler effect). Fig. 1-6 (a,b,c, and d) show the U Mon. changes with phase of light variation in (a) radial velocity observed by Preston (1964); (b) U-V color index observed by Preston *et al.*(1963) and Serkowski (1970); (c) polarization difference in two colors (B-V & U-V) by Serkowski (1970); and (d) the position angle in different color also by Serkowski (1970). This figure illustrates some of U Mon's properties we just mentioned above. Fig. 1-7 presents the qu-plane loci (or the polarization versus position angle) variation for both U Mon. and R Sct. from Serkowski (1970).

Serkowski suggests that his observations may be explained by non-spherical oscillation of a star that is embedded in a circumstellar cloud. The presence of such
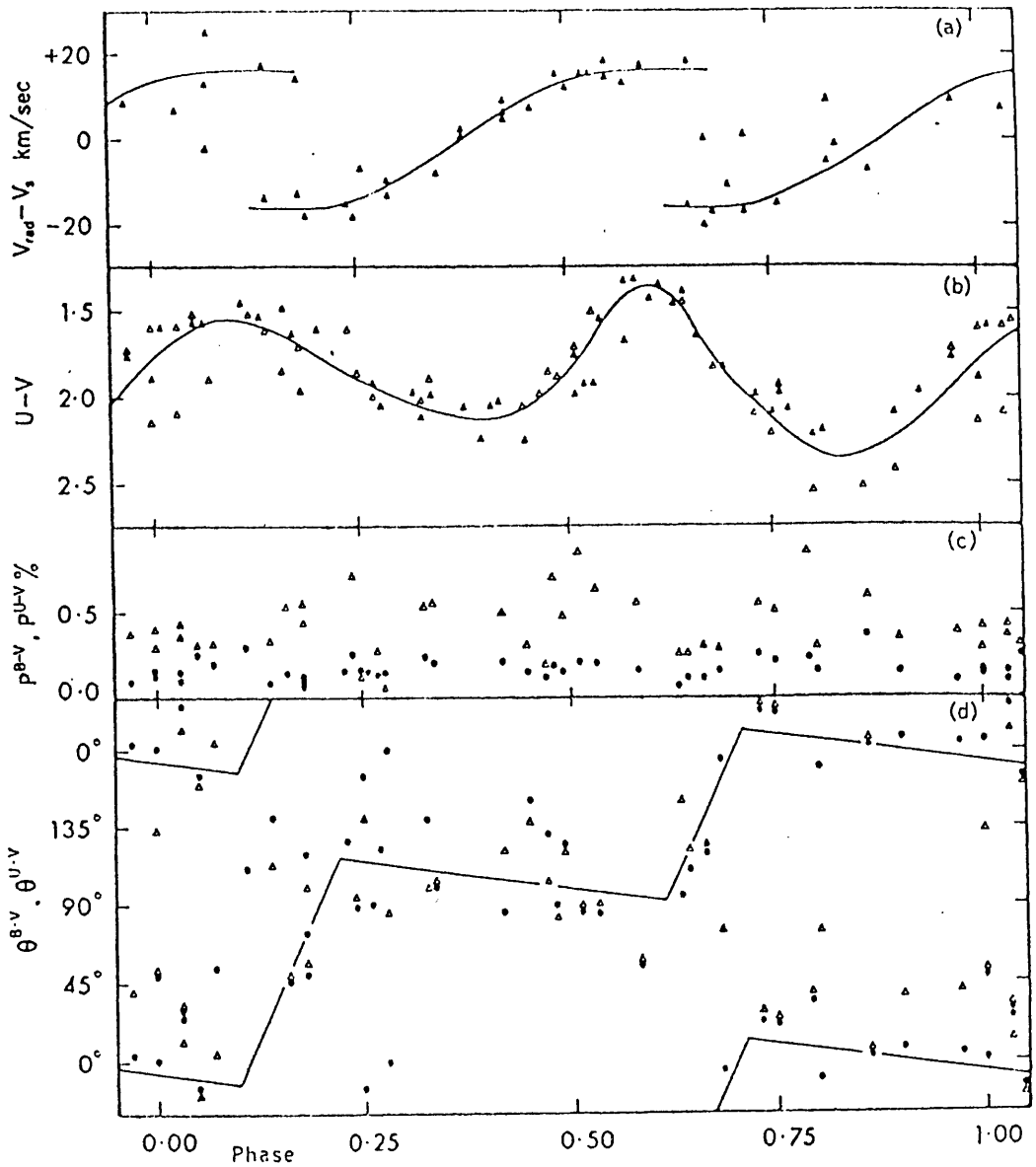
Fig. 1-6. Changes of U Mon. with phase of the light variation. (a) radial velocity observed by Preston (1964); (b) U-V color index observed by Preston *et al.*(1963) and Serkowski (1970); (c) polarization difference in two colors by Serkowski (1970); and (d) the position angle in different colors (Serkowski 1970).
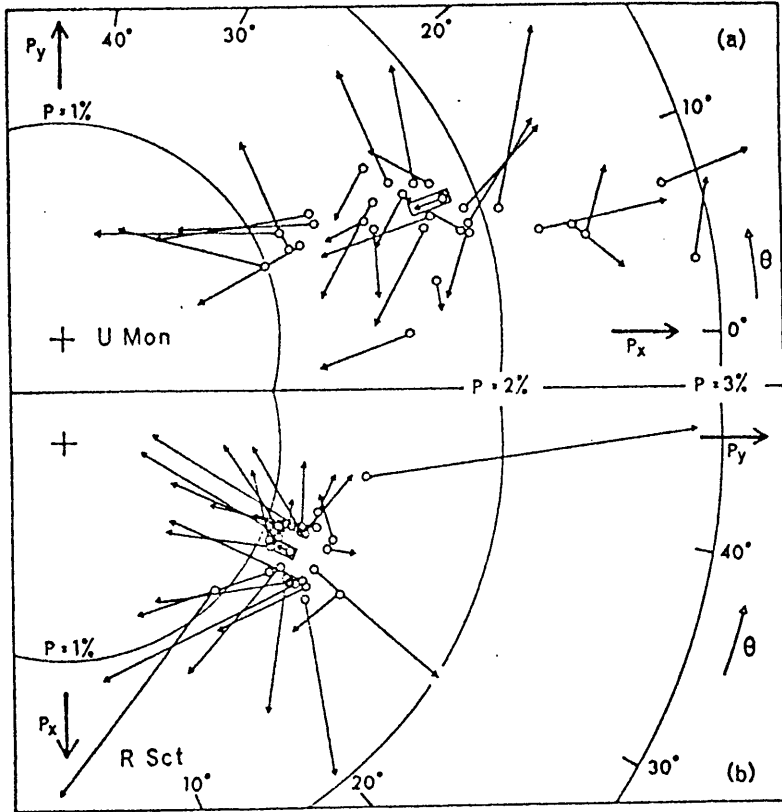
Fig. 1-7. The qu-plane (or the polarization with the position angle) for both U Mon. and R Sct. (*from Serkowski 1970*). The yellow observations are open circles, and the ultraviolet are the tips of the arrows.

a cloud is proved by the observation of Gehrz and Woolf (1970) for U Mon. because of a large infrared excess .Gehrz (1971) combined visual and infrared observations for four RV Tauri stars and concluded that there must be nonradial pulsation occurring, the strength of which is given by studying the radial velocity curves in Fig. 1-6a, and relating them to the curves expected from nonradial oscillators (see Unno *et al.* 1979, and Shawl 1974).

Preston *et al.* (1963) calculated the mean period of the light variation of U Mon. using their photometric observations, to be 92.23 days, while Serkowski (1970) obtained a period of 91.3 days using his photometric observations. In the early stages of this thesis, the author applied a second order power spectrum method to the polarimetric data (see Appendix A), and obtained almost the same period from the polarimetric observation as Serkowski (1970).

The changes in polarization of R Sct. are less regular than those of U Mon. In addition , R Sct. shows a different type of position angle variation (Serkowski 1970). Several observations have been made recently for RV Tauri stars, e.g. the observations of Henson, Kemp, and Kraus (1985) for AC Herculis in the B band, over one cycle of 75.46-day period. They found a clear correlation between the light and polarization changes,

the variability in the polarization being similar to that observed in U Mon. by Serkowski (1970). They suggest the mechanism to be either nonradial pulsation in the star or radial pulsations propagating into an asymmetrical circumstellar medium.

A small number of polarimetric observations are reported by Raveendran and Kameswara Rao (1988) and by Raveendran, Kameswara, and Anandaram (1989), for the RV Tauri star AR Puppis — in total about sixteen observations, compared to about forty by Serkowski (1970), and thirty by Henson, Kemp, and Kraus (1985). They found a high polarization in one direction (about 14.6%). The wavelength dependence becomes steeper toward ultraviolet. However, in my opinion their polarimetric observations are not sufficient to be useful, unlike the photometric data.

Some polarimetric observations have been published for luminous red variable stars (for a good review see Shawl 1974). We are especially interested in Mira variable stars, which show variable polarization and wavelength dependence, and are known to be pulsating stars (Becker 1987). Recently in a photographic image of the pulsating Mira star O Ceti reported by Karovska, Nisenson, and Papaliolios (1992) in *Sky & Telescope*, they found one of Mira's atmospheric axes to be extended up to 20% longer than the other, giving the star an oval

shape. Similar results are reported in Wilson *et al.* (1991).

Another kind of pulsator is the β Cep. stars. These early-type stars have a very short period ($\simeq 0.^{d}25$), which makes a spurious data modulation inevitable, especially in observations of only a few nights (Clarke 1986). From five nights of observation of the β Cep. star BW Vulpeculae, Odell (1981) observed variable polarization. He concluded that the variation in the polarization is caused by the star's pulsation, and that this pulsation cannot be radial or ellipsoidal, but requires higher orders of oscillation to explain the polarimetric variation.

Polarimetric measurements for three β Cep. stars, β Cru, α Vir, and σ Sco. are reported by Clarke (1986). He concluded that the polarimetric periodicities are close to the fundamental photometric period , but showed them to be spurious results. This is because of the way in which the measurements were assembled from a few hours observations per night on a small number of nights. But he concluded that α Vir does display a real variable polarization, possibly caused by stellar instability (e.g. pulsation) or binary nature.

Star Spots are an alternative explanation for variable polarization. The supergiant α Orionis shows a complex behavior of polarization wavelength dependence,

which can be explained by the combined effects of Rayleigh scattering in the photosphere and scattering by circumstellar dust (Serkowski 1971). But if the photosphere is the location of the Rayleigh scattering, then asymmetry is necessary there to produce a net and observable polarization (Doherty 1986). This asymmetry can be caused by convection cells as proposed by or - as previously discussed - by nonradial pulsations (see Schwarzschild 1975, and Schwarz and Clarke 1984) . From the available observational data of α Orionis shown by Tinbergen, Greenberg, and Jager (1971), and Schwarz and Clarke (1984), we obtain a complex wavelength dependence (Fig. 1-8), with systematic variations of the polarization with the time (Fig. 1-9). UBV measurements for the polarized dust shell around α Orionis done by Borgne, Mauron, and Leroy (1986), show that the shell has no significant departure from spherical symmetry. They suggest non-spherical particles in the shell.

Now one asks, what can be added to the above knowledge !.

§1.5. The Aim of this Research :

In any stellar system, there are internal forces such as nuclear, gravity, magnetic field ... etc. which govern (e.g.) the star's shape, photosphere brightness
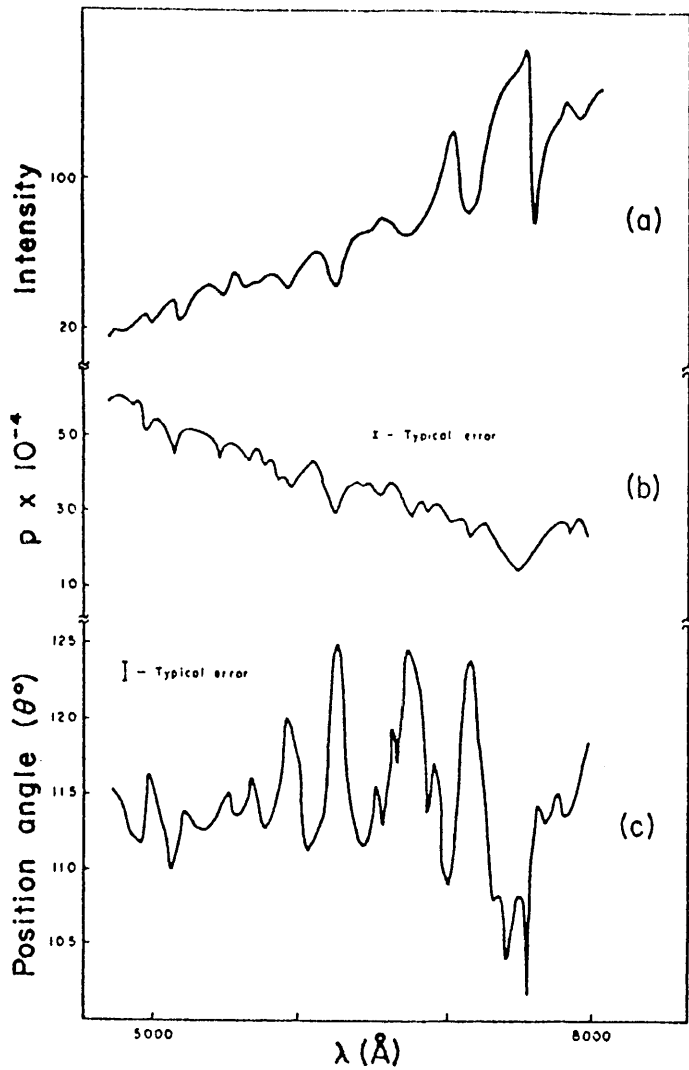
Fig. 1-8. (a) The Spectrum normalized to 100 units at 7000 Å, (b) the degree of polarization, and (c) the position angle of the polarization of α Ori as recorded by the Royal Observatory Edinburgh Mark I spectropolarimeter on 1979 Dec. 1,2, and 3 (Clarke & Schwarz 1984).
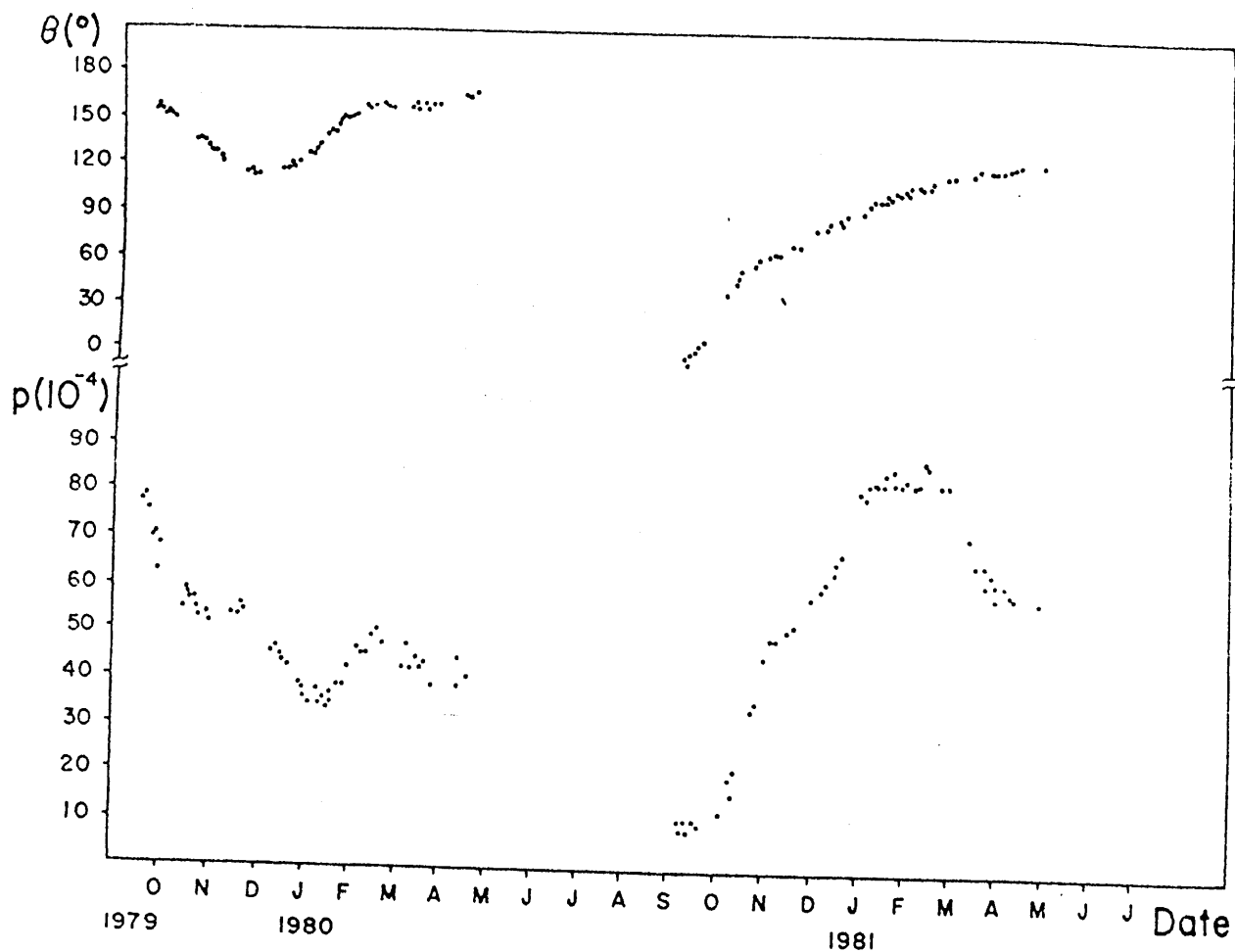
Fig. 1-9. Hayes's polarimetric data for α Ori are presented as a plot of p and θ_p against time. The units for p are 10^{-4} (i.e. 0.01%) while θ_p is in degrees in the equatorial frame (*from* Schwarz & Clarke 1984).

distribution , chemical distribution of the star and also of the circumstellar matter, if the star ejects material. These internal forces may govern the envelope shape, the envelope separation from the stellar surface, and the envelope aspect in the sky (i.e. the envelope inclination). Moreover, there are external forces such as the gravitational force of the Galaxy and of companion stars, which may influence (e.g.) the stellar orientation in the sky, the stellar rotational velocity, and the stellar velocity in the universe. All these influences of internal and external forces will affect the polarized and unpolarized light produced by the stellar system.

On the another hand, in the observer frame there will be a spectropolarimeter to measure stellar polarized and unpolarized light. The observer will apply theory to reduce the effect of the earth's atmosphere and the interstellar polarization and ending with the polarization of the star light normalized to the total light received from the star, since the observer cannot know the exact value of the total stellar light.

In this thesis we will try to present a model which relates the stellar system to the observer's frame, by parametrizing (but not calculating) the physical effects of internal and external forces on the stellar system, to predict the normalized polarization in the

observer frame, neglecting any noise from the interstellar matter and the earth's atmosphere.

For this we will use the extended envelope approach, which was discussed above in Sec. (1.2.2), but with the new factor of an anisotropic point light source being introduced, applying Simmons' (1982) technique of representing the scattered flux and Stokes' parameters as sums of multipole contributions. But here each contribution will take the form of a product of three factors, the first one arising purely from the anisotropic flux of the star, the second from the density distribution of the scatterers, and the third from the phase function of the scattering mechanism, although Thomson and Rayleigh scattering are used as scattering mechanisms throughout this thesis. Also we will not discuss the wavelength dependence of the polarization.

In the next Chapter, we will write our general equations for the scattered flux and Stokes' parameters, including arbitrary functions to describe the stellar flux, the density distribution, and the scattering mechanism. We will then solve the equations for the special case of an anisotropic light source surrounded by a spherical envelope of Thomson or Rayleigh scatterers, using non-spherical stars to provide some results to illustrate the technique. In Chapter Three we

solve the general equations for anisotropic stars with arbitrarily shaped envelopes, using the non-spherical star and envelope as a special case to compare the results with those of Chapter Two. In Chapter Four, anisotropy due to a non-uniform photosphere is considered, using spots as an example. Also in this chapter, a model is developed for variation in the projected area of a spot of arbitrary size while the star rotates. The Fifth Chapter summarizes our conclusions and discusses future work. Finally there are four appendices, A) Some analysis of Serkowski's (1970) observations for U Mon., B) The projected area of an ellipsoid, C) Some numerical values of the expressions used in the model, and C) Information about the spherical harmonic and Clebsh-Gordon coefficients.

Each chapter starts with a brief introduction, followed by the theoretical methodology and discussion of the results, and ends with a short summary of the chapter.

2. NON-SPHERICAL STAR

CONTENTS :

§2.1. Introduction :

In Section (1.2.2) we saw that most of the previous work which calculated the polarization from extended envelopes, has treated the light source as isotropic and unpolarized. In this Chapter we consider the effects of anisotropy of the stellar light source in the simplest case, in order to illustrate its basic effect, by assuming the envelope to be spherical as we will see later.

§2.2. Theory :

To illustrate the basic effect of source anisotropy, we first consider the case of a Rayleigh or Thomson scattering envelope that has spherical symmetry about the star. For simplicity, it is assumed that the star is small compared to the size of the envelope, thus allowing each scattering particle to be considered as being illuminated by radiation from a unique direction. Thus scatterer occultation (e.g. Brown & Fox 1991) and finite star depolarization effects (e.g. Cassinelli et. al. 1987) are small, and treatment is simplified of the geometry of the light source as seen from any scattering point. The basic effect that we are describing is simply that if the star radiates anisotropically, then the

51

light scattered from even a spherical shell will have a greater contribution of polarization directions from those parts of the envelope that are more thoroughly illuminated. In general, this will lead to non-cancellation of contributions when integrated over the volume and there will be a net polarization, though the envelope itself is spherical.

To quantify this, we follow Simmons (1982,1983) in using two cartesian coordinate systems centered on the star. The star's frame (X,Y,Z) has spherical coordinates (r,Θ,Φ) with OZ the stellar rotation axis, while the other frame (x,y,z) relates to the observer with spherical coordinates (r,θ,ϕ). The star is centered at O with Oz toward the observer and the x-z plane containing the Z-axis (see Fig. 2-1). The former system is rotated relative to the latter through Euler angles (α,β,γ) (cf. Messiah 1962). Consequently the scattering angle will be θ, and the polarization angle (direction) ϕ, relative to Oz for any scattering point. In general the scatterer density may be written as $n(r,\Theta,\Phi)$, and the flux of unpolarized radiation from the star is $F(r,\Theta,\Phi)$. Then following Simmons (1982) and with zero circular polarization – assuming the light source is unpolarized neglecting any magnetic field (Angel 1974) – the (un-normalized) scattered flux and Stokes parameters (F_{sc},Q,U) of the scattered radiation at the Earth
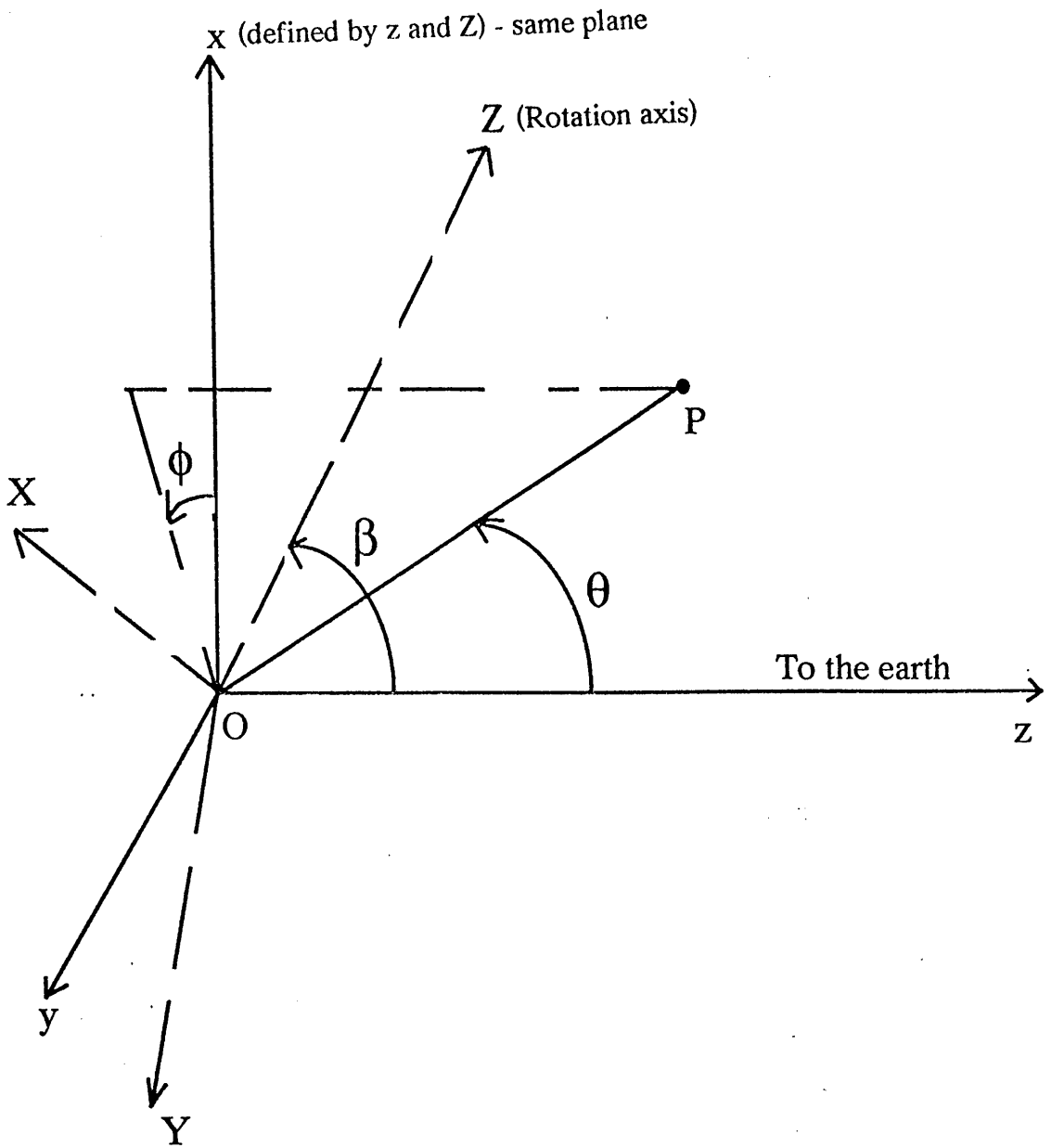
Fig. 2-1. Definitions of the star and the observer frames, O is the emitting anisotropic star (point source) and P is a general scattering point in the envelope. OZ is the rotation axis, where θ is the scattering angle, and ϕ is the polarization direction. For the Euler angles $\alpha=0$, β is the angle between Oz-axis and OZ-axis and γ is measured from X-axis in X-Y plane. The scattering plane is P'OP.

(distance D) are given by :

$$\left.\begin{array}{c} F_{sc} \\ Z^* \end{array}\right\} = \frac{1}{2 k^2 D^2} \iiint n(r,\theta,\phi) \quad F(r,\theta,\phi) \quad r^2$$

$$\times \begin{cases} (i_1 + i_2) \\ (i_1 - i_2) \exp(-2i\phi) \end{cases} \qquad dr \sin\theta \, d\theta \, d\phi \quad (2-1)$$

where $Z^* = Q - iU$ with $i = \sqrt{-1}$, $k = 2\pi/\lambda$ is the wave number, and i_1 and i_2 are the scattering functions as defined by van de Hulst (1957) , where for Thomson (electron) or Rayleigh scattering :

$$i_1 \pm i_2 = \frac{3 k^2}{8 \pi} \sigma (1 \pm \cos^2\theta) \qquad (2-2)$$

(see Brown & McLean 1977) where the value of the cross section factor σ is chosen according to whether Thomson scattering (σ will be independent of k) or Rayleigh scattering (σ is a function of k^4) is being considered.

In relation to previous models we see that the basic result of source anisotropy is to introduce the factor $F(r,\theta,\phi)$ inside the integral. This complication of allowing both F and n to be anisotropic immediately suggests that the effects on Q and U will depend on whether the two functions enhance or offset one another. We defer the discussion of this general case to Chapters Three and Four , and concentrate here on the simplification of considering a spherical envelope so as to investigate the effect of anisotropy in the stellar

radiation field. With this simplification, we write
$n=n(r)$.

The function $F(r,\theta,\phi)$ in Eq. (2-1) describes the radiative properties of the star in the observer's frame, but it is more natural to describe the behavior in terms of the flux F in the stellar coordinate system (r,θ,Φ). Providing that F varies smoothly, we may express it in terms of spherical harmonics, viz :

$$F(r,\theta,\Phi) = \sum_{\ell=0}^{\infty} \sum_{m=-\ell}^{m=\ell} F_{\ell m}(r) \; Y_{\ell m}(\theta,\Phi) \qquad (2\text{-}3a)$$

Using the rotation matrices described by Messiah (1962) (*cf.* Simmons 1983) to convert from the star's frame (θ,Φ) to the observer's frame (θ,ϕ)), we have:

$$Y_{\ell m}(\theta,\Phi) = \sum_{n=-\ell}^{n=\ell} R_{nm}^{(\ell)}(\alpha,\beta,\gamma) \; Y_{\ell n}(\theta,\phi) \qquad (2\text{-}3b)$$

and by substituting this in equations (2-3a), we obtain the flux as a function of θ and ϕ :

$$F(r,\theta,\phi) = \sum_{\ell=0}^{\infty} \sum_{m=-\ell}^{m=\ell} F_{\ell m}(r) \sum_{n=-\ell}^{n=\ell} R_{nm}^{(\ell)}(\alpha,\beta,\gamma) \; Y_{\ell n}(\theta,\phi) \qquad (2\text{-}4)$$

$Y_{\ell n}(\theta,\phi)$ are as defined by Jackson (1975) (*cf.* Simmons 1982), viz:

$$Y_{\ell n}(\theta,\phi) = \alpha(\ell,n) \; P_{\ell}^{n}(\cos\theta) \; \exp(in\phi) \qquad (2\text{-}5)$$

with $\alpha(\ell, n) = \sqrt{\dfrac{(2\ell+1)}{4\pi}\dfrac{(\ell-n)!}{(\ell+n)!}}$

and

$$P_\ell^n(x) = (-1)^n (1-x^2)^{n/2} \frac{d^n}{dx^n} P_\ell(x)$$

where the $P_\ell(x)$ are Legendre polynomials,

$$R_{nm}^{(\ell)}(\alpha,\beta,\gamma) = \exp(-i\, n\, \alpha)\; r_{nm}^{(\ell)}(\beta)\;\exp(-i\, m\, \gamma) \qquad (2\text{-}6)$$

and $r_{nm}^{(\ell)}(\beta)$ are defined by Wigner formula :

$$r_{nm}^{(\ell)}(\beta) = \sum_t (-1)^t \sqrt{\frac{(\ell+n)!\;(i-n)!\;(\ell+m)!\;(\ell-m)!}{(\ell+n-t)!\;(\ell-m-t)!\;t!\;(t-n+m)!}}$$

$$\times\;[\cos(\tfrac{1}{2}\beta)]^{2\ell+n-m-2t}\;[\sin(\tfrac{1}{2}\beta)]^{2t-n+m} \qquad (2\text{-}7)$$

In Eq. (2-7) the summation extends over all integer values of t for which the factorials have meaning ,i.e. for which the arguments of the factorials are positive or zero . The number of terms in this sum is $1+\eta$, where η is the smallest of the four numbers $\ell\pm n$ and $\ell\pm m$ (*cf.* Messiah, 1962).

We note that in expression (2-2), the scattering function factors can be expressed as :

$$1+\cos^2\theta = \frac{4}{3}\left[\sqrt{4\pi}\; Y_{00}^* + \sqrt{\frac{\pi}{5}}\; Y_{20}^*(\theta,\phi)\right] \qquad (2\text{-}8)$$

and ,

$$\sin^2\theta\;\exp(-2i\phi) = 4\sqrt{\frac{2\pi}{15}}\; Y_{22}^*(\theta,\phi) \qquad (2\text{-}9)$$

so that, on substitution in the integrals contained in Eq. (2-1), together with the other expressions above,

and using the properties of spherical harmonics, F_{sc} and Z^* can be written as:

$$F_{sc} = \frac{\sigma}{4\pi D^2}\left[\sqrt{4\pi}\; R_{00}^{(0)}(\alpha,\beta,\gamma)\; \Gamma_{00}\right.$$

$$\left. + \sqrt{\frac{\pi}{5}}\sum_{m=-2}^{m=2} R_{0m}^{(2)}(\alpha,\beta,\gamma)\; \Gamma_{2m}\right] \qquad (2\text{-}10)$$

and

$$Z^* = \frac{3}{4\pi}\frac{\sigma}{D^2}\sqrt{\frac{2\pi}{15}}\sum_{m=-2}^{m=2} R_{2m}^{(2)}(\alpha,\beta,\gamma)\; \Gamma_{2m} \qquad (2\text{-}11)$$

where ,

$$\Gamma_{\ell m} = \int_0^\infty n(r)\; F_{\ell m}(r)\; r^2\; dr \qquad (2\text{-}12a)$$

with

$$F_{\ell m}(r) = \int_0^\pi \int_0^{2\pi} F(r,\theta,\Phi)\; Y_{\ell m}^*(\theta,\Phi)\; dr\; d\Phi\; \sin\theta\; d\theta \qquad (2\text{-}12b)$$

The above expressions are exact and allow calculation of the scattered flux and Stokes parameters for any $F(r,\theta,\phi)$. That is due to the orthogonality of the spherical harmonics of $F(r,\theta,\phi)$ with those of the scattering function (in Eqs, (2-8) and (2-9)), so all harmonics of the order ℓ or $|m|$ higher than 2, are zero for the case of Thomson and Rayleigh scattering. It is at once clear that Q and U will reduce to zero, and that F_{sc} will only depend on the Γ_{00} term in Eq. (2-11), if the star radiates isotropically while, in general, the degree and direction of polarization will depend on the properties of the coefficients $\Gamma_{\ell m}$ describing the

stellar anisotropy . These expressions are exact, hence the conclusions concerning a particular star's flux can easily and justifiably be generalized to any arbitrary flux distribution function (e.g. non-spherical star due to rotation, pulsation, magnetic effects or an X-ray companion, star spots or any other anisotropic flux) . To illustrate this we now consider a specific case.

§2.3. ELLIPSOIDAL BLACK BODY STAR :

Assuming the case of a black body star of uniform surface temperature, the surface intensity is isotropic, and seen from a distant point, $F(r,\theta,\Phi)$ can be expressed in terms of the projected area $A_P(\theta,\Phi)$ of the star as viewed from the scattering element direction (θ,Φ). Hence:

$$F(r,\theta,\Phi) \simeq I_\ast \, \Delta\Omega = \frac{I_\ast \, A_P(\theta,\Phi)}{r^2} \qquad (2-13)$$

where $I_\ast$ is the isotropic intensity of the stellar surface and $\Delta\Omega$ is the solid angle subtended by the scattering element. For an ellipsoidal star with axes (a,b,c) along (X,Y,Z) (see Fig. 2-2), A_P is given by :

$$A_P = \pi \left| \sqrt{(b \, c \, \lambda)^2 + (a \, c \, \mu)^2 + (a \, b \, \nu)^2} \right| \qquad (2-14)$$

where $(\lambda,\mu,\nu) = (\cos\Phi \sin\theta , \sin\Phi \sin\theta , \cos\theta)$ are the (X,Y,Z) direction cosines of the direction (θ,Φ).

Inserting Eqs. (2-13,2-14) in Eq. (2-12), we

obtain :

$$\Gamma_{\ell m} = I_* \, N \, f_{\ell m} \qquad\qquad (2\text{-}15)$$

where

$$N = \int_0^\infty n(r) \; dr \qquad\qquad (2\text{-}16)$$

and

$$f_{\ell m} = \int_0^\pi \int_0^{2\pi} A_P(\Theta,\Phi) \; Y_{\ell m}^*(\Theta,\Phi) \; d\Phi \, \sin\Theta \; d\Theta \qquad (2\text{-}17)$$

Note that $f_{\ell m}$ are now functions of the star's shape and size only (i.e. of a,b,and c). From the numerical integrations expressed by equation (2-17) we get : $f_{2,-1} = f_{21} = 0$, and the imaginary parts of f_{22} and $f_{2,-2}$ are zero also , giving $f_{22} = f_{2,-2}$. The terms $f_{\ell m}$ are obviously real for $\ell = m = 0$ but are also real for $\ell = 2$ and $m = \pm 2, 0$, and their values are of consequence to the problem. Note that the $f_{\ell m}$ describing the stellar anisotropy play the same role as the shape factor (γ) of Brown & McLean (1977) – the latter is related to the oblateness or prolateness of the envelope, where the former is related to the stellar shape (oblateness or prolateness).

From the properties of Euler angles, we can choose α as zero, β as the inclination (i_s) of the OZ-axis (the rotation axis of the star) to the line of sight (Oz-axis), and γ as the azimuth of the OZ-axis from the Ox-axis measured about the Oz-axis, which we denote as
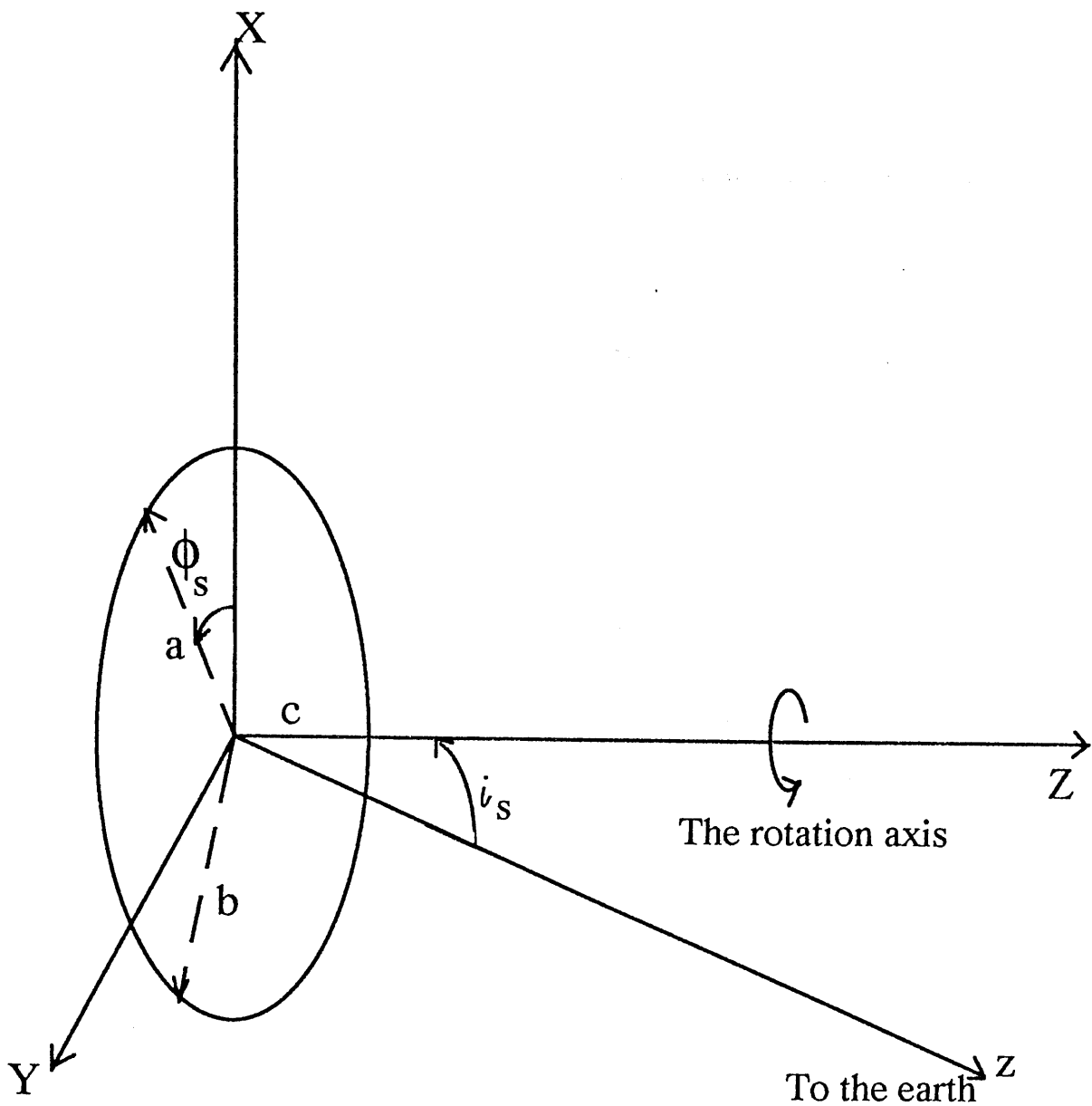
Fig. 2-2. The ellipsoidal star coordinate system, where the c-axis is along the Z-axis (the rotation axis).

ϕ_s. Thus ϕ_s measures the rotational position of the star relative to the observer (see Fig. 2-2). So the un-normalized Stokes parameters and scattered flux will be given by :

$$F_{sc} = \frac{\tau \ I_*}{4 \ \pi \ D^2} \left[\sqrt{4 \ \pi} \ f_{00} + \sqrt{\frac{\pi}{5}} \left\{ \sqrt{\frac{3}{2}} \ f_{22} \ \sin^2 i_s \ \cos 2\phi_s + \frac{1}{2} \ f_{20} \ (3 \ \cos^2 i_s - 1) \right\} \right] \qquad (2-18)$$

$$Z^* = \frac{3 \ \tau \ I_*}{4\pi \ D^2} \ \sqrt{\frac{2 \ \pi}{15}} \left[\frac{1}{2} f_{22} \left\{ (1+\cos^2 i_s) \ \cos 2\phi_s - 2i \ \cos i_s \ \sin 2\phi_s \right\} + \sqrt{\frac{3}{8}} \ f_{20} \ \sin^2 i_s \right] \qquad (2-19)$$

where, $R_{00}^{(0)}(\alpha,\beta,\gamma) = 1$ \qquad (2-20)

and τ is the envelope optical depth, equal to $\sigma \ N$ (Simmons 1982).

For most practical applications (also in the observational situation), one is interested in the normalized scattered flux and Stokes parameters defined by $[F_{sc}, Q, U]/F_{tot}$, where the total flux received F_{tot} comprises the combination of the scattered flux F_{sc} plus the direct flux from the star F_{dir}. This direct flux component is given by $I_* A_p(i_s, \phi_s)/D^2$, where A_p here is the projected area of the star seen from the Earth for $\theta = i_s$ and $\phi = \phi_s$. So we can write the normalization factor F_{norm} as :

$$F_{norm} = (I_*/D^2) \left[A_P(i_s, \phi_s) + (D^2/I_*) F_{sc} \right] \qquad (2\text{-}21)$$

Because f_{00}, f_{20}, and f_{22} are purely functions of a,b and c (i.e the star size, some of their values are presented in Appendix C), we have the normalized Stokes parameters and normalized scattered flux (henceforth called q, u and F_{scn}, respectively) as functions of ϕ_s, i_s, τ, a, b and c (for Rayleigh scattering τ will be a function of k^4).

We can write from eqs. (2-18), (2-19) and (2-21) the expression for normalized scattered flux as :

$$F_{scn} = \frac{\tau \sqrt{\pi}}{4\pi \, F_{norm}} \left\{ 2 f_{00} + \sqrt{\frac{1}{5}} \left[\sqrt{\frac{3}{2}} f_{22} \sin^2 i_s \cos 2\phi_s + \frac{1}{2} f_{20} (3 \cos^2 i_s - 1) \right] \right\} \qquad (2\text{-}22)$$

The normalized Stokes parameters can be written as :

$$q = \frac{3 \tau}{4\pi \, F_{norm}} \sqrt{\frac{2 \pi}{15}} \left\{ \frac{1}{2} f_{22} (1 + \cos^2 i_s) \cos 2\phi_s + \sqrt{\frac{3}{8}} f_{20} \sin^2 i_s \right\} \qquad (2\text{-}23)$$

and,

$$u = \frac{3 \tau}{4\pi \, F_{norm}} \sqrt{\frac{2 \pi}{15}} \, f_{22} \cos i_s \, \sin 2\phi_s \qquad (2\text{-}24)$$

from which the degree of polarization $p = \sqrt{q^2 + u^2}$ and the polarization direction, given by $\phi_P = \frac{1}{2} \tan^{-1}(u/q)$, can be determined.

It is clear from Eqs. (2-23) and (2-24), that the degree of the polarization p will depend on $\sin^2 i_s$, but with more complicated form (mainly due to the variation of the direct flux with the inclination) than that shown in Eq. 1-2. The latter equation was derived by Brown and McLean (1977) for a general isotropic point source within a nonspherical extended atmosphere. The current work proves that even when the star is considered as an anisotropic light source, the polarization equation is still found to be of a similar form.

Application of this general anisotropic source model, also generalizes the work of Gnedin et. al. (1976), which was a two dimensional model for ellipsoidal effects in close X-ray binaries.

§2.3.1. ANALYTICAL EXPRESSIONS FOR THE SPECIAL CASE $_{a=b}$

For the special case of a=b, we can calculate f_{00}, f_{20}, and f_{22} from Eq. (2-17) as :

$$f_{00} = \frac{\pi^{3/2} c^2 a}{\sqrt{c^2 - a^2}} \{ x \cos(\sin^{-1} x) + \sin^{-1} x \} \qquad (2-25a)$$

$$f_{20} = \sqrt{\frac{5}{\pi}} \; \sqrt{\frac{\pi^2 \quad c^2 \; a}{c^2 - a^2}} \; \left\{ \frac{3}{x^2} \left(\frac{-1}{32} \sin 4(\sin^{-1} x) + \frac{1}{8} \sin^{-1} x \right) \right.$$

$$\left. - \frac{1}{2} x \cos(\sin^{-1} x) - \frac{1}{2} \sin^{-1} x \right\}$$

$$(2\text{-}25b)$$

and,

$$f_{22} = 0 \hspace{4cm} (2\text{-}25c)$$

where,

$$x = \sqrt{1 - a^2/c^2} \hspace{3cm} (2\text{-}25d)$$

f_{22} reduced to zero, because when a=b, Ap will be independent of ϕ (i.e. symmetric about the equator). So the integration over ϕ will be zero, which is expected for such symmetric star to have a polarization p only in one direction (here q), therefore the polarization p will be in one direction (here q) which depends only on f_{20}, with zero u.

§2.4. CALCULATION OF POLARIZATION AND THE SCATTERED FLUX

Using the expressions (2-21 to 2-24) from the previous section, and by solving the integrals numerically, the polarization can be calculated for an ellipsoidal star, for either Thomson or Rayleigh scattering (depending on which value of the optical depth τ we use, noting that for Rayleigh scattering τ

will be a function of k^4). Because we deal with a small optical depth envelope, a working value of $\tau = 0.1$ will be used here for illustration unless otherwise stated.

The un-normalized scattered flux (Fsc) is usually smaller than the direct flux (Fdir), but for small a,b or c, Fdir may decrease very rapidly compared with Fsc, so the common assumption that Fdir>>Fsc (i.e. the normalization factor will be proportional to $A_P(i_s, \phi_s)$ only) is not applicable here when the Stokes parameters are normalized. If the usual approximation (i.e. Fdir>>Fsc) is made here, then the equations will give non-physical values of p and Fscn, since in fact there is no projected area seen by the observer for a disk star viewed edge on.

The projected area A_P is the determining factor in this application of the model, as it affects p, Fscn and Fnorm (which are functions of f_{00}, f_{20} and f_{22}). We expect the maximum polarization to occur for maximum scattered light and for minimum projected stellar area (direct flux) along the line of sight, in the extreme case the normalized scattered flux constituting the total observed flux (Fscn is equal to the unity). For minimum scattered light and projected stellar area, the normalized scattered flux will be unity again, but the polarization will be small due to there being less

scattered (polarized) light. The minimum polarization is expected to be zero on symmetry grounds for directions in which the projected stellar area appears circular.

By considering an ellipsoidal star, the general anisotropic source model can be used in cases such as a single fast rotating star, as an approximation to a Roche ellipsoid in binaries, and non-radially oscillating stars. Though the polarizing effects caused by radiative transfer within a non-spherical photosphere are usually small unless the distortion is very great (Haisch & Cassinelli 1976, and Collins & Buerger 1974), the effect of an anisotropic source with scattering by a surrounding shell can produce high values of polarization as will be shown below.

§2.4.1 OBLATE AND PROLATE STARS :

In Sec 1.3.1. we discussed the effect of fast rotation on stars, and found that the star can take either oblate or prolate shapes, depending on the angular momentum and the strength of the magnetic field. Dynamically stable shapes are possible with c and b shrinking to about 0.1 of a.

From the above analysis, we calculate a maximum polarization of about 20% for a flat disk star viewed

edge on (a=b=1 and c=0 with i_s=90° and ϕ_s=0°), when zero projected stellar area will be observed (no direct light), and only the scattered flux is seen. The value of maximum polarization is the same for any optical depth τ, because the p and F_{scn} dependence on τ disappear, so $F_{norm} \simeq F_{scn}$ (Figs. 2-3 (a and b) and 2-4 (a and b)).

In general the polarization increases with inclination i_s and with optical depth τ (Figs. 2-3 a and b). Note that for Maclaurin spheroids the c-axis of the star will shrink while a=b=1, which means the sizes of a and b-axes increase compared to c-axis. In the case of Jacobi ellipsoids, c-axis will expand as a=b=1, so the sizes of a and b-axes will decrease compared to c-axis. Moreover, for a distortion δr (as a fraction of the spherical radius of the star), the star will give more polarization if δr is subtracted from (e.g.) the c-axis, the star shrinking toward a Maclaurin spheroid, than if δr is added to (e.g.) the c-axis, distorting the star toward a Jacobi ellipsoid, since the former will have more surface area than the latter. This explains why the maximum polarization from Jacobi ellipsoids is much less than that from Maclaurin spheroids, and why in general Maclaurin spheroid light sources (c ranging from 1 to 0, with a=b=1, or a/c=b/c from 1 to ∞) have larger polarization increases as i_s increases than that for

Jacobi ellipsoid sources (c ranging from 1 to 100, or a/c=b/c from 1 to 0.01).

For the normalized scattered flux F_{scn} variation with c (Figs. 2-4 a and b), the strength also increases as for the Maclaurin spheroids above, but is reduced for Jacobi ellipsoids, because F_{scn} is the ratio of F_{sc} to F_{norm}, both of them approaching zero as c approaches infinity, so the ratio F_{scn} will go to unity.

§2.4.2 NON-SPHERICAL LIGHT SOURCE :

A question now arises as to which values describing the geometries above are realistic in terms of real physical situations. An example of an oblate Maclaurin spheroid source is a single fast rotating star. For X-ray binaries the Roche lobe can be approximated to a prolate Jacobi ellipsoid. A study of these two configurations is as follows:

§2.4.2.1 SINGLE STAR :

Rotating stars can undergo considerable distortion. For the most rapidly rotating models of main-sequence stars, the expected distortion (fractional reduction in polar radius) is about 0.01 for stars of about 60 $M_\odot$, and by about 0.15 for stars of 0.6 $M_\odot$ (Solar masses, see
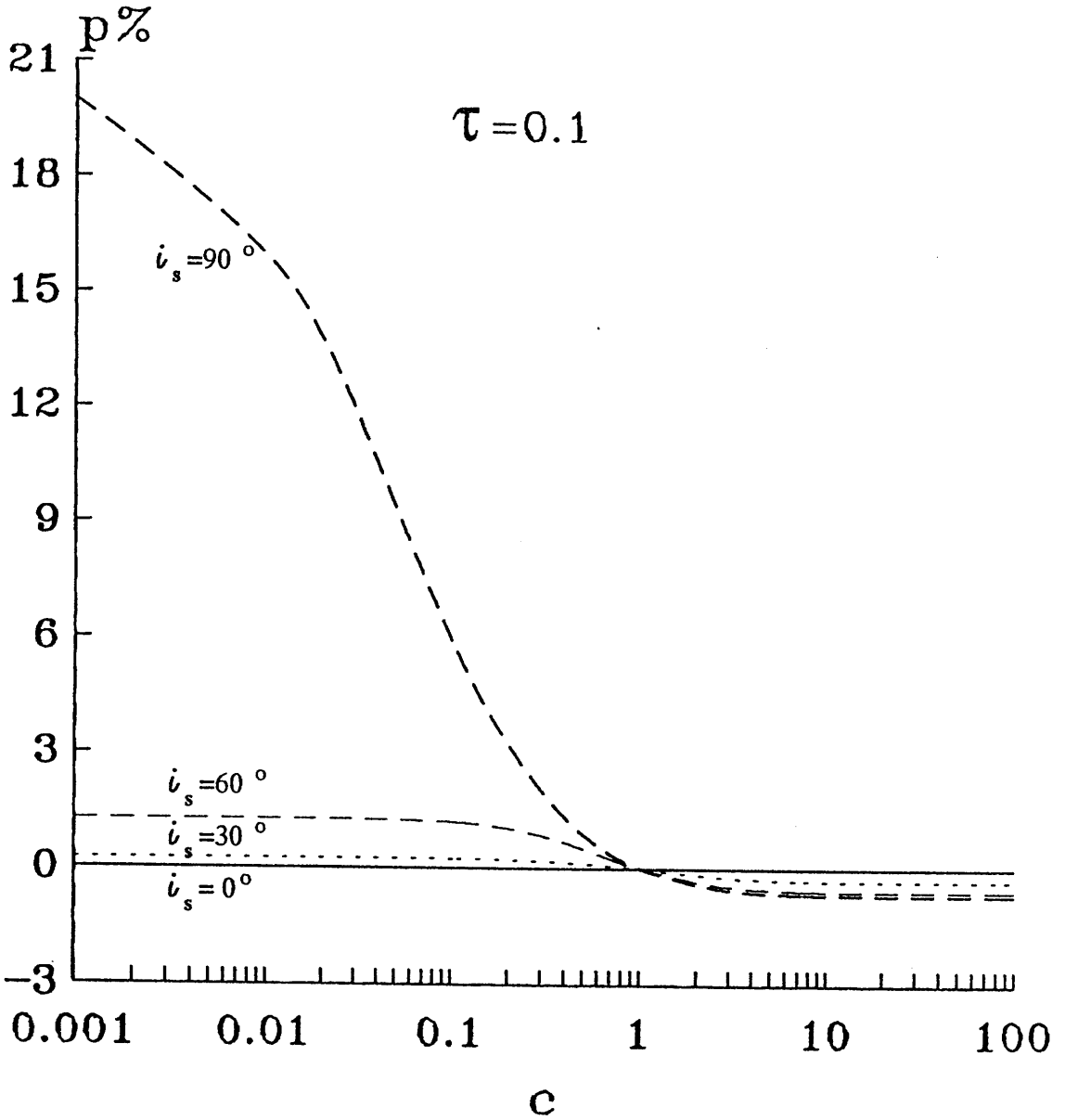
Fig. 2-3a.

Fig. 2-3. The percentage normalized polarization p
for Maclaurin spheroids (oblate shapes, c from zero to
1), and Jacobi ellipsoids (prolate shapes, c from 1 to
100), at a=b=1 and $\phi_s=0^0$ for different inclinations i_s.
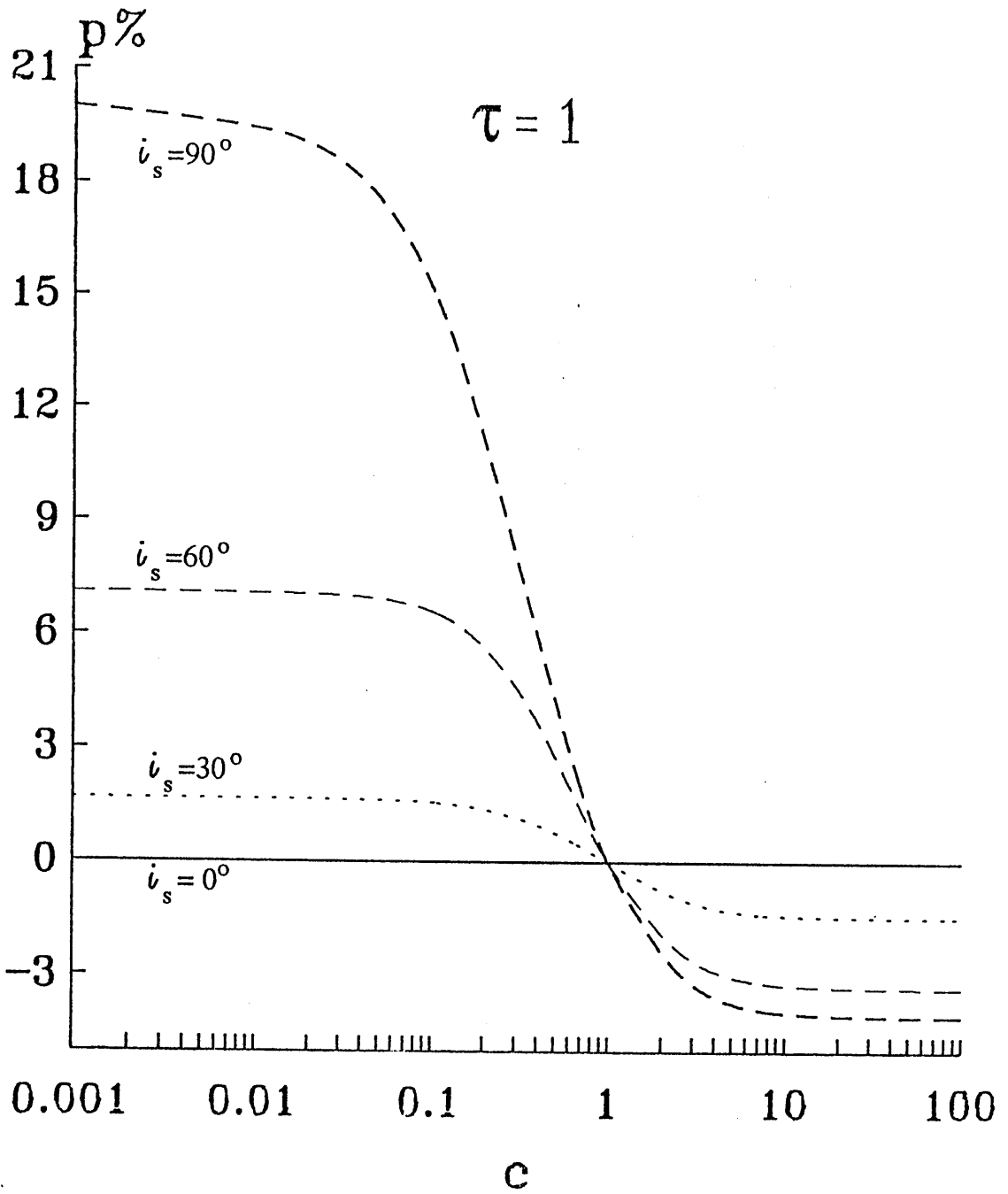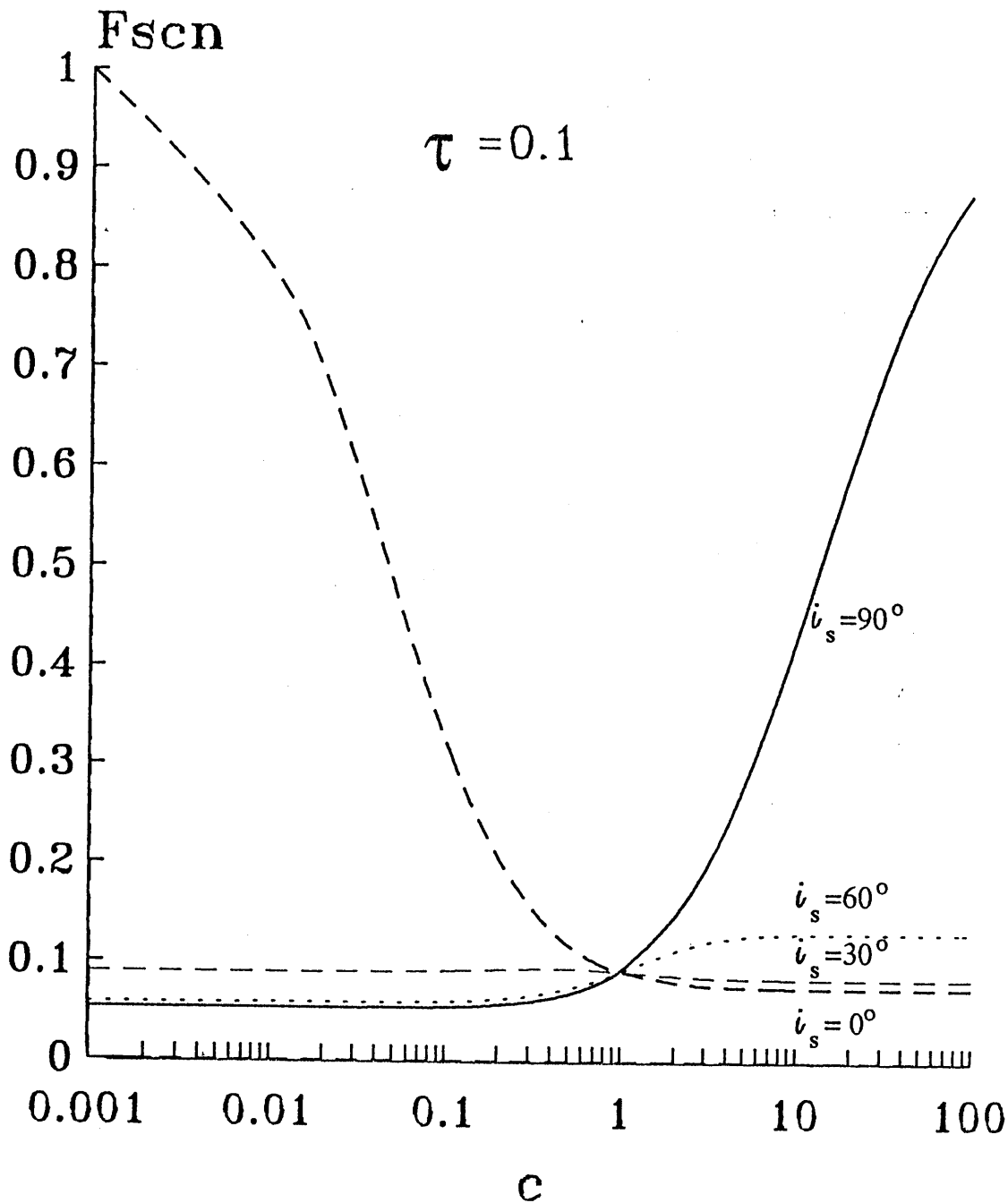a. for $\tau=0.1$. b. for $\tau=1.0$.

Fig. 2-3b.

Fig. 2-4a.

Fig. 2-4. The normalized scattered flux Fscn for Maclaurin spheroids (oblate shapes, c from zero to 1), and Jacobi ellipsoids (prolate shapes, c from 1 to 100), at a=b=1 and $\phi_s=0°$ for different inclinations i_s. a. for $\tau=0.1$. b. for $\tau=1.0$.
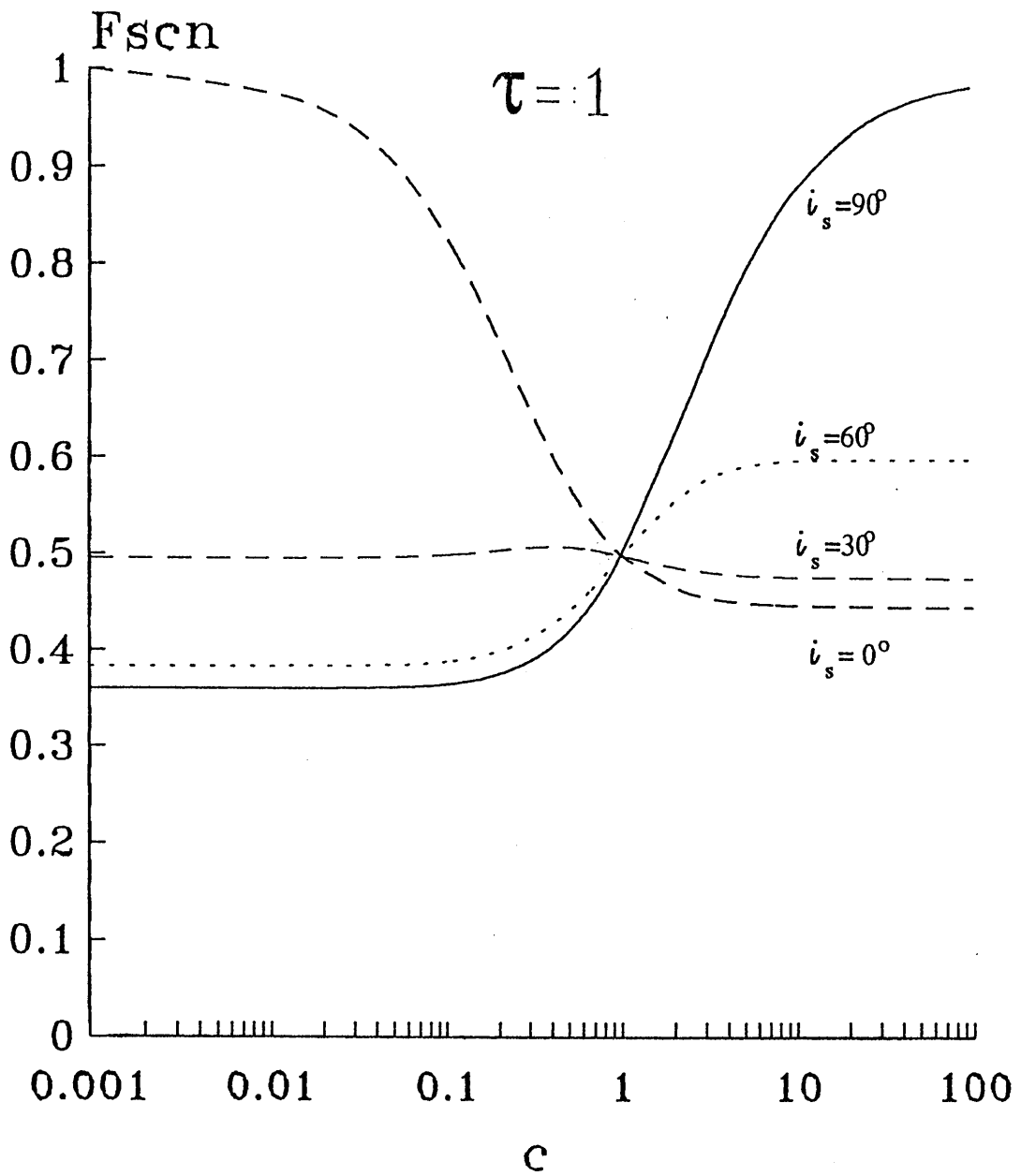
Fig. 2-4b.

Tassoul 1978 and Papaloizou & Whelan 1973). Ostriker and Bodenheimer (1968) modelled rotating white dwarfs, and showed that the ratio of equatorial to polar radius can be up to 4.32, which would produce a polarization p of about 2.6% for a spherical envelope with $\tau=0.1$ (Fig. 2-3a).

As an example, for a star with a=b=1 and c=0.9 (for $\tau=0.1$), the polarization p is expected to be about 0.1% at $i_s=90°$ decreasing to zero at $i_s=0°$, and the normalized scattered flux F_{scn} is about 0.1 of the total flux (see Figs. 2-3a and 2-4a).

The variations of the polarization p and the scattered flux F_{scn} with rotation angle ϕ_s (or with time t) of this star are zero, due to there being no changes in the projected area with rotation angle for different inclinations.

§2.4.2.2 BINARIES :

The shape of a star filling its Roche lobe can be approximated by an ellipsoid (Chandrasekhar 1963, Gnedin et. al. 1976 and Bochkarev et. al. 1979). From the Chandrasekhar (1963) analysis we found that ellipsoidal figures of equilibrium are expected when the major axis becomes about double the size (up to seven

times) of the two minor axes for any binary mass ratio, where before the double sized or after the seven times size, the Roche lobe will be a conical shape(see Tassoul 1978). Furthermore X-ray binaries such as Cygnus X-1 and Centaurus X-3 have only a single optical component.

As an example of such binaries, for a binary with b=2 (as major axis) and a=c=1 (as minor axes), we expect the maximum polarization p of 0.45% (Figs. 2-5). The variation of q and u with the stellar rotation is (as expected) a circle for $i_s=0°$, but becomes more elliptical for larger i_s's, and eventually linear at $i_s=90°$ (Figs. 2-5). The locus is described here twice in one rotational period, due to the symmetry in the shape variation. For the normalized scattered flux F_{scn} , the value is constant at about 0.08 for $i_s=0°$. As i_s increases, the level of F_{scn} grows and develops an oscillation with orbital phase, achieving a peak value of 0.15 at $i_s=90°$ and $\phi_s=90°$ or $\phi_s=270°$.

§2.4.3 NON-RADIALLY OSCILLATING STARS :

A non-radially oscillating star can be approximated as distorting through a time series of ellipsoidal shapes as the star axes (a,b and c) vary from unity. Such possible orthogonality in the oscillations was mentioned by (e.g) Serkowski (1970) in relation to his

74

observation of two RV Tau stars. These stars show a change in the brightness of about 5 magnitudes, which may be due to large oscillation in the shape and projected area of the star. Such variations will affect the scattered flux F_{scn} as well as the direct flux F_{dir}, and result in an interesting variation in the polarization, both in value and direction. Many variable stars have this kind of oscillation (e.g. Omicron Ceti, W Vir and RR Lyrae). The distortion from sphericity may be up to 90% (i.e. c/a or b/a =0.1, see Sect. 4.1). Many assumptions are involved in the calculation and the observation of these values, but assumption of at least 20% distortion will be quite acceptable here in order to discuss the polarimetric characteristics of such stars for oscillations in one, two or three axes of the star (This was recently proved for one axis by the observation of Karovska *et al.* 1992 for Omicron Ceti, see Sec. 1.4).

The Total flux is (as defined above in Sec. 2.3) a combination of the scattered flux and the direct flux F_{dir}, but the latter will be unity for isotropic stars. So we can define the added flux as the flux due to anisotropy only (neglecting the isotropic part) and to the scattering flux, or :

$$F_{add} = F_{tot}/F_{norm} - 1 \qquad\qquad (2-26)$$

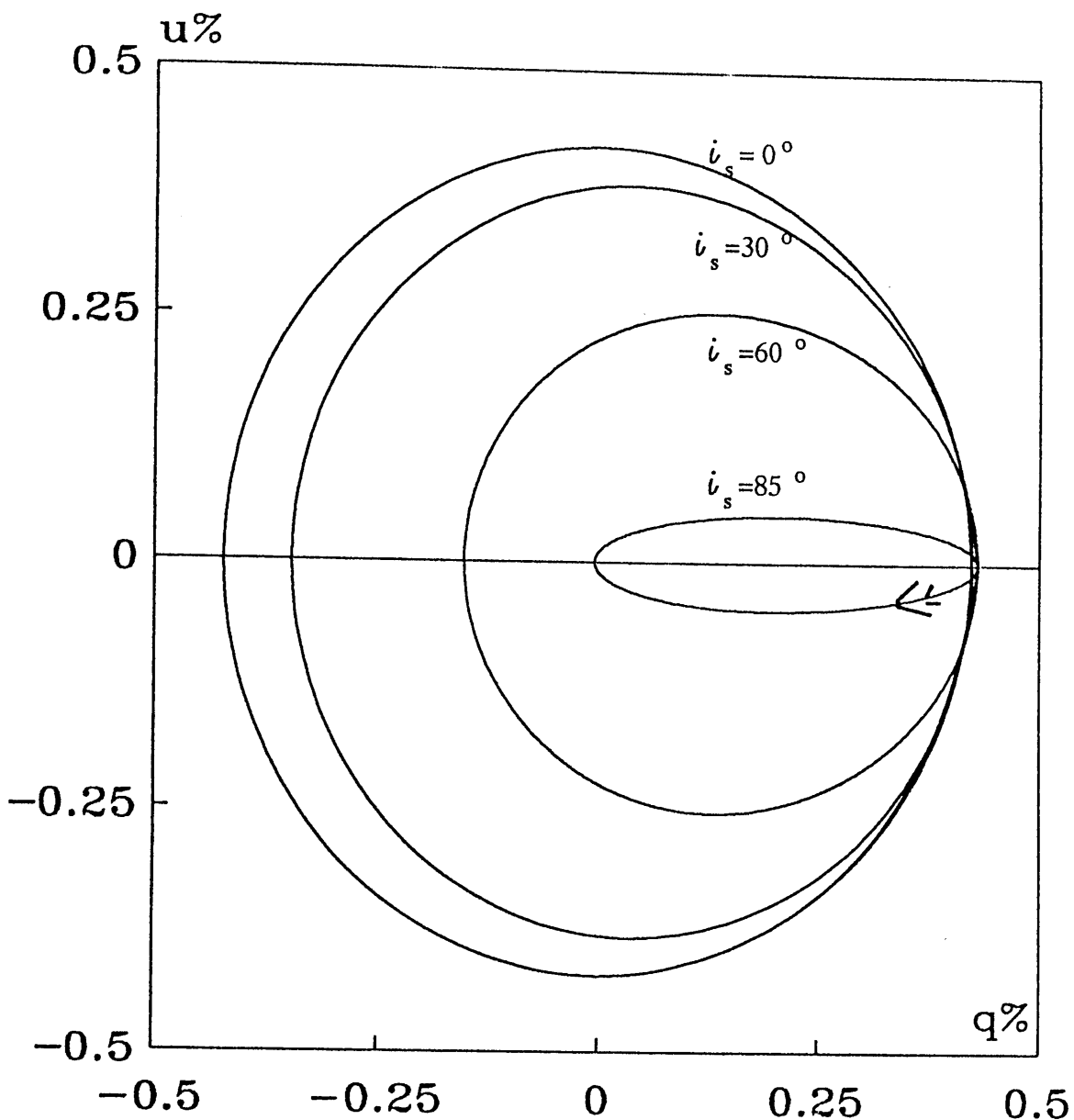which give an indication about the light variation in some of the following Figures.

Fig. 2-5. The plot of qu-plane for a rotating binary of b=2, a=c=1. for i_s=0°,30°, 60° , and 85°.

§2.4.3.1 Stellar Oscillation in one axis only:

Before presenting any results, we note that the spherical harmonic ℓ values used in our polarimetric modeling have no direct relation to the $\ell=2$ values of the second harmonic oscillation theory.

Consider a non-rotating star oscillating in b with time t in the form:

$$b = 1 + \delta \cos(\omega t + \Delta) \qquad\qquad (2\text{-}27)$$

where δ is the fractional distortion amplitude from spherical , $\omega = 2\pi/\Pi_p$ where Π_p is the pulsation period, and Δ the phase, but with constant a and c. So for a distortion (full amplitude) of order 0.2 (i.e $\delta=0.1$) in the b-axis with a=c=1, and $\Delta=0$, the maximum absolute polarization p will be about 0.1% and F_{scn} about 0.9. Fig. 2-6 shows p and F_{scn} variation for this kind of pulsation with time (t/Π_p), when the star at $\phi_s=0°$ or π (the star is non-rotating so ϕ_s remains fixed). There is no inclination dependence here since the pulsations are along the b-axis and a=c=1, so the projected area (for $\phi_s=0°$ or π) will be the same for any i_s .The polarization angle switches through $90°$ each time p passes through zero, i.e. as the star goes from oblate to prolate.

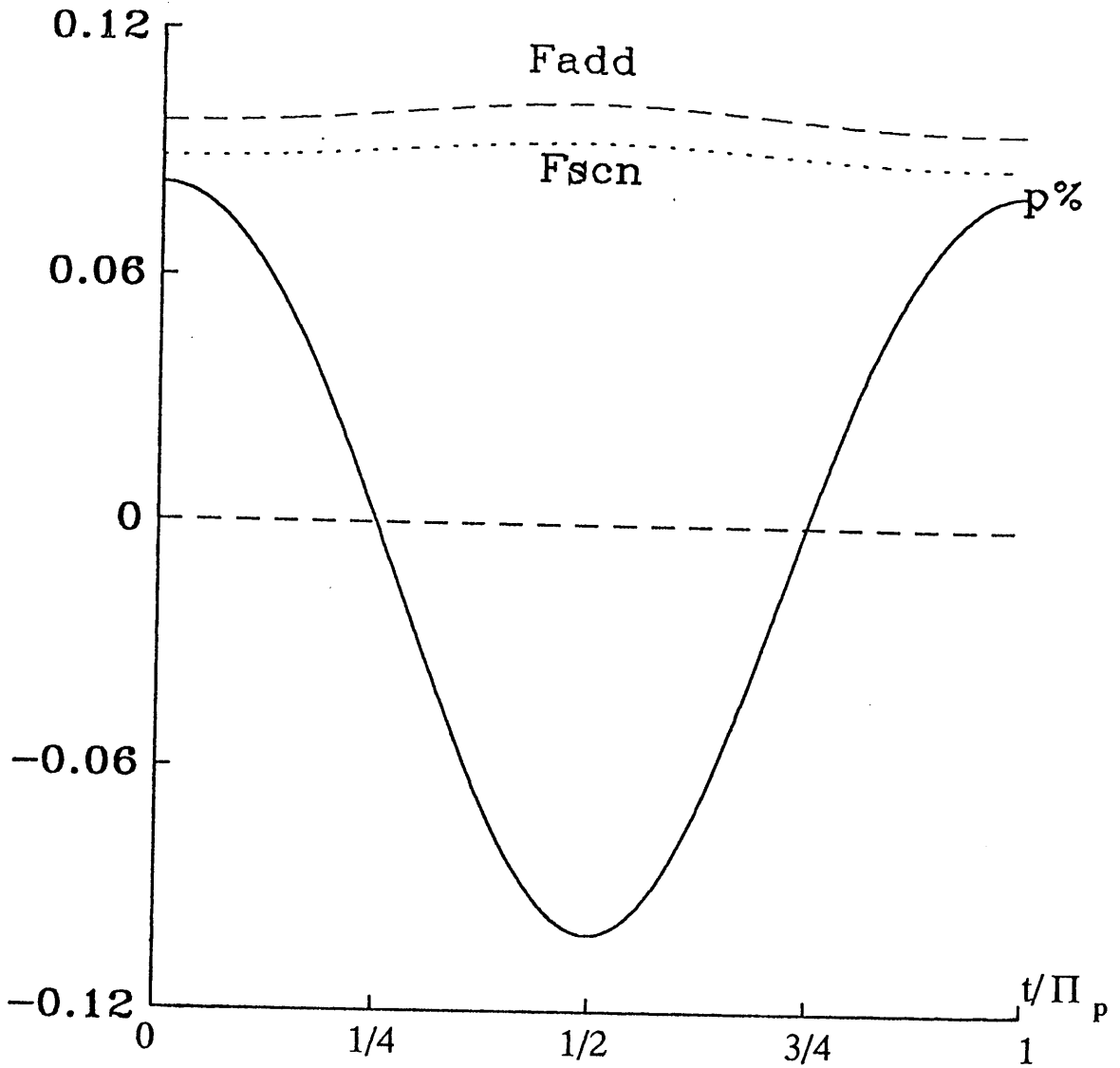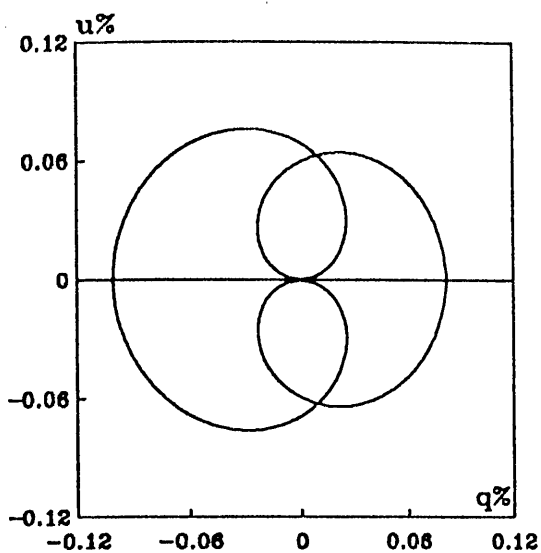Evidently the form of the variations of the Stokes'

Fig. 2-6. The plot of p and Fscn with the time as t/Π_P, for a non-rotating star, having an oscillation in the b-axis once per pulsation period Π_P, with δ=0.1 and Δ=0. See text for discussion.

parameters will depend in this case (when the oscillation in b-axis only) on both the rotation period Π_r and the pulsation period Π_p. There are dynamical reasons to expect these two periods to be related (Becker 1987). We shall deal with three cases :

I - For $\Pi_p=\Pi_r$ (here we have $\omega t=\phi_s$), and again with $\Delta=0$, $\delta=0.1$ with a=c=1, Figs. 2-7 (a,b, and c)plot the changes in the qu-plane as the star rotates, and (d) plot the stellar parameters variation with ϕ_s. Here the loci are described once per rotation period, and are double lobed due to the changing shape of the pulsation during rotation. These lobes shrink in u with increasing i_s . F_{scn} shows small variations, and has values about 0.09.

II - For $\Pi_p=n\Pi_r$, where n is an integer number (e.g. n=2, so $\omega t=2\phi_s$), as expected the loci will be described twice per Π_p due to the symmetry(Figs. 2-8 a,b,c and d). This combined effect of rotation and pulsation may explain the multiple modes observed in some pulsating stars (e.g. β Cep., Becker 1986). The pattern gets more complicated and shrinks as i_s increases. The values of F_{scn} are (as in case I) about 0.09, with small variations.

III - And for $\Pi_p=\nu\Pi_r$, where ν is a rational number
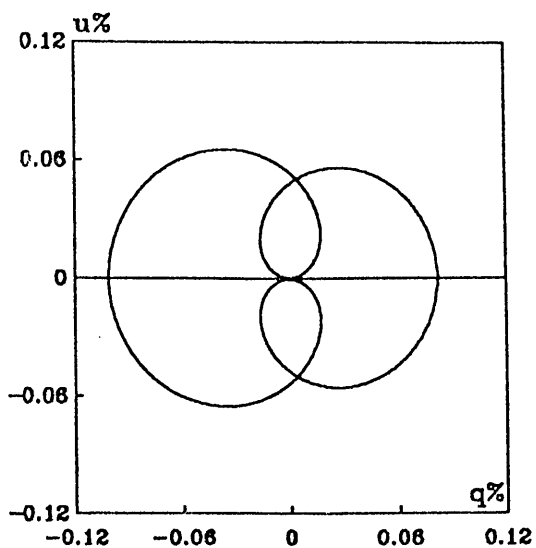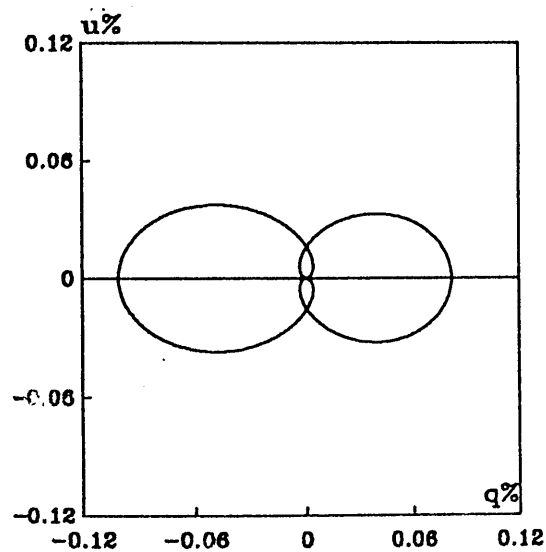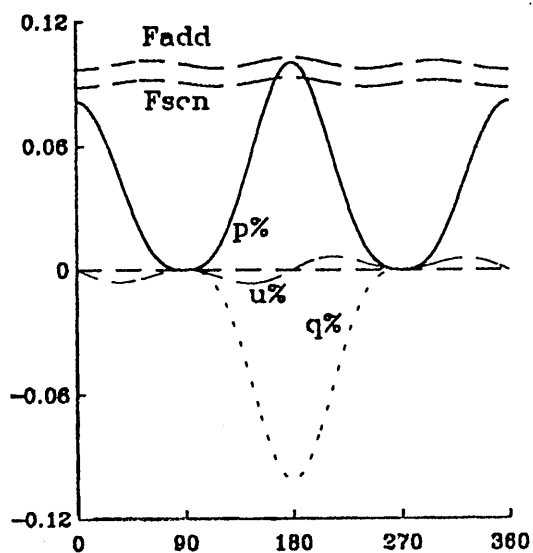
Fig. 2-7 a-d. The qu-plane for a rotating star, with
oscillation in b of δ=0.1, Δ=0 and ωt=φs (i.e. the
pulsation period = the rotation period) a. for i_s=0°, b.
for i_s=30°, c. for i_s=60° and d. for i_s=85°.
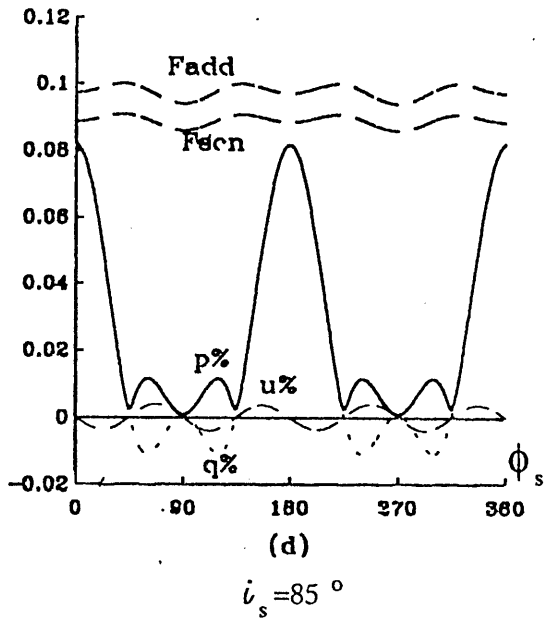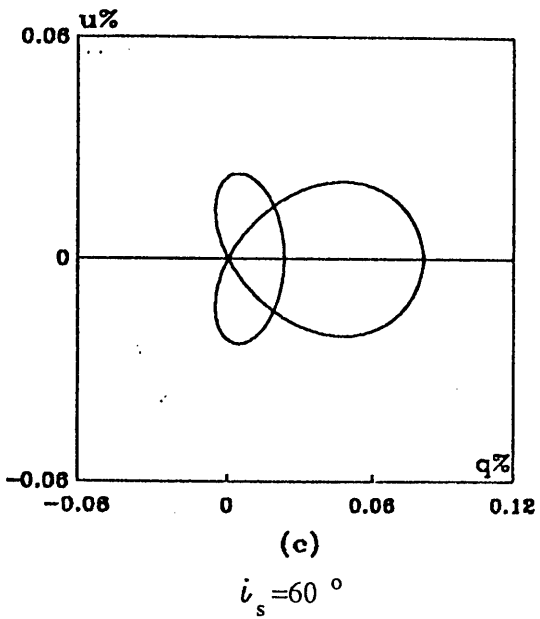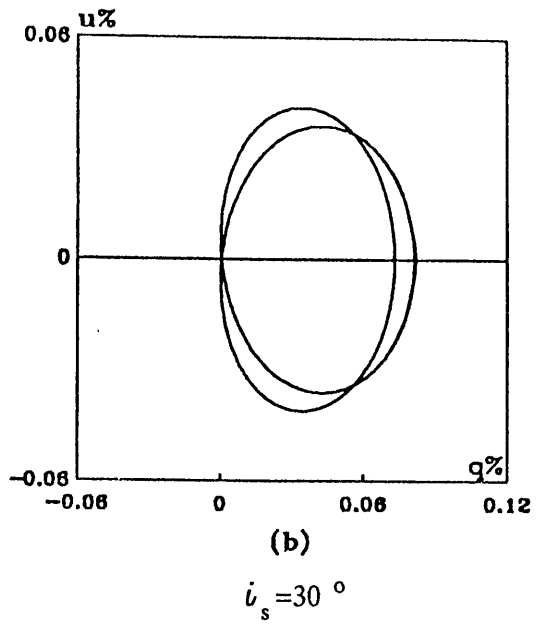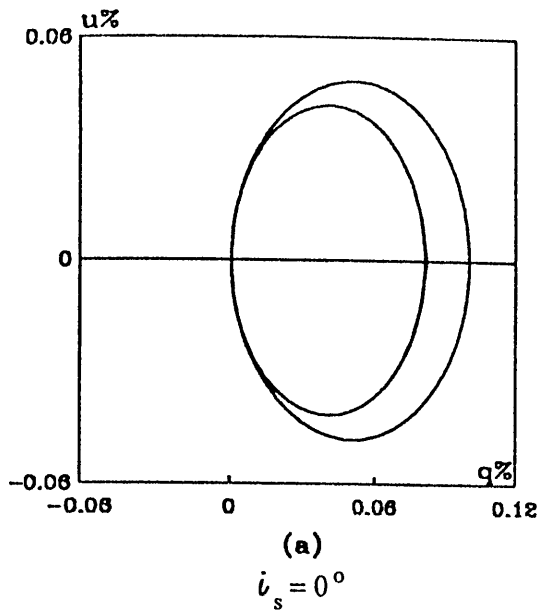
Fig. 2-8 a-d. As in Figs.2-7, but $\omega t=2\phi_s$ (i.e. the pulsation period is double the rotation period). a. for $i_s=0^0$, b. for $i_s=30^0$, c. for $i_s=60^0$ and d. for $i_s=85^0$.
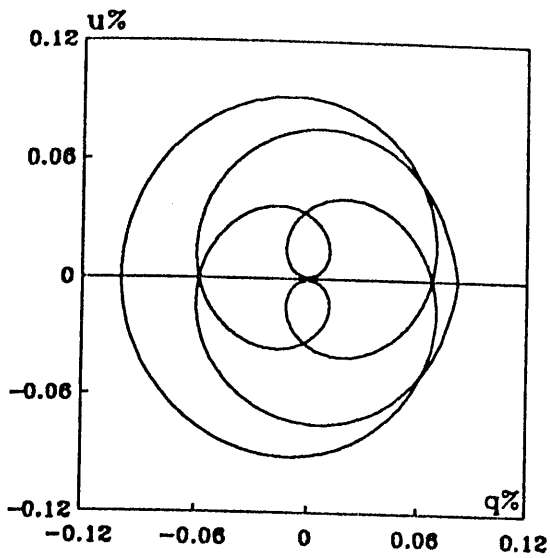
(a)

$i_s = 0°$
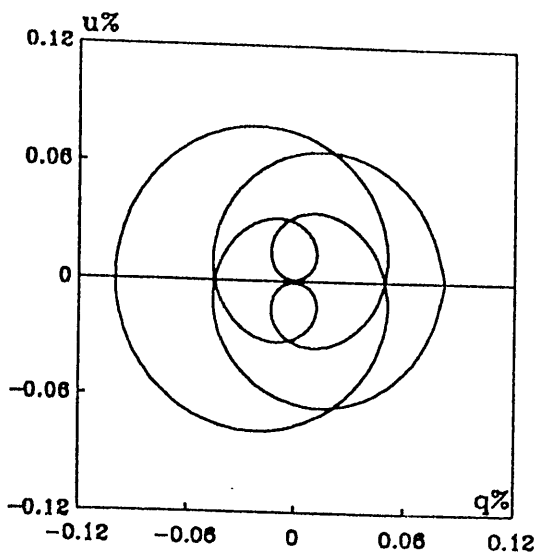
(b)
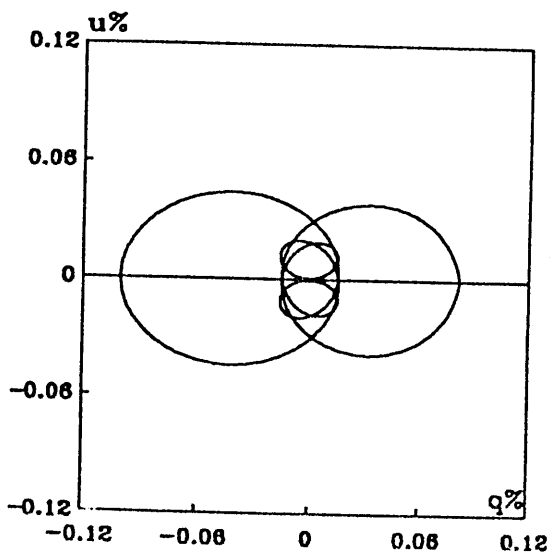
$i_s = 30°$

(c)
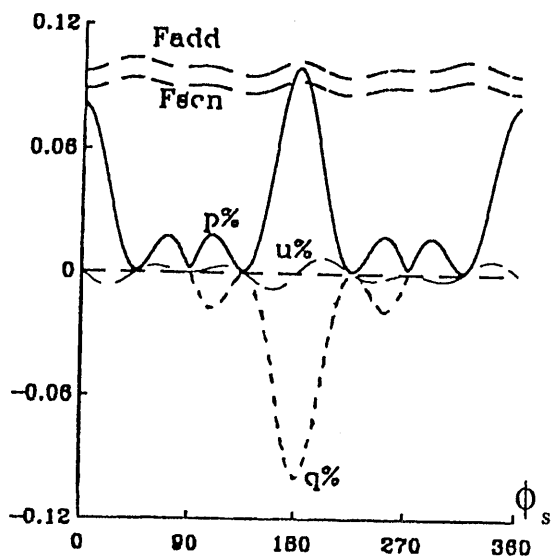
$i_s = 60°$

(d)

$i_s = 85°$

Fig. 2-9 a-d. As in Figs.2-7, but ωt=φs/2 (i.e. the pulsation period is half of the rotation period). a. for $i_s=0°$, b. for $i_s=30°$, c. for $i_s=60°$ and d. for $i_s=85°$.

rather than an integer, one Π_r will not show all the variation occurring in p, q, u and F_{scn}, instead we get 'commensurable' rotation/pulsation periods on which q and u patterns repeat. For example for $\nu=\frac{1}{2}$ (i.e. $\omega t=\phi_s/2$) , then interval $2\Pi_p$ will include a complete cycle of changes. Figs. 2-9 (a,b,c and d) show the qu-loci for $2\Pi_p$, the pattern being more complicated than the last two cases . F_{scn} is as in cases I and II. If ν is an irrational number, then qu-locus will not close -i.e. there will be no commensurability and the observed (q,u) may appear 'chaotic'.

So for observational polarimetric data, lobes in the qu-loci may be explained as stellar oscillations (if there is not any local concentration of scatterers, see Clarke and McGale 1986). If a period analysis method (see e.g. Cuypers 1987) is applied to such polarimetric data, two main periods are expected to occur. The dominating one will be the rotation period, and the other the pulsation one, due to the latter having less effect on polarization than the former.

§2.4.3.2 STELLAR OSCILLATION IN TWO AXES :

The above analysis is easily generalized to pulsations along several axes, as Serkowski suggests for U Mon (Serkowski 1970). If a star oscillates in one of

its (e.g.) equatorial axes, the star will (mostly) react by oscillating in the opposite direction (e.g.) polar axis. Astrophysically the latter distortion is expected to be smaller than the former, due to other forces (e.g. rotational effects). In order to demonstrate the effect on the polarization, consider two cases (1) where the star is pulsating but not rotating and (2) when it is also rotating.

(1) Using Eq. (2-26) for b with $\delta=0.1$, $\Delta=0°$ and $\omega=2\pi/\Pi_P$, and for c with $\delta=0.05$, $\Delta=\pi/2$ and $\omega=4\pi/\Pi_P$ (i.e. the c-axis undergoes two pulsations per Π_P), with a=1, Figs. 2-10 plot p and F_{scn} versus time (t/Π_P), for different i_s and for $\phi_s=0°$. Because pulsation in the c-axis will be in the line of sight at $i_s=0°$, its effect will be very small, so results for $i_s=0°$ (Fig. 2-10a) will be almost the same as for a one axis pulsator (Fig. 2-6). Thus the maximum absolute p is about 0.1% and F_{scn} about 0.09. But as i_s increase the effect of the pulsation in the c-axis gets larger, and the variation of p with time gets more complicated. The maximum p also shows a small increase as i_s increases. This is clearly due to the changes in the projected area. But the variation in F_{scn} is very small, with a value about 0.09.

(2) The effects of rotation for a star of the same

dimensions are shown on the qu-plane in Figs. 2-11 (a,b,c and d). The loci are double lobed with one of the lobes shrinking as i_s increases, because at $i_s=0°$ the pulsation in c-axis direction is on the line of sight which will show no effects on the polarization. As i_s increases, the pulsation in c-axis will produce polarization in the opposite direction of that produced by the b-axis pulsation, which will decrease the polarization in some directions.

§2.4.3.3 STELLAR OSCILLATION IN THREE AXES :

Finally we consider the case of stellar pulsation in three directions. For a-axis pulsation with $\delta=0.05$, $\Delta=\pi/2$ and $\omega=2\pi/\Pi_p$, b-axis pulsation with $\delta=0.1$, $\Delta=0$ and $\omega=2\pi/\Pi_p$ and c-axis pulsation with $\delta=0.08$, $\Delta=\pi/2$ and $\omega=4\pi/\Pi_p$. Fig. (2-12) shows plots of p and F_{scn} against t/Π_p for such a non-rotating star. Figs. (2-13 a,b,c and d) show the qu-plane loci for a rotating star of the above values, but with $\omega t=2\phi_s$ for a and c-axis pulsation and $\omega t=\phi_s$ for b-axis pulsation , are shown in Fig. 2-12 a,b,c and d. In general the Figures get more complicated as the number of oscillating axes increases, and the value of the maximum p increases as well, but by a small factor. Evidently, as the number of parameters describing the variations of the stellar motions increases, so does the complexity of the behavior of p,
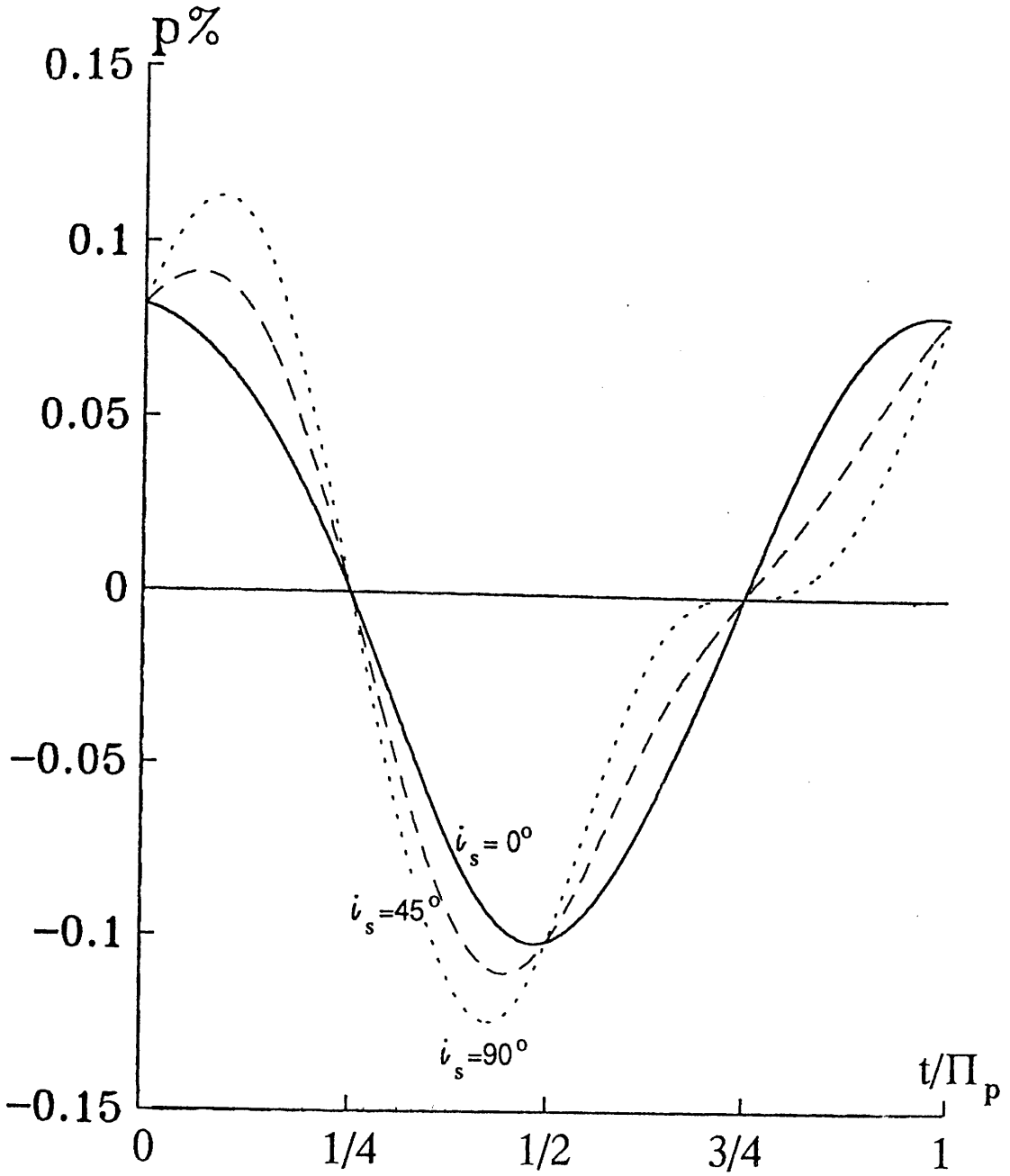
Fig. 2-10. Plot of p% and Fscn with time as t/Π_p for a non-rotating star, having oscillations in two axes, b-axis with $\delta=0.1$, $\Delta=0$ and $\omega=2\pi/\Pi_p$, and c-axis with $\delta=0.05$, $\Delta=\pi/2$ and $\omega=4\pi/\Pi_p$, for $i_s=0^0$, 45^0, and 90^0.
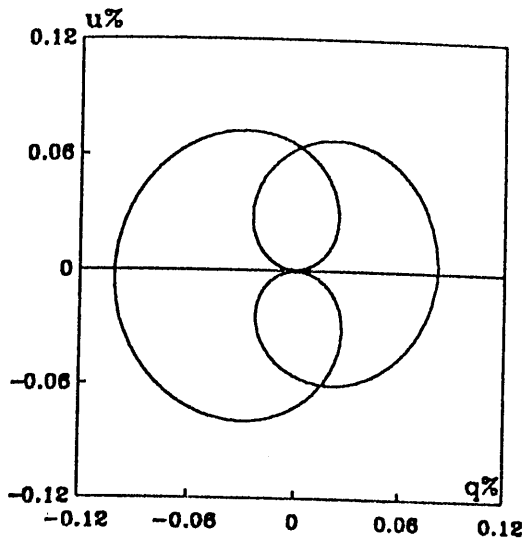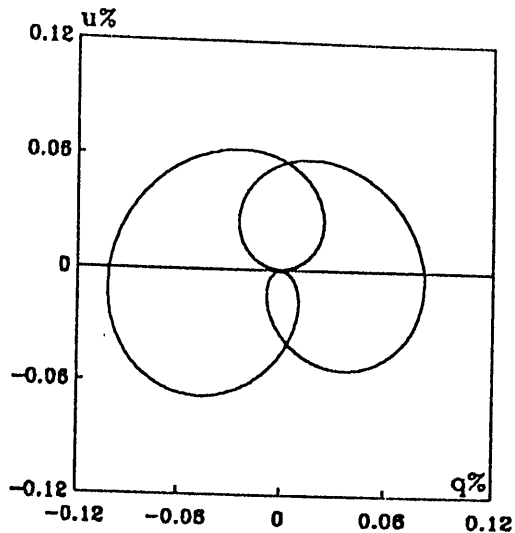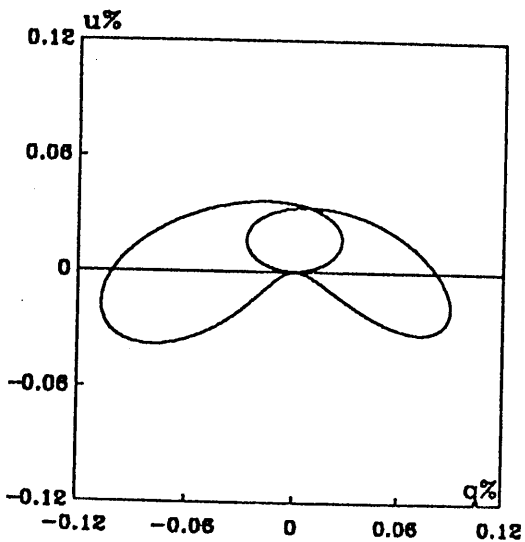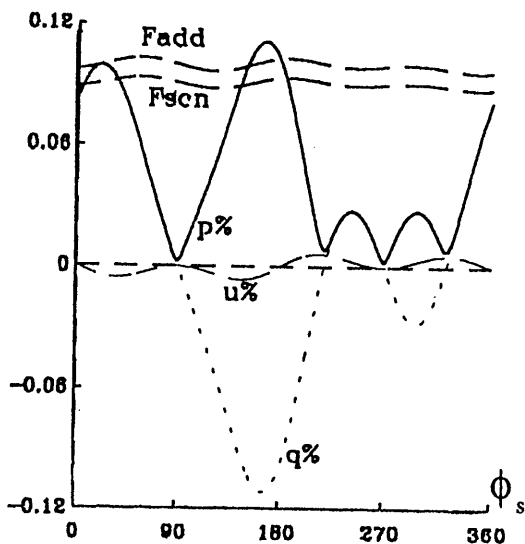
Fig. 2-11 a-d. The qu-loci for a rotating star with the same values as in Figs. 2-10 - see text for the discussion. a. for $i_s=0^0$, b. for $i_s=30^0$, c. for $i_s=60^0$ and d. for $i_s=85^0$.
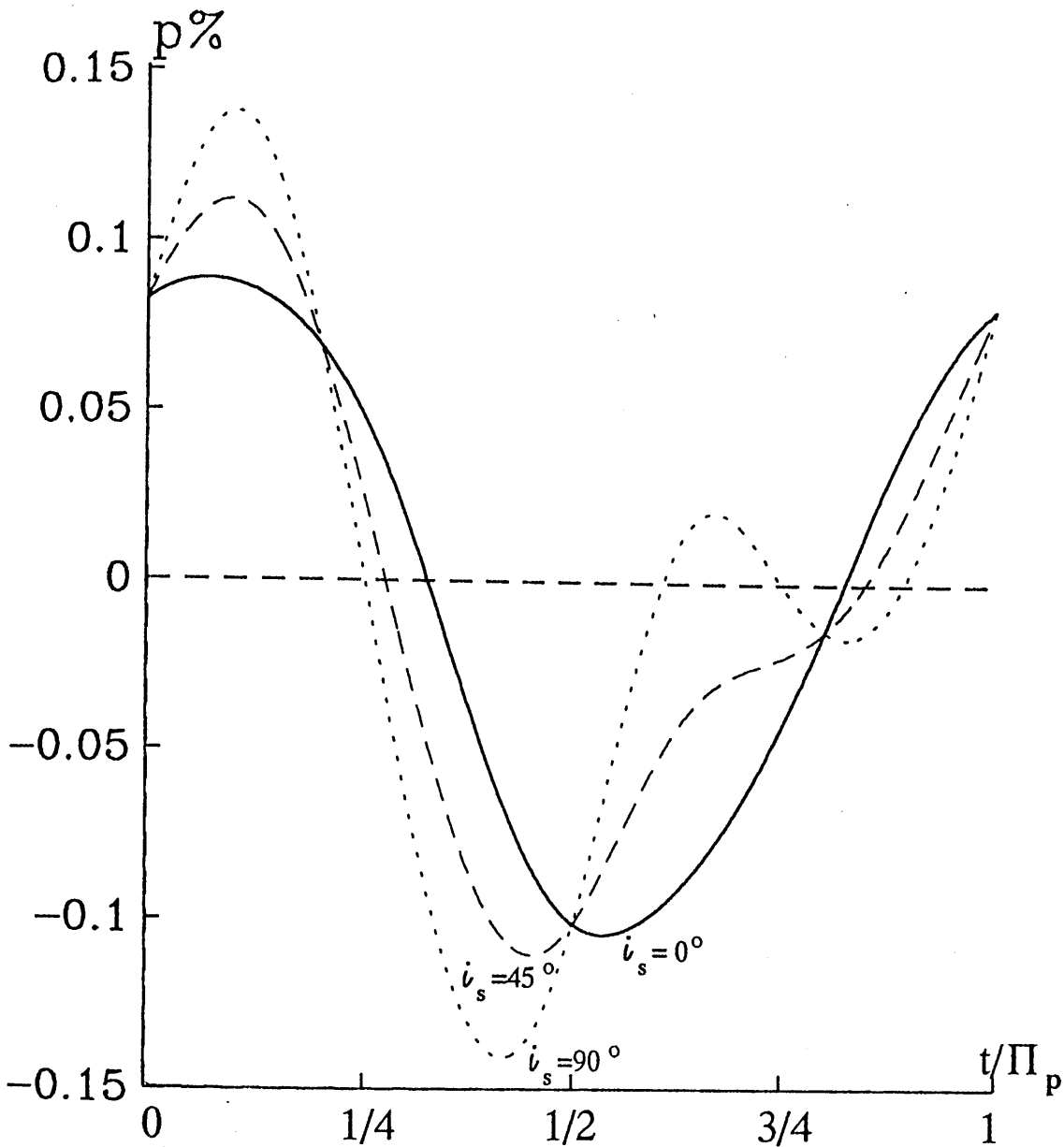
Fig. 2-12. Plot of p% and F_{scn} with time as t/Π_p for a non-rotating star, having oscillations in three axes, a-axis with $\delta=0.05$, $\Delta=\pi/2$ and $\omega=4\pi/\Pi_p$, b-axis with $\delta=0.1$, $\Delta=0$ and $\omega=2\pi/\Pi_p$, and c-axis with $\delta=0.08$, $\Delta=\pi/2$ and $\omega=4\pi/\Pi_p$, for $i_s=0^0$, 45^0, and 90^0.
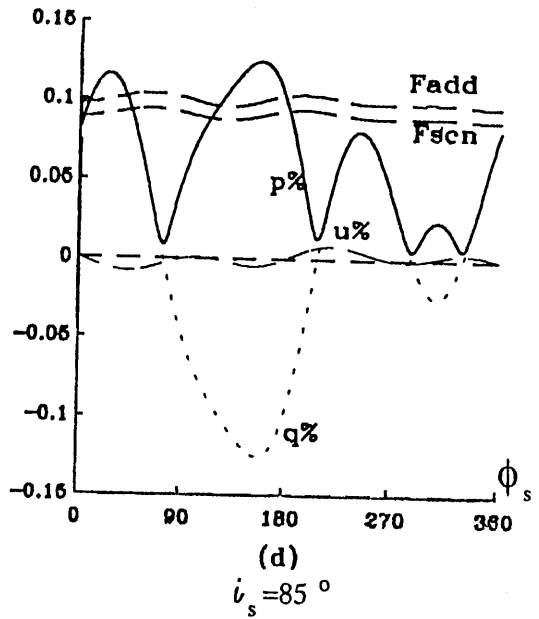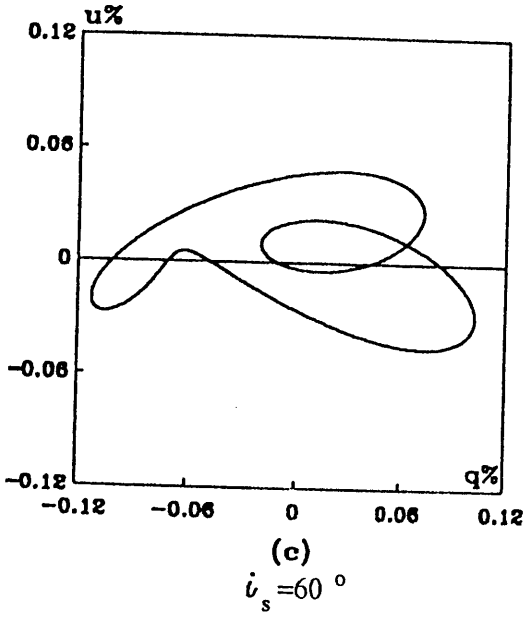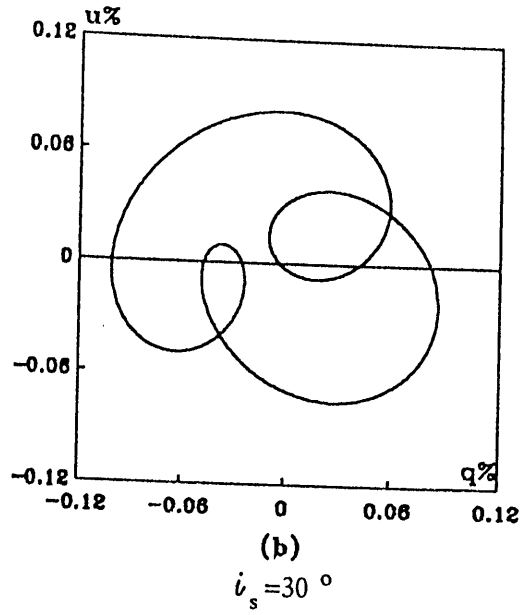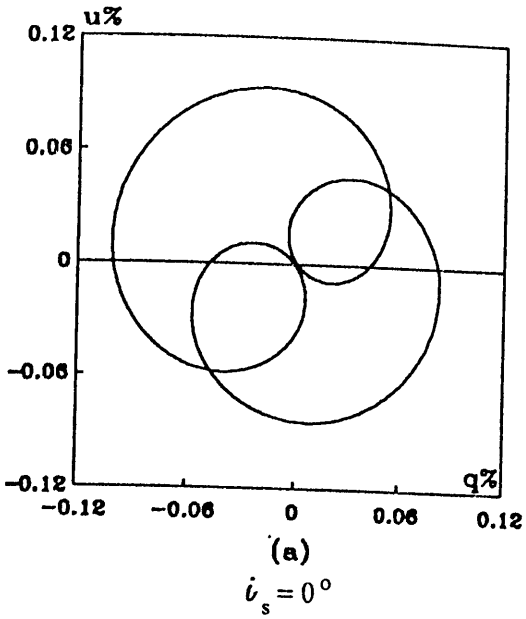
Fig. 2-13 a-d. qu-loci for a rotating star with the same values Figs. 2-12 - see text for the discussions. a. for *i*s=0⁰, b. for *i*s=30⁰, c. for *i*s=60⁰ and d. for *i*s=85⁰.

q, u and F_{scn}.

In general, the shrinking of one of the double lobed of the qu-loci, can be explained by pulsation in more than one stellar axes. More accurate data and more complicated analyses are needed to ascertain whether two or three axes are pulsating, and to calculate the pulsating period for each axis. The rotation period however is expected to dominate in period analysis.

SUMMARY :

Expressions have been developed to describe the flux and polarization of radiation scattered by a spherically symmetric envelope for a central point stellar light source radiating anisotropically. These are obtained in terms of spherical harmonics of the light source anisotropy function. Such anisotropy can arise from stellar spots, or from distortion of the stellar shape by rotation, pulsation, or magnetic effects. In the most extreme case of a flat disk-like star, the net polarization can be as high as 20% when the system is viewed edge on, all of the observed light then being scattered light.

Explicit expressions for the Stokes parameters are obtained for the case of a uniform ellipsoidal stellar

light source, and used to illustrate the dependence of the results on the stellar shape. It is shown that observationally important polarizations can arise in this way by the scattering of light from stars with realistic degrees of distortion, even on spherical envelopes. The time dependence of the polarization is computed for rotating and for pulsating ellipsoidal stars. When both rotation and pulsation occur, complex loci in the (q,u) plane result.

CHAPTER THREE

3. ELLIPSOIDAL LIGHT SOURCE AND ELLIPSOIDAL CIRCUMSTELLAR ENVELOPE:

CONTENTS :

§3.1. Introduction :

Since the linear polarization from many stars is mainly produced by scattering on circumstellar matter (Kruszewski et. al. 1968, Serkowski 1970, Dyck et. al. 1971 and Shawl 1975), it is important to represent the circumstellar matter as an arbitrarily shaped envelope.

In this chapter the generalized results of Chapter Two are presented, by allowing both the point light source and the particle density distribution functions to be arbitrarily anisotropic, but we still consider only the case of optically thin envelopes and Thomson or Rayleigh scattering.

§3.2. General expression for Scattered Flux and Polarization:

As in Sec. 2-2, we will neglect the effects of finite star depolarization (e.g Cassinelli et. al. 1987), and of scatterer occultation (e.g. Brown and Fox 1991), by assuming the star to be small compared to the size of the envelope.

We define three cartesian coordinate systems

centered on the star, as follows (*see* Fig. 3-1) :

I - The observer reference frame (x,y,z) with spherical coordinates (r,θ,ϕ), the line of sight being the Oz-axis. As in Sec. 2-2, θ is then the scattering angle, and ϕ the polarization angle (direction) , relative to Oz for any scattering point.

II - The star's frame (X,Y,Z) with spherical coordinates (r,θ,Φ), where OZ is a convenient stellar axis (such as rotation) lying in the x-z plane of the observer's frame. This system is rotated relative to the former one through Euler angles (α,β,γ).

III - The envelope frame (X',Y',Z') with spherical coordinates (r,θ',Φ').

In general the scatterer density is $n(r,\theta',\phi')$, and the flux of the radiation (assumed unpolarized) from the star is $F(r,\theta,\Phi)$. Then following Eq. 2-1 (*also see* Simmons 1982), the (un-normalized) scattered flux and Stokes parameters (F_{sc},Q,U) of the scattered radiation at the Earth (distance D) are given now in this form :

$$
\left.\begin{array}{c} F_{sc} \\ Z^* \end{array}\right\} = \frac{1}{2\,k^2\,D^2} \iiint n(r,\theta',\phi')\ F(r,\theta,\Phi)\ r^2
$$

$$
\times \begin{cases} (i_1 + i_2) \\ (i_1 - i_2)\,\exp(-2i\phi) \end{cases} dr\,\sin\theta\,d\theta\,d\phi \qquad (3-1)
$$
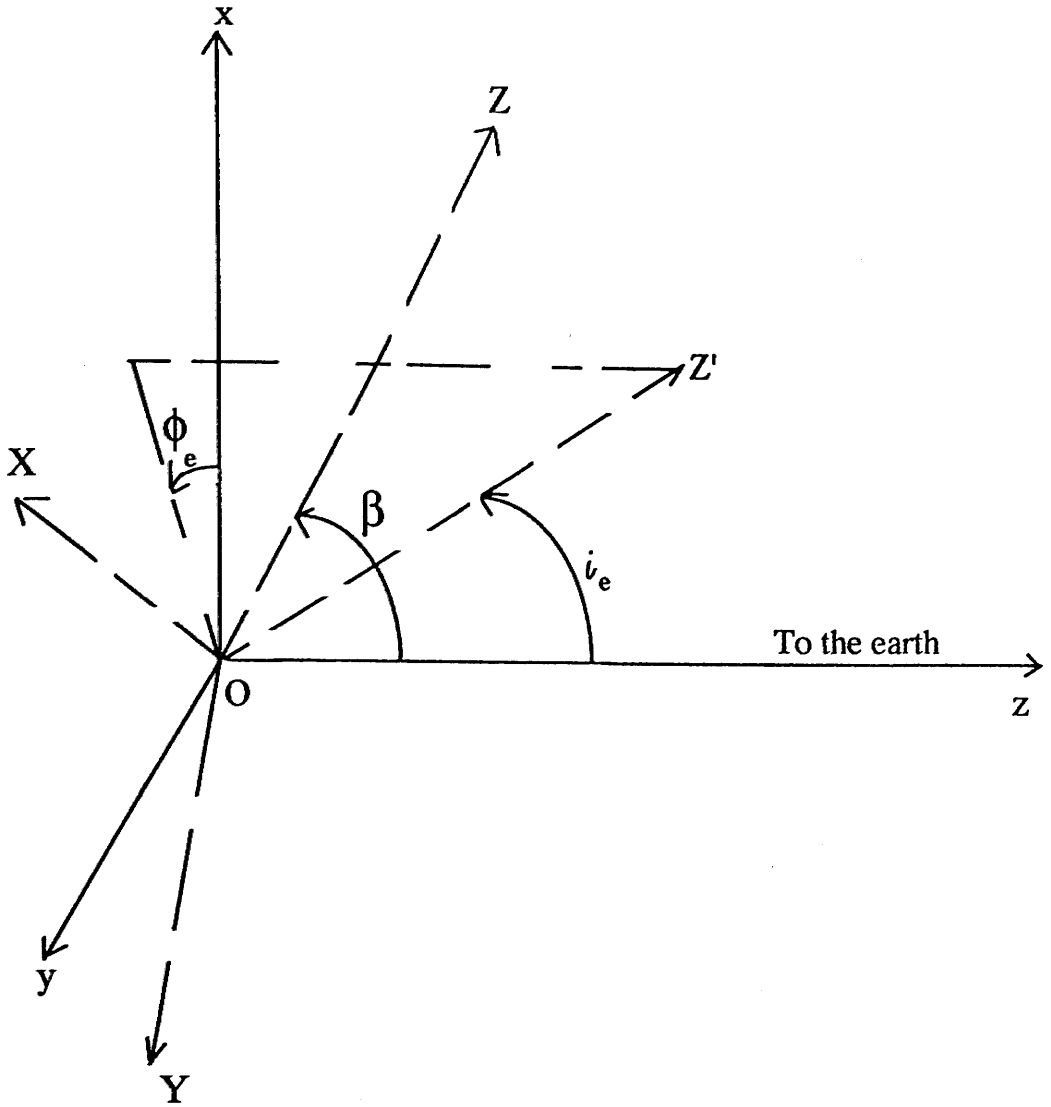
Fig. 3-1. The three coordinate systems, where O is the anisotropic light source, OZ'-axis is the axis of rotational symmetry of the envelope, which has an inclination i_e from the observer direction z. The angle ϕ_e is the azimuth of the envelope in the observer frame, and defines the envelope rotation (*see* the text).

with the same definitions of Eq. (2-1).

Providing that F varies smoothly, it may be expressed in terms of spherical harmonics in the observer frame (θ, ϕ) (see Eqs. (2-3 to 2-7), viz :

$$F(r,\theta,\phi) = \sum_{\ell=0}^{\infty} \sum_{m=-\ell}^{m=\ell} F_{\ell_m}(r) \sum_{n=-\ell}^{n=\ell} R_{nm}^{(\ell)}(\alpha,\beta,\gamma) \; Y_{\ell_n}(\theta,\phi) \qquad (3-2)$$

Generally we can expand the density distribution scatterers – in the observer frame, then it will be $n(r,\theta,\phi)$ – in terms of spherical harmonics, hence :

$$n(r,\theta,\phi) = \sum_{\ell'=0}^{\infty} \sum_{m'=-\ell'}^{m'=\ell'} n_{\ell',m'}(r) \; Y_{\ell',m'}(\theta,\phi) \qquad (3-3)$$

Evidently, if the envelope is uniformly rotating, this density could be also be expressed by using rotation matrices, but for present, we leave Eq. (3-3) in its general form. The $Y_{\ell_m}(\theta,\phi)$ in Eqs. (3-4 and 3-5) are as defined in Sec. 2-2 (cf. Jackson 1975).

Using the properties of the product of two spherical harmonics , we can express the multipoles of $n(r,\theta,\phi)$ and $F(r,\theta,\phi)$ as :

$$n(r,\theta,\phi)\ F(r,\theta,\phi)\ =\ \sum_{\ell\ell'\ mm'}\ n_{\ell'_m'}(r)\quad F_{\ell_m}(r)\quad \times$$

$$Y_{\ell'_{m'}}(\theta,\phi)\quad Y_{\ell_m}(\theta,\phi)\qquad (3-4)$$

or as

$$n(r,\theta,\phi)\ F(r,\theta,\phi)\ =\ \sum_{\ell\ m\ n}\ R^{\ell}_{nm}(\alpha,\beta,\gamma)\qquad \sum_{\ell'\ m'}\quad \times$$

$$C^{LM}_{\ell\ell'_{nm'}}\quad Y_{LM}(\theta,\phi)\qquad (3-5)$$

where $C^{LM}_{\ell\ell'_{mm'}}$ are Clebsh-Gordon coefficients , arising from the products of two spherical harmonics. Only terms satisfying the following two conditions contribute to the sum in Eq. (3-4) :

  (1) $n + m' = M$ (3-6)

and,

  (2) $|\ell - \ell'| \le L \le \ell + \ell'$ (3-7)

and are given by :

$$C^{LM}_{\ell\ell'_{nm'}}=(-1)^{M}\ \sqrt{\frac{(2\ell+1)(2\ell'+1)(2L+1)}{4\pi}}\ \begin{pmatrix}\ell & \ell' & L\\ 0 & 0 & 0\end{pmatrix}\begin{pmatrix}\ell & \ell' & L\\ n & m' & M\end{pmatrix}\ (3-8)$$

(*cf.* Messiah 1962, where values of the Clebsh-Gordon coefficients and the rotation matrices are tabulated , e.g. see Rose (1957), see also appendix C)

The scattering function factors can be expressed as in Sec. 2-2 :

$$1+\cos^{2}\theta\ =\ \frac{4}{3}\left[\ \sqrt{4\pi}\ Y_{00}+\sqrt{\frac{\pi}{5}}\ Y_{20}(\theta,\phi)\right]\qquad (3-9a)$$

and ,

$$\sin^2\theta \ \exp(-2i\phi) = 4 \ \sqrt{\frac{2\pi}{15}} \ Y^*_{22}(\theta,\phi) \qquad (3\text{-}9b)$$

so that, on substitution in the integrals contained in Eq. (3-1), together with the other expressions above, and using the properties of spherical harmonics, F_{sc} and Z^* can be written as:

$$F_{sc} = \frac{\sigma}{4\pi D^2} \sum_{\ell\ m\ n} R^\ell_{nm}(\alpha,\beta,\gamma) \sum_{\ell'\ m'} \times$$

$$\left[\sqrt{4\pi} \ C^{00}_{\ell\ell',nm'} + \sqrt{\frac{\pi}{5}} \ C^{20}_{\ell\ell',nm'} \right] S_{\ell\ell',mm'} \qquad (3\text{-}10)$$

and

$$Z^* = \frac{3}{4\pi}\frac{\sigma}{D^2} \sqrt{\frac{2\pi}{15}} \sum_{\ell\ m\ n} R^\ell_{nm}(\alpha,\beta,\gamma) \sum_{\ell'\ m'} C^{22}_{\ell\ell',nm'} \ S_{\ell\ell',mm'}, \quad (3\text{-}11)$$

where,

$$S_{\ell\ell',mm'} = \int_0^\infty F_{\ell m}(r) \qquad n_{\ell',m'}(r) \qquad r^2 \ dr \qquad (3\text{-}12)$$

where,

$$F_{\ell m}(r) = \int_{-1}^{1} \int_0^{2\pi} F(r,\theta,\phi) \ Y^*_{\ell m}(\theta,\phi) \quad d\cos\theta \ d\phi \qquad (3\text{-}13a)$$

and,

$$n_{\ell',m'}(r) = \int_{-1}^{1} \int_0^{2\pi} n(r,\theta',\phi') \ Y^*_{\ell',m'}(\theta',\phi') \quad d\cos\theta' \ d\phi' \qquad (3\text{-}13b)$$

Eqs. (3-13) describe the effects of each function (F and n) in the appropriate - stellar or envelope frame - (*cf.* Simmons 1982).

Eqs. (3-5) and (3-8) show that the scattered flux

and the Stokes parameters can be expressed as sums of increasing order of multipole contribution . This helps to separate the effects of anisotropy in the flux F and in the density distribution function n, and to study how they can cooperate together to produce polarization.

If the functions are smooth the summations will converge rapidly, so the first few terms (ℓ & $\ell' \leq 2$) will give a reasonable approximation. Due to the conditions of Eqs. (3-6) and (3-7) the summation over ℓ, ℓ', m, and m' in Eqs. (3-10) and (3-11) will be limited. For functions, describing the stellar flux and the circumstellar density distribution of the scattering particles symmetrically about stellar and envelope polar axis, respectively, $S_{\ell\ell', mm'}$ =0 for odd values of ℓ and ℓ'.

For a spherical envelope ($n(r,\theta,\phi)=n(r)$) and anisotropic light source, Eqs. (3-10 and 3-11) reduce to Eqs. (2-10 and 2-11) of Sec. 2-2. On the other hand, for an isotropic point light source within an arbitrary shaped envelope, these Eqs. (3-10 and 3-11) reduce to the results of Brown and McLean 1977 and Simmons 1982. It is obvious that for a spherical star and envelope, the scattered flux will equal the optical depth (if we neglect attenuation) and that the polarization will be zero.

§3.3. ELLIPSOIDAL LIGHT SOURCE AND ELLIPSOIDAL CIRCUMSTELLAR ENVELOPE:

As an illustration of the above general formulation, we will take the case ,discussed in Sec.2-3, of a black body star of uniform surface temperature, but now with this star within an ellipsoidal circumstellar envelope. For such star of isotropic surface intensity (I_*), $F(r,\Theta,\Phi)$ can be expressed (as seen from a distant point), in terms of the projected area $A_P(\Theta,\Phi)$ of the star as seen from direction (Θ,Φ). Hence:

$$F(r,\Theta,\Phi) \simeq I_* \, \Delta\Omega = \frac{I_* \, A_P(\Theta,\Phi)}{r^2} \qquad (3\text{-}14a)$$

where I_* is the isotropic intensity of the stellar surface and $\Delta\Omega$ is the solid angle subtended by the scattering element. For this star the axes (a,b,c) will be along (X,Y,Z) (see Fig. 3-2), A_P is given by :

$$A_P = \pi \left| \sqrt{(b\,c\,\lambda)^2 + (a\,c\,\mu)^2 + (a\,b\,\nu)^2} \right| \qquad (3\text{-}14b)$$

where $(\lambda,\mu,\nu) = (\cos\Phi\,\sin\Theta\,,\,\sin\Phi\,\sin\Theta\,,\,\cos\Theta)$ are the (X,Y,Z) direction cosines of the direction (Θ,Φ) (see appendix B). So we obtain :

$$F_{\ell m}(r) = \frac{I_*}{r^2} \int_0^\pi \int_0^{2\pi} A_P(\Theta,\Phi) \, Y_{\ell m}^*(\Theta,\Phi) \, d\Phi \, \sin\Theta \, d\Theta \qquad (3\text{-}15)$$

Let us take the circumstellar envelope to be the

same as that of Simmons 1982, i.e. an ellipsoidal shell of arbitrary thickness and uniform density . The density distribution, which has an axis of rotational symmetry OZ', has an inclination angle i_e with the line of sight. We shall consider only the case of rotation of OZ' about the line of sight, but not any other direction, with an azimuthal angle ϕ_e in the observer frame (see Fig. 3-2). We then have (Simmons 1982) :

$$n_{\ell,m'}(r) = 2\pi\ (R_1 - R_2)\ n_0\ K_{\ell'}\ Y_{\ell,m'}(i_e, \phi_e) \qquad (3\text{-}16)$$

where we define :

$$n(r, \theta', \Phi') = \begin{cases} n_0 & \text{when} \quad r_2(\mu) \le r \le r_1(\mu) \\ 0 & \text{otherwise} \end{cases} \qquad (3\text{-}17a)$$

Here n_0 is the uniform number density of particles within the column bounded by r_1 and r_2, where :

$$r_{1'2}(\mu) = \frac{R_{1,2}}{\sqrt{1 + (A_r^2 - 1)\ \mu^2}} \qquad (3\text{-}17b)$$

and $\quad \mu = \cos(\zeta) \qquad (3\text{-}17c)$

R_1 and R_2 are the outer and inner equatorial axis length , and A_r is the ratio of the length of the equatorial axis to the polar axis (see Fig. 3-2). The angle ζ is the angle between the radius vector and the axis of symmetry, which is related to our frames by the addition theorem of spherical harmonics (This explains the appearance of $Y_{\ell,m'}(i_e, \phi_e)$ in Eq. (3-16) – see Simmons 1982 and Jackson 1975. Finally $K_{\ell'}$ is given by :
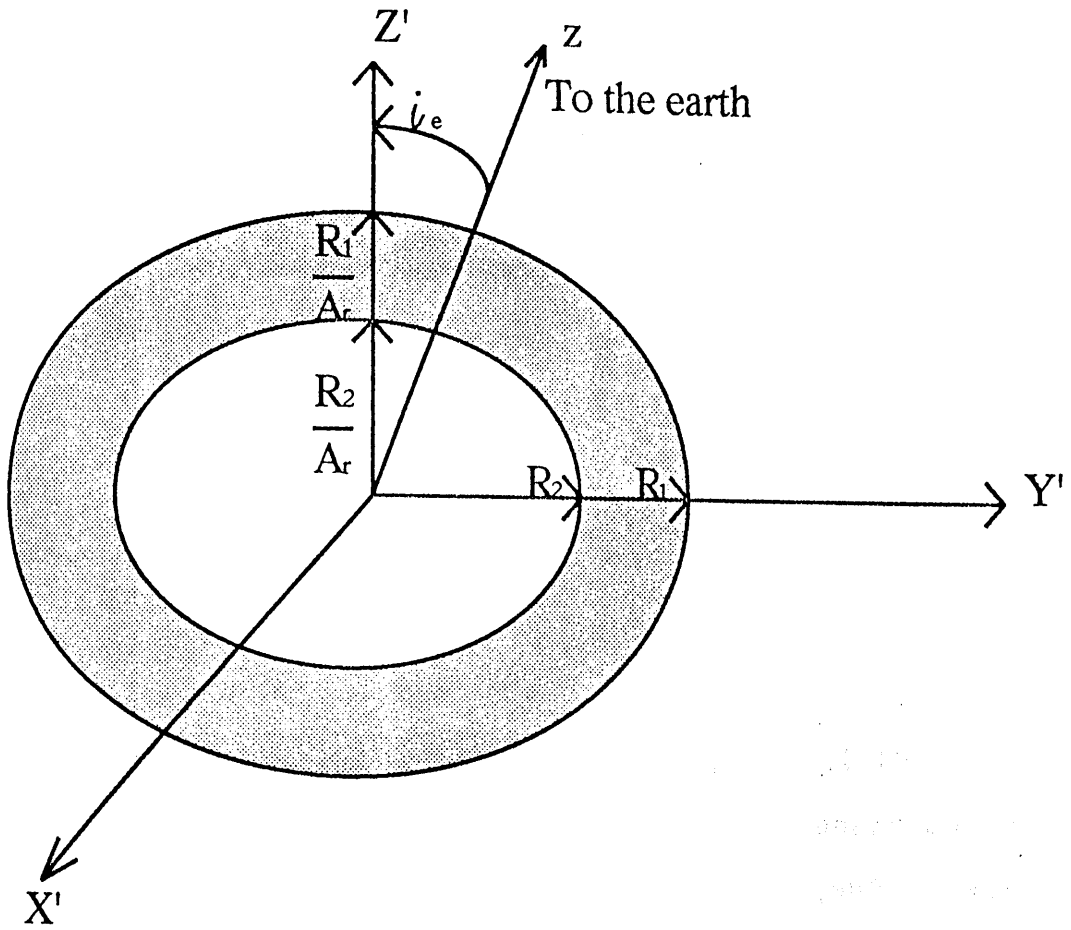
Fig. 3-2. The ellipsoidal envelope, with a thickness (R_1-R_2), and A_r is the ratio of the equatorial axis to the polar axis.

$$K_{\ell'} = \int_{-1}^{1} \frac{P_{\ell'}(\mu)}{\sqrt{1 + (A_r^2 - 1)\,\mu^2}}\; d\mu \qquad (3\text{-}18)$$

Inserting Eqs. (3-15) to (3-18) in Eq. (3-12), we obtain :

$$S_{\ell \ell'\, mm'} = I_x\; N\; f_{\ell m}\; K_{\ell'}\; Y_{\ell',m'}(i_e,\phi_e) \qquad (3\text{-}19)$$

where,

$$N = 2\pi\; (R_1 - R_2)\; n_0 \qquad (3\text{-}20)$$

and,

$$f_{\ell m} = \int_0^{\pi} \int_0^{2\pi} A_P(\Theta,\Phi)\; Y_{\ell m}^{*}(\Theta,\Phi)\; d\Phi\; \sin\Theta\; d\Theta \qquad (3\text{-}21)$$

Note that the multipoles of the flux $f_{\ell m}$ are now functions of the star's shape and size only (i.e. of a,b,and c). Moreover, the multipoles of the envelope $K_{\ell'}$ are also functions of the envelopes shape and size only (i.e. of A_r). This combination of $K_{\ell'}$ and $f_{\ell m}$ will have a great effect on both the polarization and the scattered flux, depending on whether the two functions enhance or offset one another.

If we describe the orientation of the star relative to the observer frame in terms of the Euler angles, then we can choose α as zero, β as the inclination (i_s) of the OZ-axis (the rotation axis of the star) to the line of sight (Oz-axis), and γ as the azimuth of the OZ-axis from the Ox-axis measured about the Oz-axis, which we denote as ϕ_s. Thus ϕ_s measures the rotational position

of the star relative to the observer (see Fig. 3-2).

As in Chapter one, we will consider the observational situation, then the normalized scattered flux and Stokes parameters as they are usually used. They are given by $[F_{sc}, Q, U]/F_{tot}$, where the total flux received F_{tot} comprises the combination of the scattered flux F_{sc} plus the direct flux from the star. We can define F_{add} as the flux normalized by F_{tot} which is added to the direct flux due to the scattered flux and the stellar shape variation (assuming that the direct flux is unity). This direct flux component is given by $I_\ast \, A_p(i_s, \phi_s)/D^2$, where A_p here is the projected area of the star seen from the Earth for $\theta = i_s$ and $\phi = \phi_s$. So we can write the normalization factor F_{norm} as :

$$F_{norm} = (I_\ast/D^2) \left[A_p(i_s, \phi_s) + (D^2/I_\ast) \, F_{sc} \right] \qquad (3-22)$$

Then the general expressions for the normalized scattered flux and Stokes parameters (F_{scn} and $Z_n^\ast$, respectively) are :

$$F_{scn} = \frac{\tau}{4\pi \, F_{norm}} \sum_{\ell \, m \, n} R_{nm}^{\ell}(0, i_s, \phi_s) \quad f_{\ell m} \sum_{\ell' \, m'} K_{\ell'} \, Y_{\ell' m'}(i_e, \phi_e)$$

$$\times \left[\sqrt{4\pi} \, C_{\ell\ell' nm'}^{00} + \sqrt{\tfrac{\pi}{5}} \, C_{\ell\ell' nm'}^{20} \right] \qquad (3-23)$$

and,

$$Z_n^* = \frac{3}{4\pi} \frac{\tau}{F_{norm}} \sqrt{\frac{2\pi}{15}} \sum_{\ell \, m \, n} R_{nm}^{\ell}(0, i_s, \phi_s) \; f_{\ell m}$$

$$\times \sum_{\ell' \, m'} K_{\ell'} \; Y_{\ell' m'}(i_e, \phi_e) \; C_{\ell\ell' nm'}^{22}, \qquad (3-24)$$

where τ is the average envelope optical depth, equal to $\sigma \, (R_1 - R_2) \, n_0$ - see Simmons (1982).

As before, the degree of polarization $p = |Z_n^*| = |Z_n|$, and the polarization direction is given by $\phi_p = \frac{1}{2} \arg Z_n$.

From Eqs. (3-23) and (3-24), we can calculate the polarization and the scattered flux, using the properties of the two factors $K_{\ell'}$ and $f_{\ell m}$, which are describing the envelope and stellar anisotropy. Due to the symmetry of the functions chosen to describe the stellar flux and the scatterer density distribution n, $K_{\ell'}$ and $f_{\ell m}$ are non-zero only for even ℓ' and ℓ, respectively.

The multipoles of the envelope $K_{\ell'}$ can be related to the shape factor γ of Brown and McLean (1979), since both are independent of the inclination (both stellar i_s and envelope i_e), and are purely dependent on the *relative* density distribution of the scattering particles.

§3.4. Discussions and Calculations :

As mentioned above the multipoles of the flux $f_{\ell m}$ are non-zero only for even ℓ, the spherical harmonics of ℓ with higher even values (i.e $\ell \geq 4$) are important only for great stellar distortion from sphericity. As an example Fig. (3-3 a and b) show the variation of $f_{\ell 0}$ for a star distorted in its c-axis. When c $\ll$ 1 the values of $f_{\ell 0}$ for $\ell > 2$ became important (Fig. 3-3a), but may be neglected, due to their being much smaller than f_{20} for the same values of c. On the opposite side, for c>2 most of $f_{\ell 0}$ are considerably larger than the case for c<1. The values of $f_{\ell 0}$ for $\ell > 2$ when c>2 is still less than f_{20}. For m>0 the values of $f_{\ell m}$ are expected to be smaller than that for m=0, but f_{2m} still be larger than $f_{\ell m}$ for $\ell > 2$. In this thesis, we will neglect the effects of $f_{\ell m}$ for $\ell > 2$.

Simmons (1982) also calculated the K_ℓ, for ellipsoidal envelopes, and his results are in agreement with the above discussion for $f_{\ell m}$. For $\ell' = 2$, a maximum value is expected for an isotropic point source star, between Ar=4 and Ar=5 (*see also* Fig. 3-4). For Ar>5 the assumptions of the above modelling fail, because the scatterers in the polar direction are much nearer to the star than that in the equatorial direction. In other words, the optical depth in the polar direction becomes

much larger than the optical depth in the equatorial direction. In addition the assumption of a *point* star (much smaller than the envelope) fails. For simplicity, we neglect these effects in the following discussion.

So we can write Fscn, and Stokes' parameters for $\ell=\ell'=2$ as :

$$F_{sc} = \frac{\sigma}{4 \pi D^2} \left[\sqrt{4 \pi} \left\{ \sum_{m=-2}^{m=2} S_m^{22\ 2-2} C_{22\ 2-2}^{00} + \right.\right.$$

$$\sum_{m=-2}^{m=2} S_m^{22\ 1-1} C_{22\ 1-1}^{00} + \sum_{m=-2}^{m=2} S_m^{22\ 00} C_{22\ 00}^{00} +$$

$$\sum_{m=-2}^{m=2} S_m^{22\ -11} C_{22\ -11}^{00} + \sum_{m=-2}^{m=2} S_m^{22\ -22} C_{22\ -22}^{00} +$$

$$\left. S_0^{00\ 00} C_{00\ 00}^{00} \right\} + \sqrt{\frac{\pi}{5}} \left\{ S_0^{02\ 00} C_{02\ 00}^{20} + \right.$$

$$\sum_{m=-2}^{m=2} S_m^{22\ 2-2} C_{22\ 2-2}^{20} + \sum_{m=-2}^{m=2} S_m^{22\ 1-1} C_{22\ 1-1}^{20} +$$

$$\sum_{m=-2}^{m=2} S_m^{22\ 00} C_{22\ 00}^{20} + \sum_{m=-2}^{m=2} S_m^{22\ -11} C_{22\ -11}^{20} +$$

$$\left.\left. \sum_{m=-2}^{m=2} S_m^{22\ -22} C_{22\ -22}^{20} + \sum_{m=-2}^{m=2} S_m^{20\ 00} C_{20\ 00}^{20} \right\} \right]$$

(3-25a)

and, Stokes' parameters :

$$Z^* = \frac{3}{4\pi}\frac{\sigma}{D^2} \quad \sqrt{\frac{2\,\pi}{15}} \quad \left\{ \quad S_0^{02\ 02}\ C_{02\ 02}^{22} \right. \qquad +$$

$$\sum_{m=-2}^{m=2} S_m^{22\ 20}\ C_{22\ 20}^{22} + \sum_{m=-2}^{m=2} S_m^{22\ 11}\ C_{22\ 11}^{22} \quad +$$

$$\sum_{m=-2}^{m=2} S_m^{22\ 02}\ C_{22\ 02}^{22} + \sum_{m=-2}^{m=2} S_m^{20\ 20}\ C_{20\ 20}^{22} \quad \left.\right\}$$

$$(3\text{-}25b)$$

where,

$$S_m^{ll'\ nm'} = R_{nm}^{l}(\alpha,\beta,\gamma)\ S_{ll'\,mm'}, \qquad (3\text{-}25c)$$

The multipoles $f_{\ell m}$ and $K_{\ell'}$ are the determining factors. We showed in Sec. 2.4. (for spherical envelope) the effect of the projected area A_p (within the shape factor $f_{\ell m}$) on the scattered flux and the polarization, showing that the polarization increases as the stellar inclination i_s increases. With an ellipsoidal envelope the ratio of the length of the equatorial axis to the polar axis of the ellipsoidal envelope A_r (within the shape factor $K_{\ell'}$) affects p and F_{scn}, even for a spherical star (as expected). For A_r approaching infinity of $\tau=0.1$ (the envelope will be a plane disk of scattering particles) and a spherical star, the polarization p and F_{scn} increase as i_e increases. The polarization for each value of i_s has a maximum between $A_r=4$ and $A_r=5$, where the model has failed for $A_r>5$ (see the discussion of Simmons (1982) calculations above), and p is zero at $i_s=0°$ (see Fig. 3-4a). Even although,

the scattered flux is small for this case (Fig. 3-4b).
For non-spherical stars the situation will be more
complicated.

The maximum polarization (as expected in Sec 2.3.)
then is produced by a disk shaped star with zero
thickness at $i_s=90°$. Here p was about 20% (of the total
light) for spherical envelope, this value increasing as
A_r increases to about 35% for $i_e=0°$, due to the envelope
becaming a disk (instead of global) of scatterers
perpendicular to the stellar disk, so the scattering
angle will be 90° which enhances the polarization. The
polarization p decreases for $i_e>30°$ to about -11% at
$i_e=90°$ (due to the scattering angles being smaller, or
the scattering particles seen by the observer being
fewer than that at $i_e=0°$, *see* Fig. 3-5). These values
are independent of τ as the case for spherical envelopes
(*see* Sec. 2.4). This maximum polarization of about 35%
of the total flux is within what expected from some
previous models (e.g. Brown and McLean 1977) with a disk
envelope illuminated by a spherical star.

In general we can apply the expressions in (3-24)
and (3-25) to the same cases in Sec. (2.4), to such
objects as a single fast rotating oblate star , a Roche
lobe filling star, or a non-radially oscillating star.
The results thus give almost the same loci in the
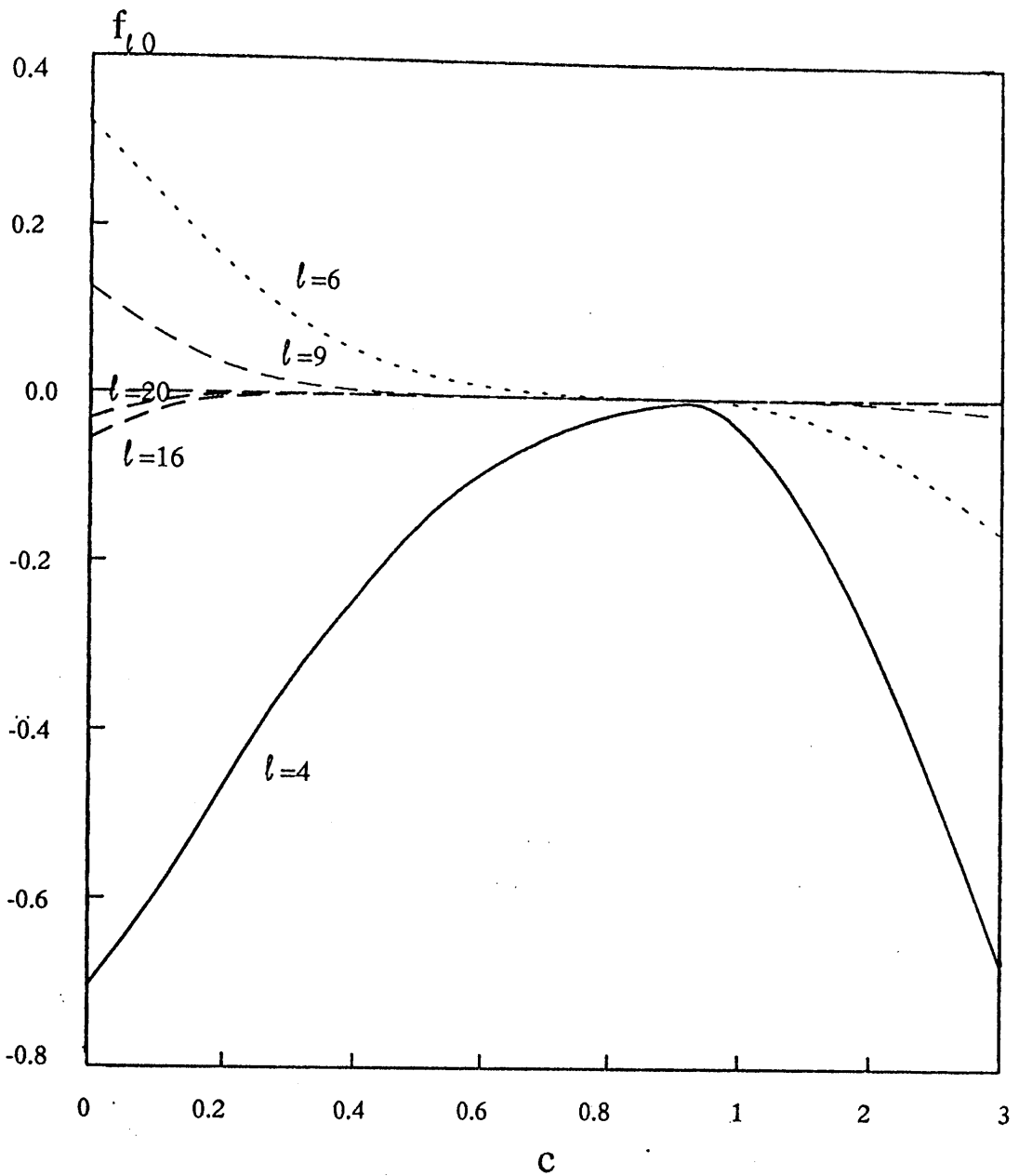
Fig. 3-3a. The values of $f_{\ell 0}$ for $\ell=0$ and 2 as c increases, where a=b=1. For $\ell=0$ the values start (at $c \simeq 0$) at about six and increase with c, $\ell=2$ the values start close to 3, decrease to zero at c=1 and continue with a negative sign.
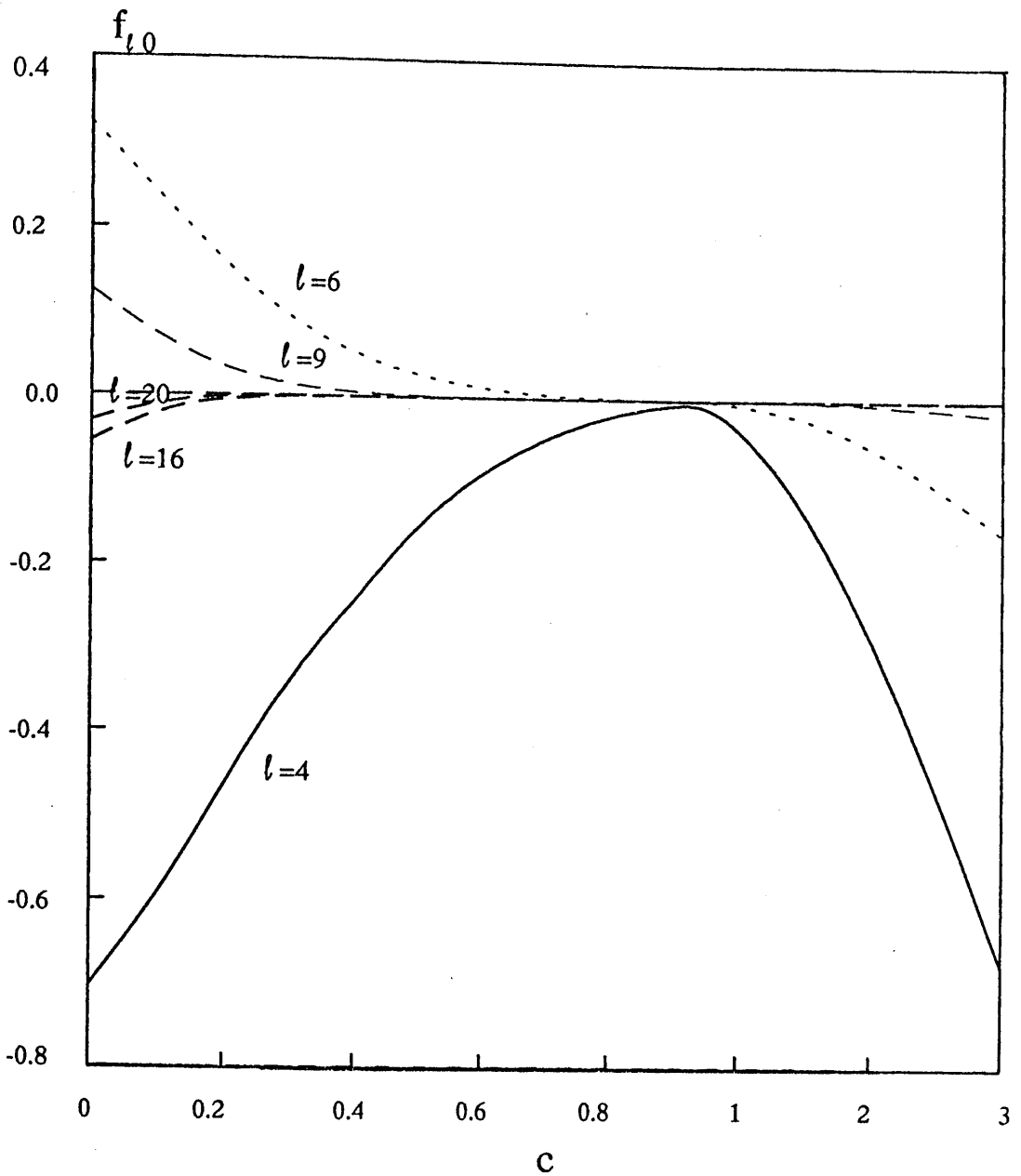
Fig. 3-3b. The values of $f_{\ell 0}$ for different $\ell > 2$ as c
increase, where a=b=1. Its clear all $\ell > 2$ are important
when c>2, and ℓ=4 may be considered when c<0.5.
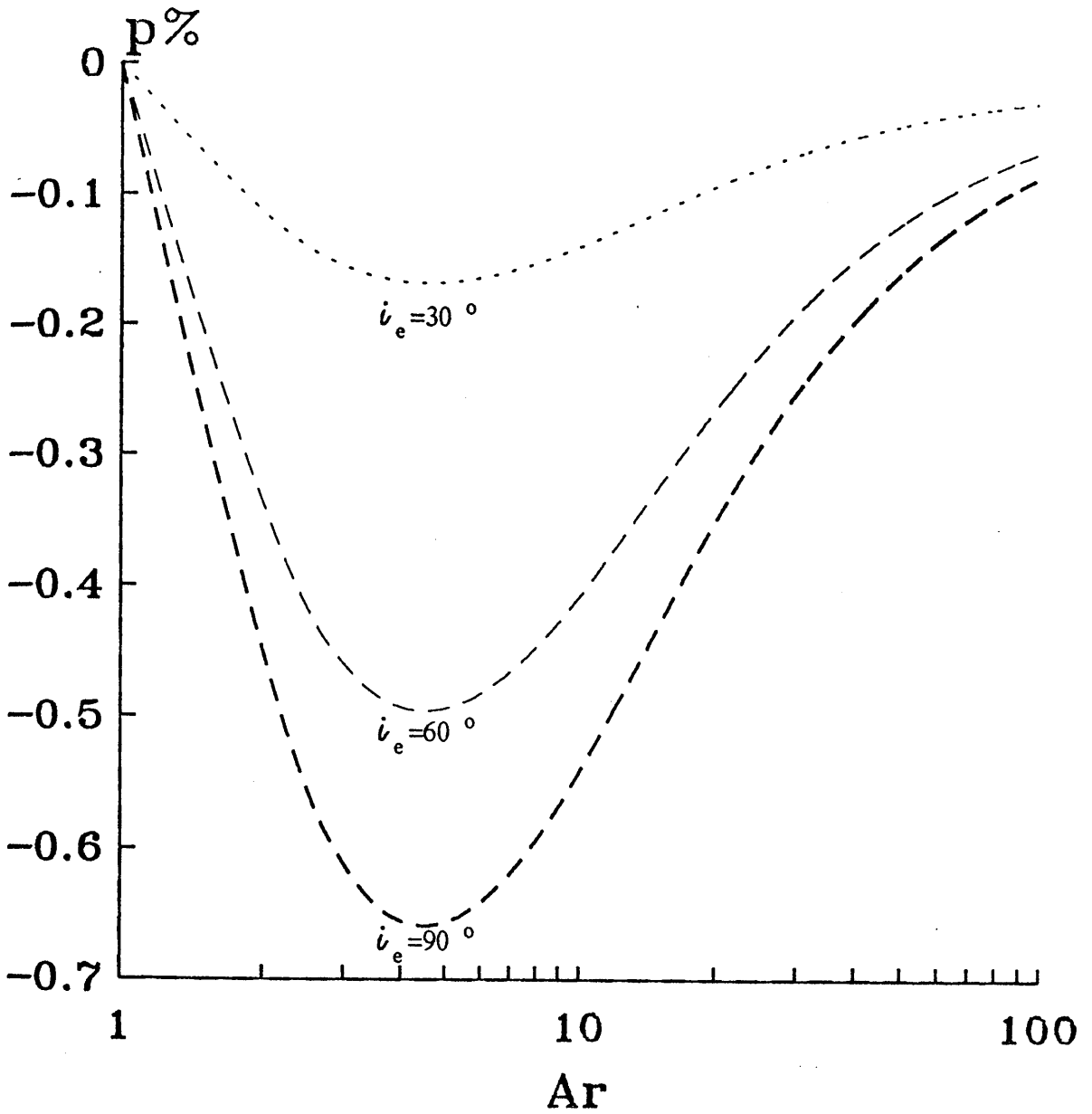
Fig. 3-4a. The polarization in % as Ar increase from 1 to 100 for a spherical star (i.e. a=b=c=1). The degree of p% is increased as the inclination of the envelope increases.
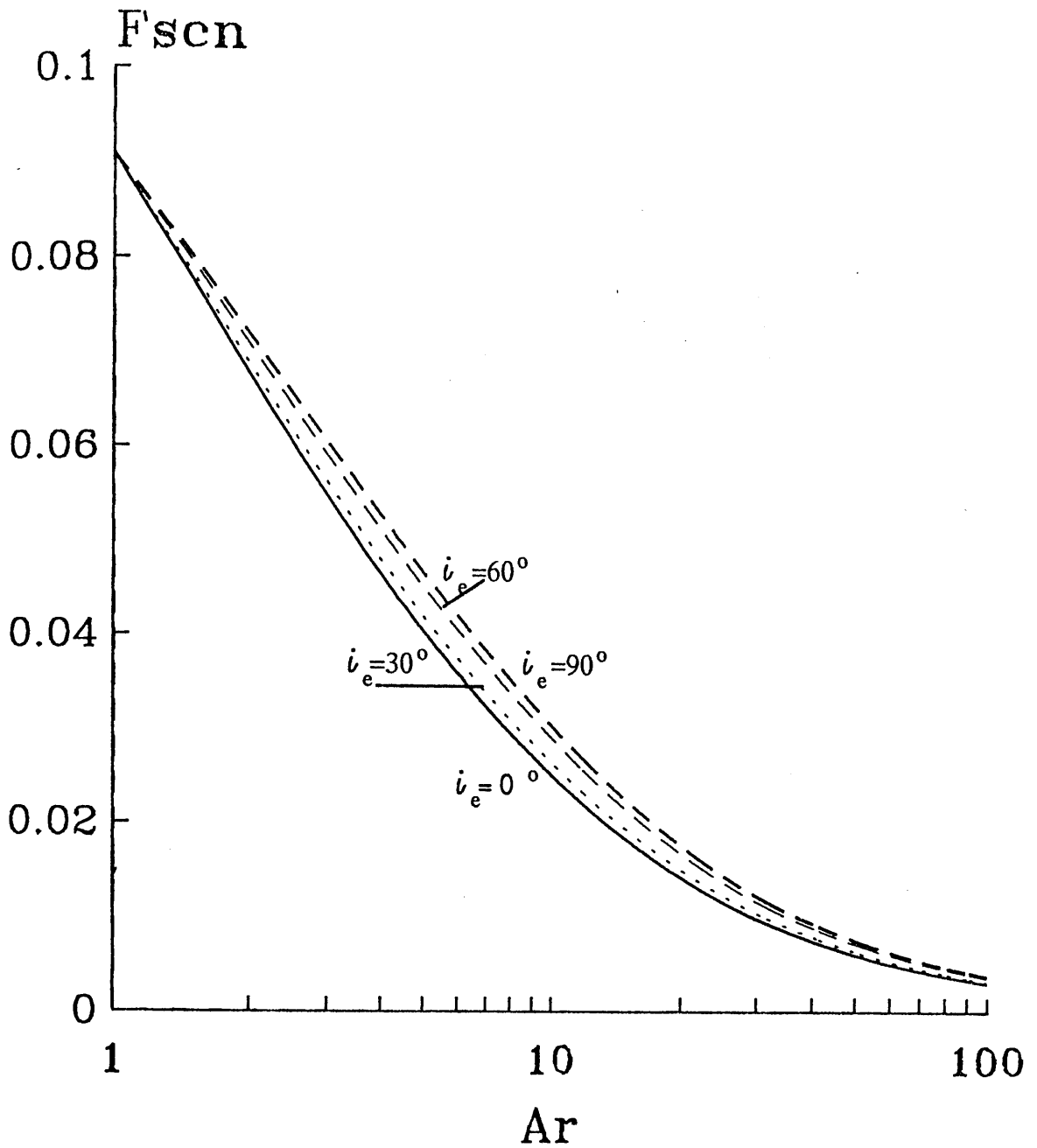
Fig. 3-4b. The normalized scattered flux F_{scn} vs. Ar. There is not much increase in F_{scn} as i_e increases.
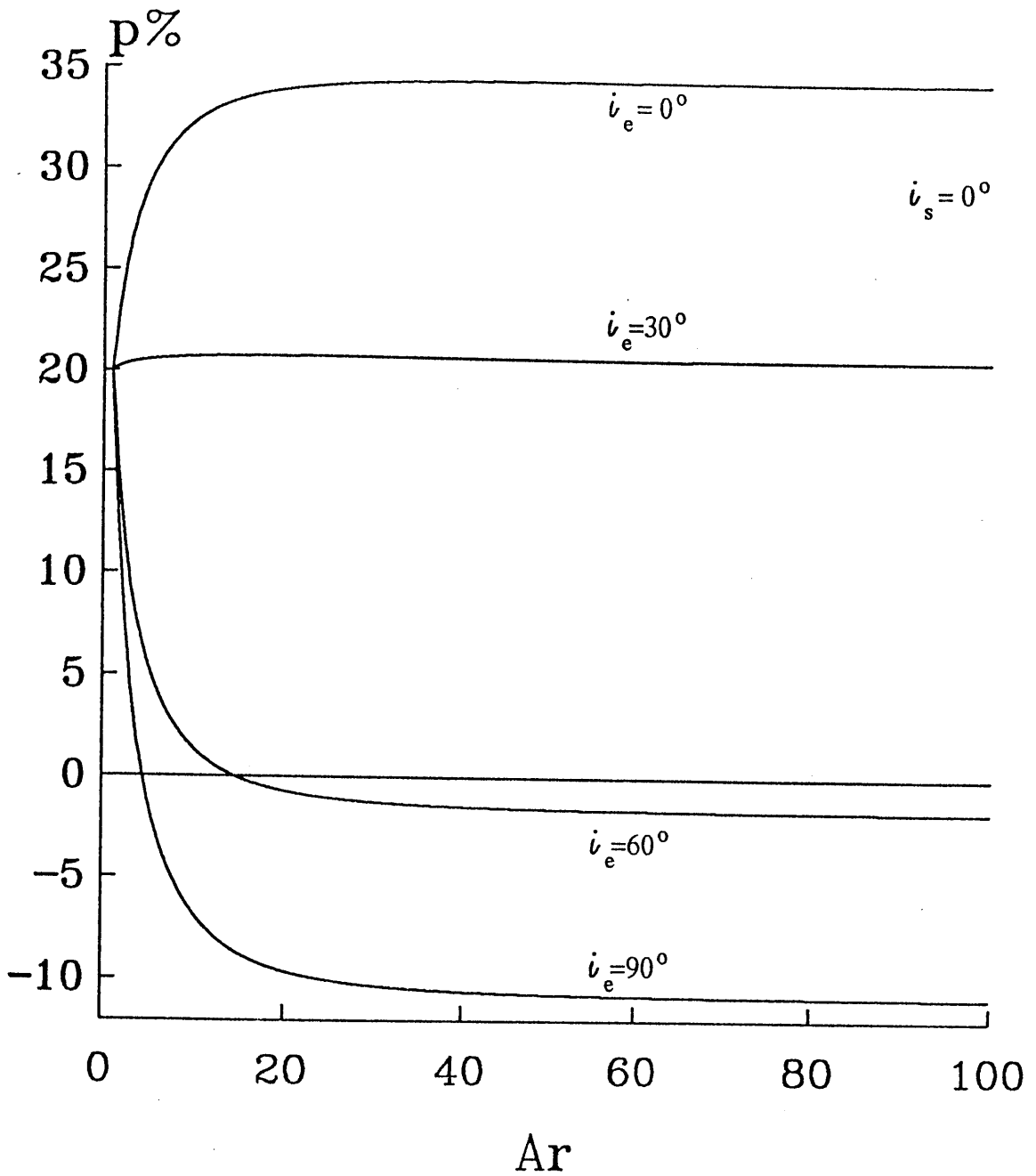
Fig. 3-5. The polarization in % from a disk like star viewed edge on (i_s= $0°$), within an extended envelope as Ar increases from 1 to 100, for i_e= $0°$, i_e=$30°$, i_e=$60°$, and i_e=$90°$.

qu-plane as in Sec. 2.4. but with smaller or larger values of q and u, as the two function of F and n offset or enhance each other. So here we will concentrate mainly on the effect of the envelope shape on the polarization for a fixed stellar shape. To show this we will choose two examples from Sec. 2.4., the binaries and pulsating stars.

§3.4.1 BINARIES :

For binary stars, assuming the same values of b=2 and a=c=1 (again with the star small compared to the envelope, with magnetic field neglected), a large envelope may be expected to be fixed, and its axis of symmetry to be parallel to the rotation axis of the binary (i.e. $i_e = i_s$). We find for $A_r = 3$ an enhancement for the maximum polarization, from about .45% (of the total light) for a spherical envelope (*see* Fig. 2-5) to about 1.1% for our ellipsoidal envelope when seen at $i_s = 90°$ (*see* Fig. 3-6), but reduced at $i_s = 0°$ to about .32% .

If a star has a strong enough oblique magnetic field, then the envelope's axis of symmetry may be parallel to the magnetic field instead of to the rotation axis of the star (in this case the binary). Figs. (3-7, 3-8, and 3-9) show this effect for three envelope inclinations (or magnetic field inclinations)
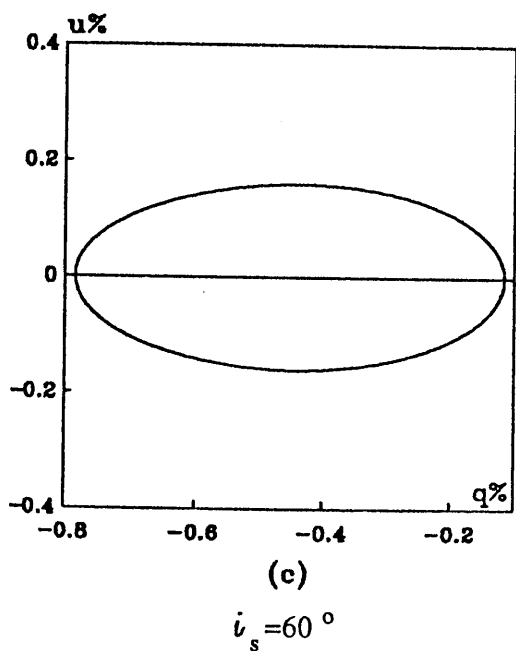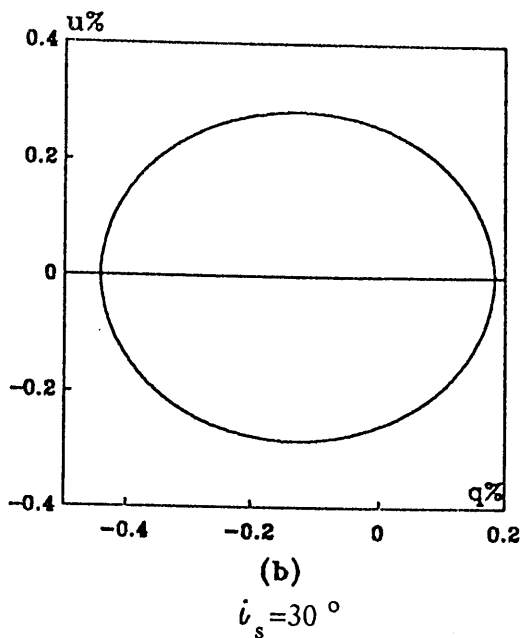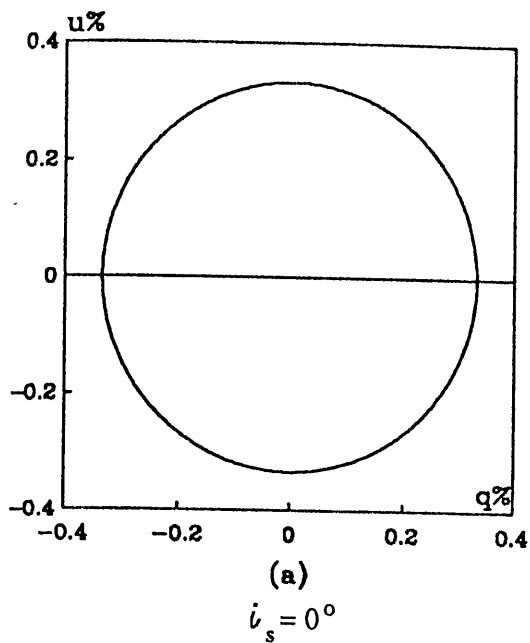
Fig. 3-6. The polarization in % from a binary of b=2 a=c=1, with a fixed envelope of Ar=3, and $i_e = i_s$. (a) i_s= 0°, (b) i_s=30°, (c) i_s=60°, and (d) i_s=90°.

$i_e=0°$, $i_e=45°$, and $i_e=90°$, respectively, for the same binary above, at different stellar inclinations ($i_s=0°$, 30°, 60°, and 90°). In general the inclination of the star affects the degree of polarization more than the inclination of the envelope. On the other hand, since the star illuminates more in the direction of its smaller axes (here a and c-axes), and the envelope has more scatterers in the direction of its longer axes, so we expect higher polarization for bigger inclination difference (i_s-i_e).

This model allows us to calculate the polarization produced by a rotating envelope for any inclination i_e, due (e.g.) to strong magnetic field. Of course such envelopes will not show any change in the polarization if they co-rotate with the star with inclination relation of $i_e=i_s$, because of the symmetry of the envelope as seen by the observer. But polarization changes can be shown for a co-rotating envelope, which has its axis of symmetry perpendicular to the stellar rotation axis, then the rotation will be about one of its equatorial axes. These envelopes will have different observable shapes as it is rotating. Any other relation between i_e and i_s will not result in a co-rotating system.

For the same binary as above but with $i_e=i_s+\pi/2$ and
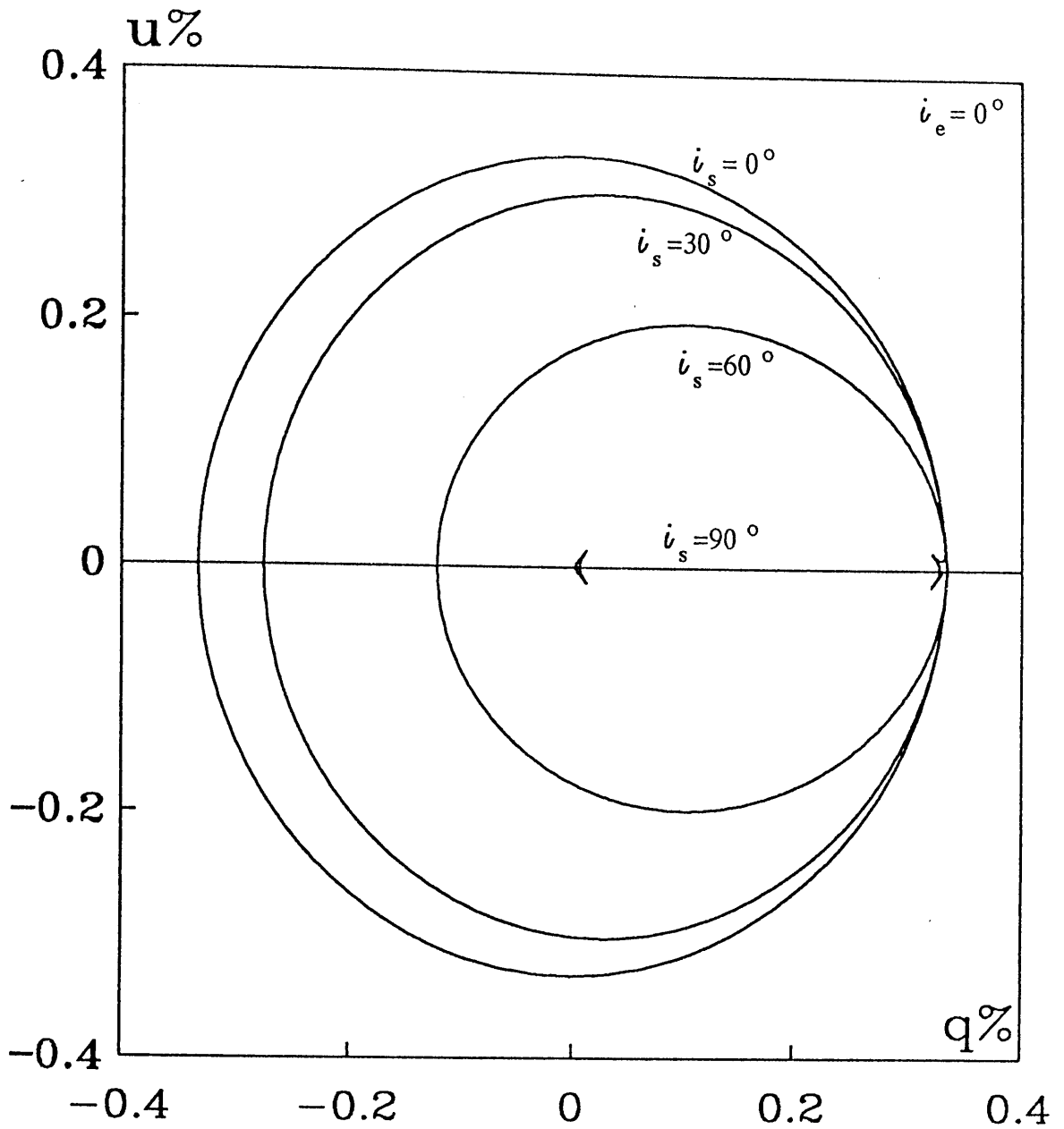
Fig. 3-7. The polarization in % from a binary of b=2 a=c=1, with a fixed envelope of Ar=3, and i_e= 0°, and different stellar inclinations i_s= 0°, 30°, 60°, and 90°.
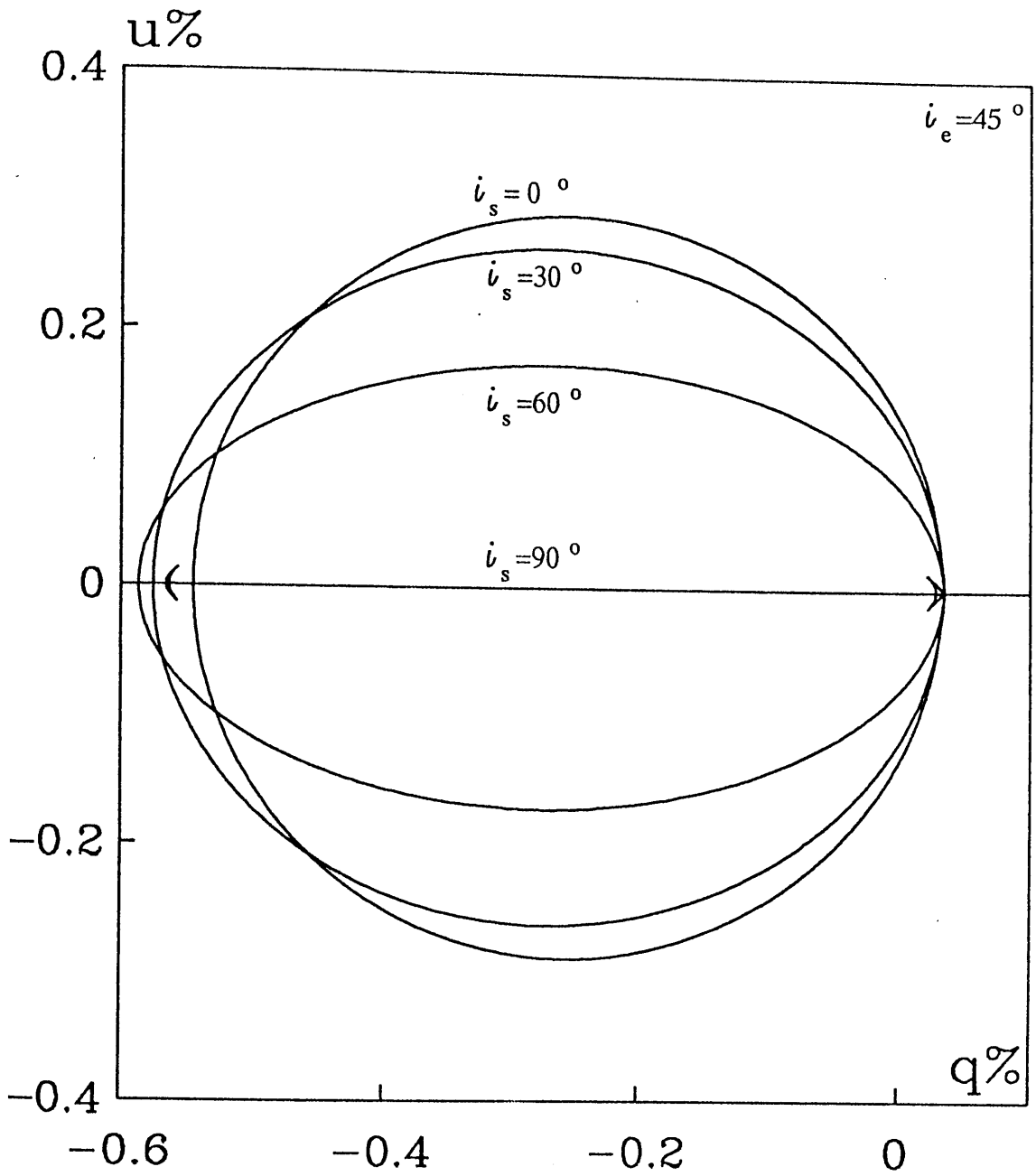
Fig. 3-8. The polarization in % from a binary of b=2 a=c=1, with a fixed envelope of Ar=3, and i_e= 45°, and different stellar inclinations i_s= 0°, 30°, 60°, and 90°.
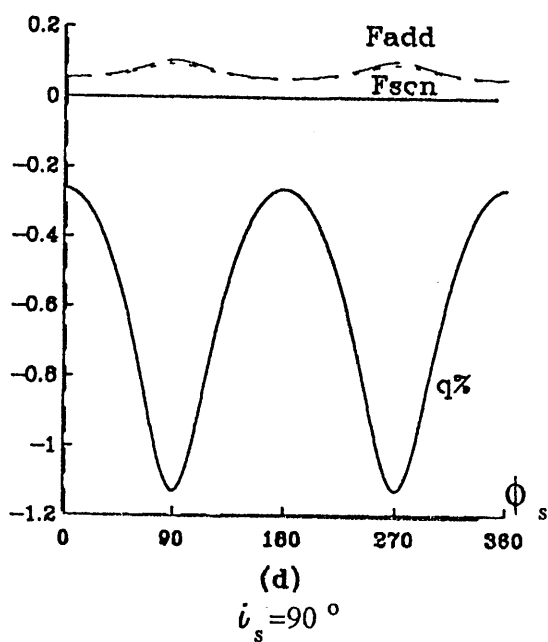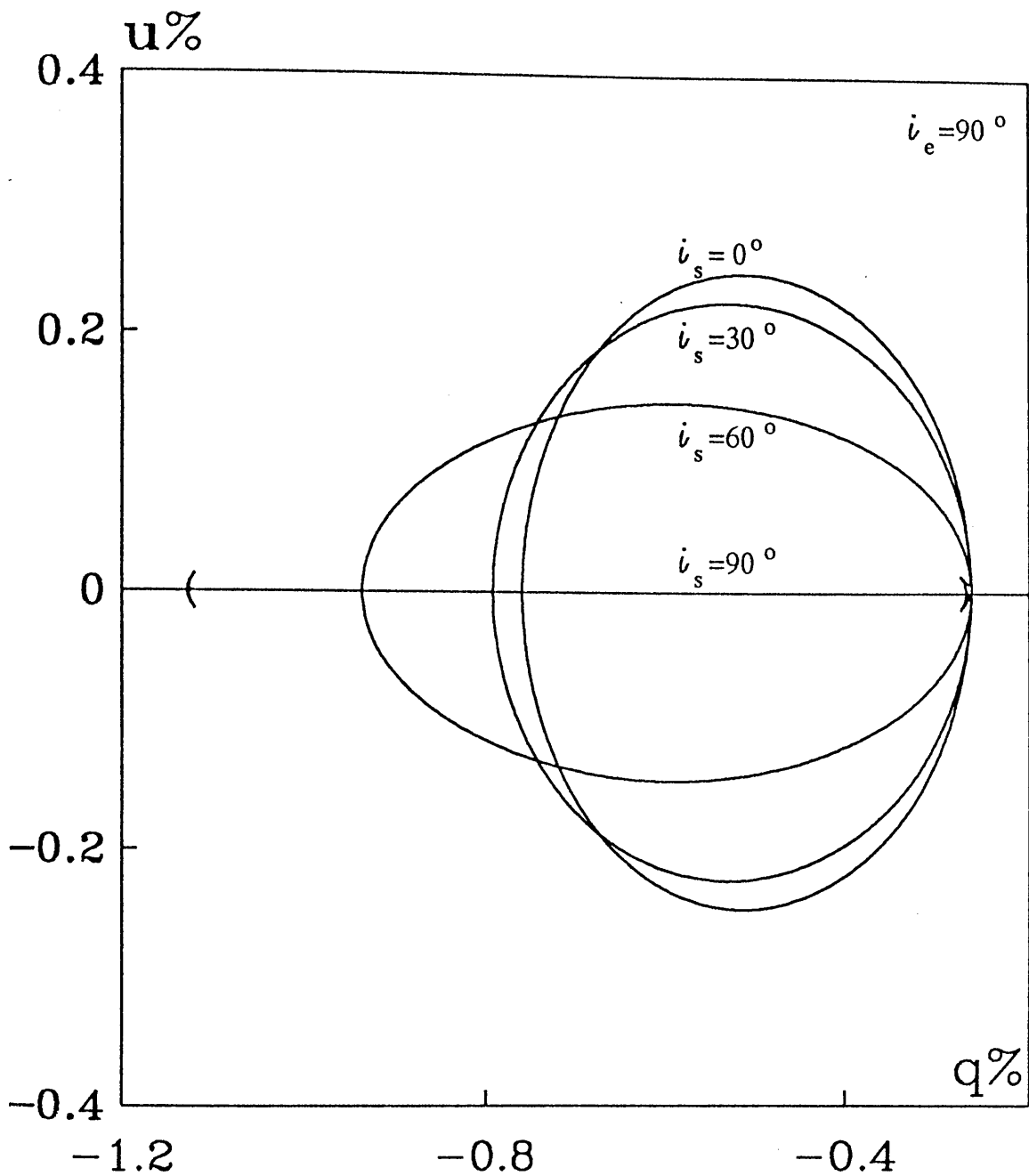
Fig. 3-9. The polarization in % from a binary of b=2 a=c=1, with a fixed envelope of $A_r=3$, and $i_e= 90°$, and different stellar inclinations $i_s= 0°$, $30°$, $60°$, and $90°$.

$\phi_s = \phi_e$ (the star and the envelope are co-rotating), the polarization seen at $i_s = 90°$ shows no variation other than that for fixed envelopes, because the distortion from sphericity for the envelope is in the direction of the line of sight, which will not affect the polarization during stellar rotation. The maximum polarization is the same for fixed and rotating envelopes, but different qu-loci occur for $i_s < 90°$ (see e.g. Fig. 3-10). Also the locus is described twice per period.

Envelope rotation may also be slower than the star, due (e.g.) to the distance between them and the weakness of the coupling gravitational force. In this case the patterns of the qu-loci become more complicated. But for a binary rotating four times faster than the envelope, with the same values of the last case, at $i_s = 90°$ the qu-loci will be the same as for a co-rotating system case, because when $i_s = 90°$ (i.e. $i_e = 0°$) the envelope will be seen by the observer to have the same symmetric shape during its rotation (since for $i_s = 90°$, u is zero, in the following figures the results for $i_s = 85°$ are shown instead). The locus for $i_s = 90°$ is described eight times per envelope rotation because of the symmetry. For $i_s < 90°$ the results are (as expected) more complicated (see Figs. 3-11 a,b,c and d).

§3.4.2 PULSATING STARS:

If a star has non-radial oscillations, such oscillations may not affect the size and shape of the large envelope. In order to show the effects for an ellipsoidal envelope, we will assume the envelope size remains the same during stellar oscillation, and that the star has three oscillating axes (i.e. a,b and c), described by the equation (*see* Eq. 2-26) :

$$x = 1 + \delta \cos(\omega t + \Delta) \qquad\qquad (3-26)$$

where x is an axis (a,b or c), δ is the fractional distortion amplitude from spherical , $\omega = 2\pi/\Pi_P$ where Π_P is the pulsation period, and Δ the phase. So as in Sec. 2.4.3.3, we assume the pulsation to be as follows : for a-axis pulsation $\delta=0.05$, $\Delta=\pi/2$ and $\omega t=2\pi t/\Pi_P$; b-axis pulsation $\delta=0.1$, $\Delta=0$ and $\omega t=2\pi t/\Pi_P$; and c-axis pulsation with $\delta=0.08$, $\Delta=\pi/2$ and $\omega t=4\pi t/\Pi_P$. For a rotating star with pulsation period equal to the rotation period, and having a co-rotating envelope, Figs (3-12 a,b,c and d) show qu-loci for different i_s's at $i_e=i_s+\pi/2$. As may be expected, at $i_s=90°$ there are no changes in the qu-plane loci from those for a spherical envelope, but a great enhancement for the polarization occurs for $i_s<90°$, approaching five times that for $i_s=90°$ for smaller i_s.

The envelope may, however, expand and contract as the star oscillates because (e.g.) the star is emitting
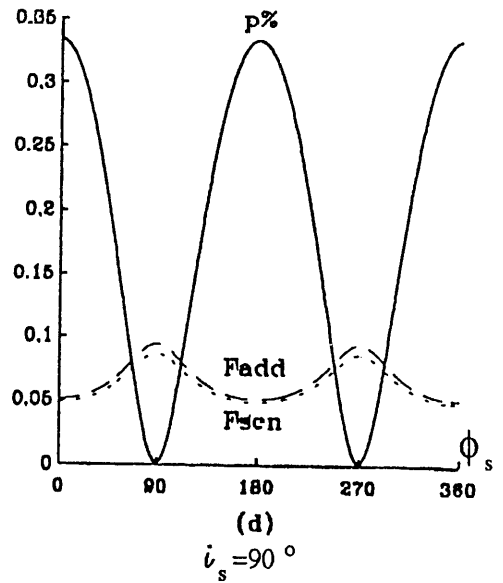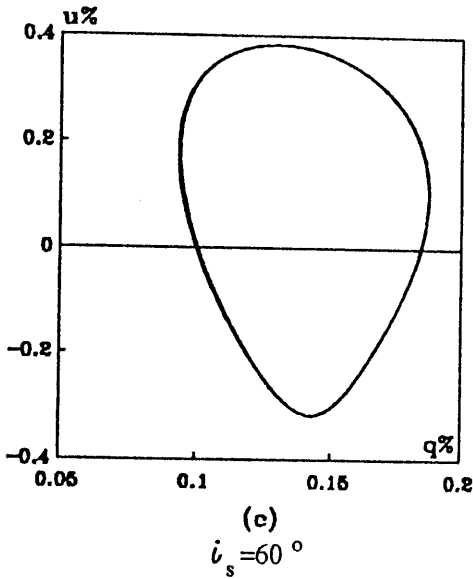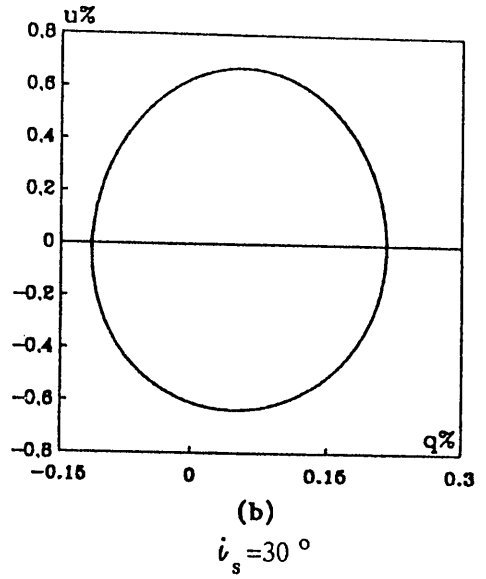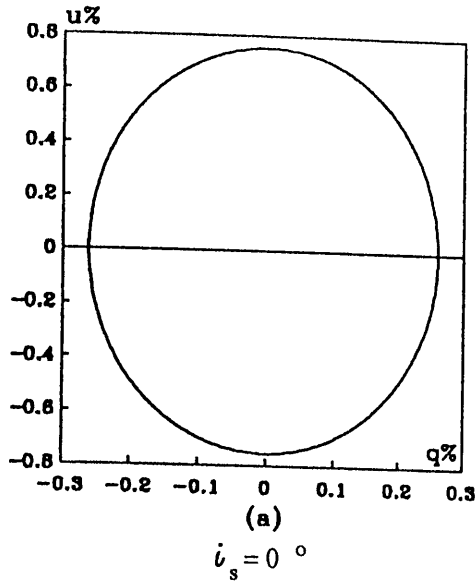
Fig. 3-10. The polarization in % from a binary of b=2 with a=c=1, with a co-rotating envelope of Ar=3, and i_e= i_s+90°, and different stellar inclinations (a) i_s= 0°, (b) i_s=30°, (c) i_s=60°, and (d) i_s=90°.
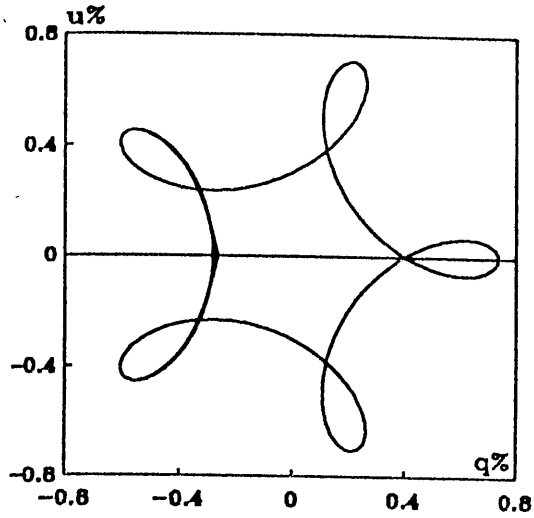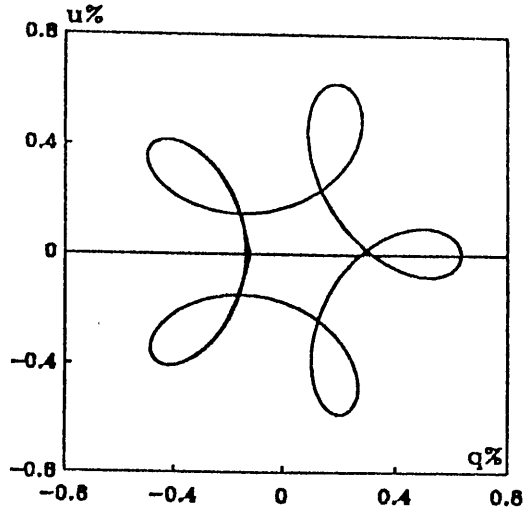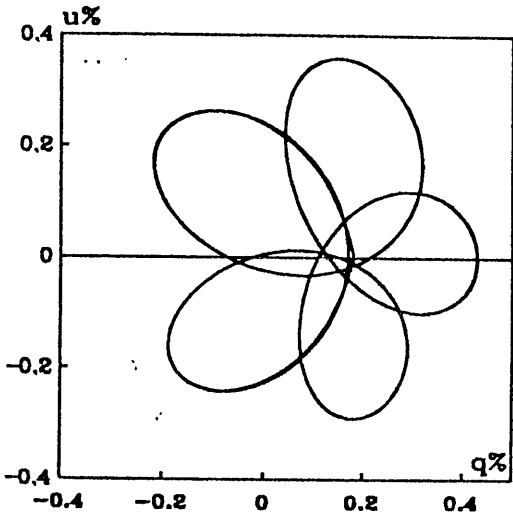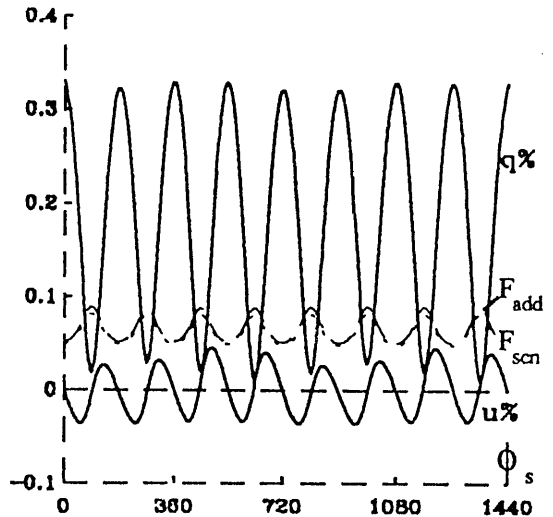
Fig. 3-11. The polarization in % from a binary of b=2 a=c=1, with slow rotating envelope of A_r=3 (the star rotates four times faster than the envelope), and i_e= i_s+90°, and different stellar inclinations (a) i_s= 0°, (b) i_s=30°, (c) i_s=60°, and (d) i_s=85°.
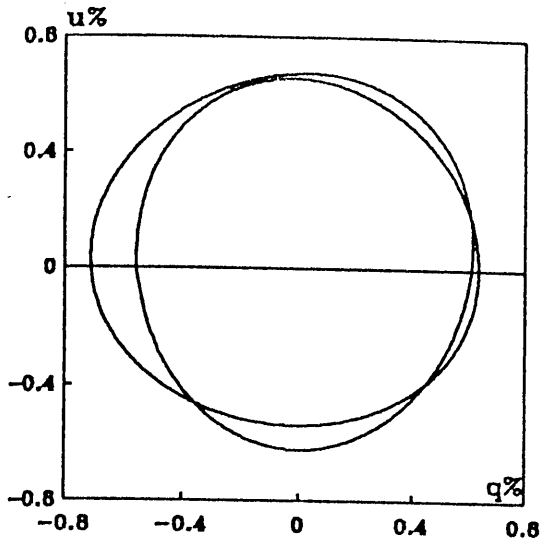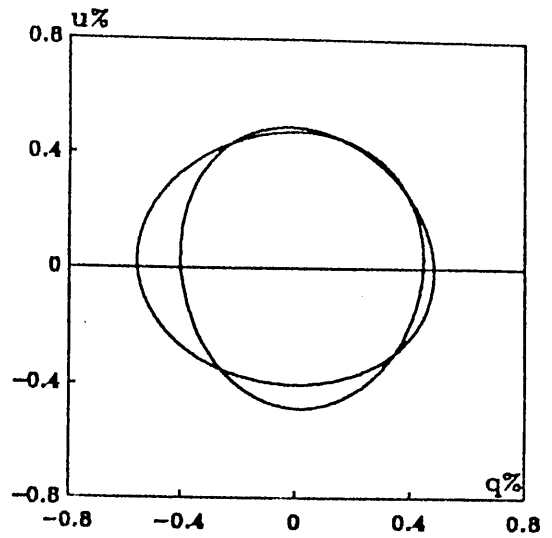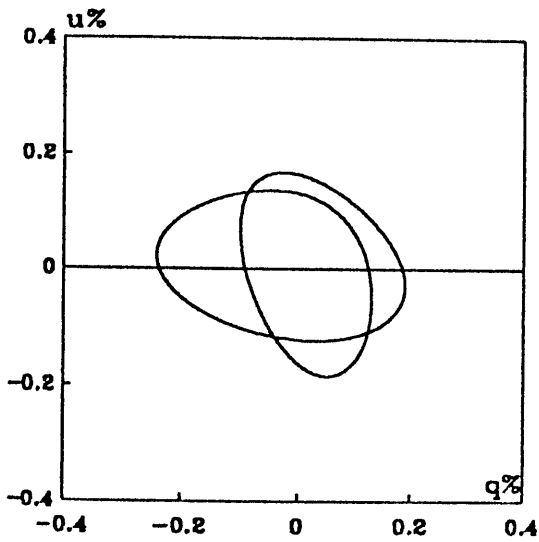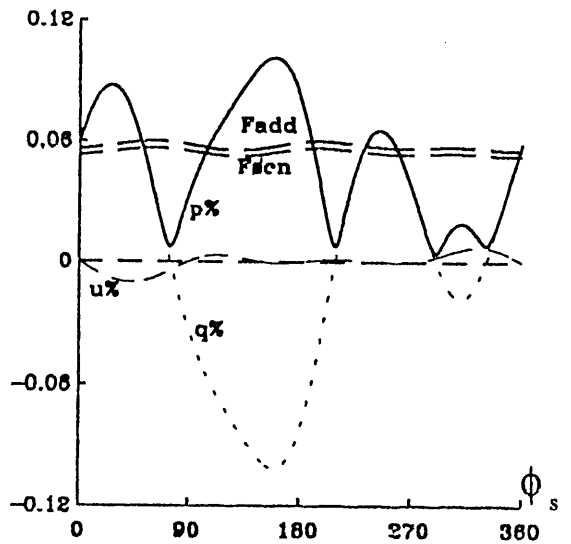
Fig. 3-12. The polarization in % from a star pulsating in its three axes (see the text), with a co-rotating envelope of Ar=3, and i_e= i_s+90°, and different stellar inclinations (a) i_s= 0°, (b) i_s=30°, (c) i_s=60°, and (d) i_s=85°.
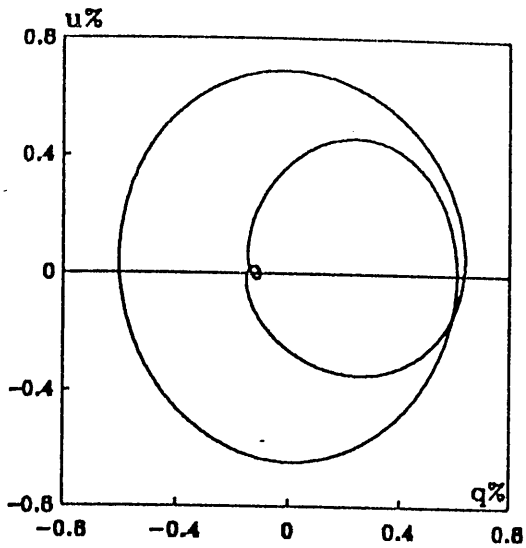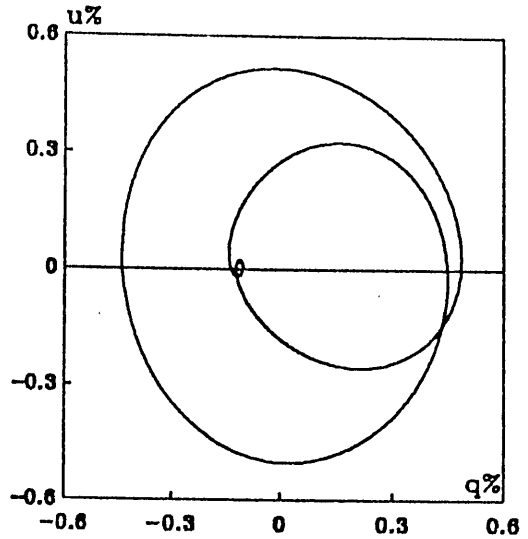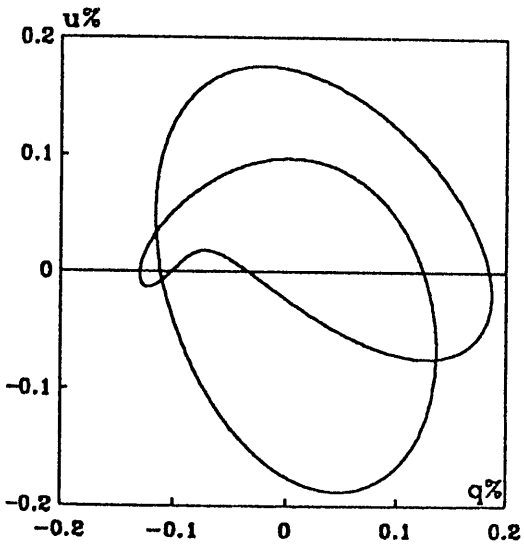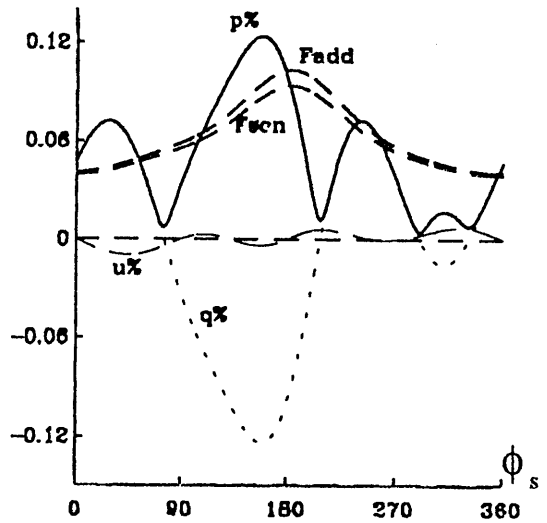
Fig. 3-13. The polarization in % from a star pulsating in its three axes, within an envelope which is expanding and contracting (see the text), and $i_e = i_s + 90°$, and different stellar inclinations (a) $i_s = 0°$, (b) $i_s = 30°$, (c) $i_s = 60°$, and (d) $i_s = 85°$.

some material or through magnetic or radiation pressure effects. The fractional distortion amplitude δ from spherical would have to be large enough to show its effects on the polarization. We use Eq. (3-26) for A_r i.e. $A_r = 3 + 2\cos(2\pi t/\Pi_p)$ for a star with the same value used for Figs. 12. A very small enhancement in the polarization is occurring for large i_s with changes in the qu-loci (*see* Figs. 3-13 a,b,c and d). At $i_e = i_s$ the results are expected to be similar to those for the binaries discussed above.

The normalized scattered flux F_{scn}, in general is less than 0.1 of the total flux, in all the cases discussed so far. Where F_{add} has a variation due to stellar rotation in most cases of about 0.05 of the total flux. In general, it will be difficult to tell directly from the polarimetric observation whether or not the envelope is spherical, however, more photometric (and if possible photographic) data about the scattering region will be needed, before applying this model to the data.

SUMMARY :

The results of Chapter two, for circumstellar polarization of scattered anisotropic starlight are generalized to include an arbitrary (rather than

spherical) envelope shape. Spherical harmonics are used to describe both the light source anisotropy and the density distribution functions. The maximum polarization from the extreme case of a flat disk-like star, viewed edge on, is increased from 20% (for spherical envelopes) to 35% for such stars within a disk-like envelope viewed face on, when all the observed light will be the scattered light.

Specific expressions for the Stokes parameters and scattered flux are obtained for the case of a uniform ellipsoidal stellar light source surrounded by an ellipsoidal envelope at a large distance from the source. These expressions are approximated to illustrate the dependence of the polarization on the shape of the star and the envelope. It is shown that observationally important polarization can arise in this way by scattering of light from stars with realistic degrees of distortion, both for non-spherical envelopes with a spherical star and vice versa. The polarization is computed for a rotating and a pulsating star with a fixed envelope. More complex loci in the qu-plane occur when both the star and the envelope are rotating.

CHAPTER FOUR

4. SPOTS

CONTENTS :

§4.1. THE SIZE OF THE SPOTS :

Starspot models are commonly used to describe the light variation of giants ,supergiants, and late-type dwarf stars (Bopp and Evans 1973, Vogt 1980, Fekel 1983 and Bopp 1987). These spots affect the isotropy of the light source, and so can produce polarization, the properties of which depends on the temperature, size and location of the spot.

Bright photospheric spots (where $T_{spot} > T_{star}$, e.g. granules or supergranules) can have temperatures above the stellar photosphere by up to 1000 K (Doherty 1986), and sizes as large as 10% of the stellar surface (Schwarzschild 1975). They can occur anywhere on the star and tend to be long-lived in the case of the giants. Dark photospheric spots (where $T_{spot} < T_{star}$, i.e. black spots) can be cooler than the star by up to 2000 K (Vogt 1981), with size up to 15% of the stellar surface, and occur within 60° north and south of the stellar equator (Bopp and Evans 1973).

Wilson et al. (1991) reported changes on the surface of α Ori. with the confirmation of hotspots. For three observing sessions (Feb. 1989; Jan. 1991; and Sep.

1991), Wilson *et al.* found in the first session a single hotspot, contributing 10% of the total flux. By the second session the star shows two spots, each approximately as bright as the original hotspot. In the last session, they again see a single hotspot, but this time it was considerably brighter (20% of the total flux).

Virtually any light curve can be generated by a suitably complex distribution of spots on a rotating star (Vogt 1981). So far, their polarization effects have not been studied in detail. In photometric studies it is common to consider projected spot area rotation only in terms of the cosine variation in the spot position angle. In this approximation the spot disappears totally when its center arrives at the limb — such as in the formulation of Bopp and Evans (1973) and the calculation of Vogt (1981). This assumption of a uniform hot spot with a cosine factor to describe the spot area was also used for polarimetric modelling of a hot spot presented by Gnedin *et. al.*(1976), Schwarz and Clarke (1984) and Doherty (1986). The approximation is acceptable for small spots (e.g. of angular extent $\psi < 5°$), but for larger spots we expect the projected spot area at the limb to have a more complicated position angle dependence as the spot crosses the limb, and also to vary with non-uniform temperature distribution within

the spot. This will affect both the light variation and the polarization.

Basically, the stellar polarization due to spots, is caused by scattering of light in a small solid angle (not by light scattering by all scatterers, as expected). To clarify this, we will take the case of a spherical envelope around a star with its rotation axis perpendicular to the line of sight, the star having an equatorial spot of angular size ψ (at the star center). When the spot is centered on the line of sight, there will be no contribution to polarization, because of polarization cancellation. But when the spot is on the limb of the star, the observer will see half of the spot, and because the spot is the source of anisotropy (on an otherwise spherical star), we expect the polarization will be due only to the light of the spot scattering by the scatterers of the envelope. However, only the scatterers on altitude θ_{alt} between $90°+\psi$ and $-(90°+\psi)$ - measured from the stellar equator - will be illuminated by the spot (see Fig. 4-1). But the polarization produced by the light scattered within $90° \leq \theta_{alt} \leq -90°$ (i.e scattering in a hemisphere so large, with a small star) will be reduced to zero due to the cancellations. But the polarization produced by scattering in the solid angle within $90° \leq \theta_{alt} \leq 90°+\psi$ above and below the equator, will have different

position angles resulting in incomplete polarization cancellations. Thus this solid angle of scatterers will produce an observable polarization, whose degree clearly depends on the size of the spot.

In this Chapter we will calculate the polarization from a point source star with spots, by using the result of the last two Chapters (two and three), which modelled the effects of source anisotropy and of the scatterer density distribution.

§4.2. THE GENERAL FORMULATION :

First we define four coordinate systems centered on the star as in Sec. 3-2, *see* Fig. 4-2:

I- The observer's frame (x,y,z) with spherical coordinates (r,θ,ϕ), the line of sight being the Oz-axis

II- The star's frame (X,Y,Z) with spherical coordinates (r,Θ,Φ), where OZ is a convenient stellar axis (such as rotation) lying in the x-z plane of the observer's frame with an inclination of i_s. This system is rotated by the azimuth angle Φ_s in the stellar frame. As in Sec. 2.2, θ is then the scattering angle, and ϕ the polarization angle (direction) , relative to Oz for any scattering point.

III- The spot's frame (x_s,y_s,z_s) with spherical coordinates (r,θ_s,ϕ_s), where the spot is on Oz_s-axis.

This system is rotated relative to the observer one through Euler angles (α, β, γ) (*cf*. Sec. 2.2 and Messiah 1961).

IV- The envelope frame (X', Y', Z') with spherical coordinates (r, θ', Φ'). This frame can be rotated from the observer frame by another set of Euler angles.

The center of any spot of angular radius ψ is at (θ_{sp}, Φ_{sp}) in the stellar frame and (θ_{sp}, ϕ_{sp}) in the observer frame. By keeping the assumption of a small point light source (compared to the size of the envelope), the scattered flux will depend on the projected area and brightness of both the star and the spots seen from the scatterers. We assume the spot to be circular in spherical stars as in most of the previous work (*see* e.g. Schwarz and Clarke 1984). The projected area of such a circular spot varies as the star rotates (depending on the angle θ_{sp} between the normal to the spot area and the line of sight) first as an ellipse by projection then to more complicated shapes as the spot crosses the limb of the star.

Using Eq. (2-1) of Sec. 2-2 for the general case of on anisotropic point light source $F'(r, \theta, \phi)$ and arbitrary distribution particles density function $n(r, \theta, \phi)$, we can write the (un-normalized) scattered flux and Stokes parameters (F_{sc}, Q, U) of the scattered

The source of the polarization

This part will not illuminated by the spot

The polarization cancellation occurs here

The star

The spot

ψ

ψ

The source of the polarization
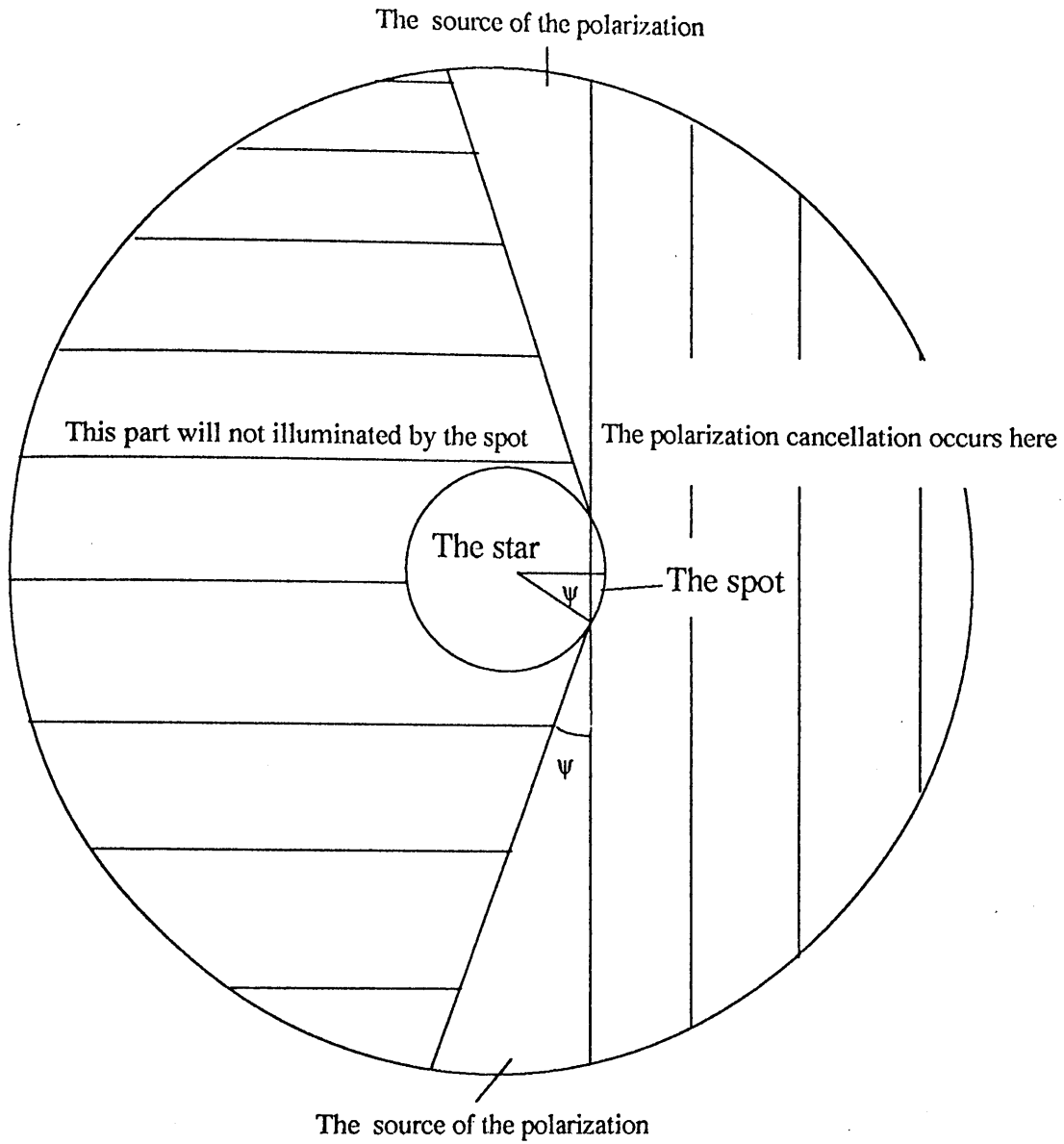
Fig. 4-1. A spot of size ψ at the stellar limb is illuminating only the scatterers in a solid angle of $\Omega = \psi$, within an altitude ϕ_{alt} between $90^\circ \leq \phi_{alt} \leq 90^\circ + \psi$ above and below the stellar equator.
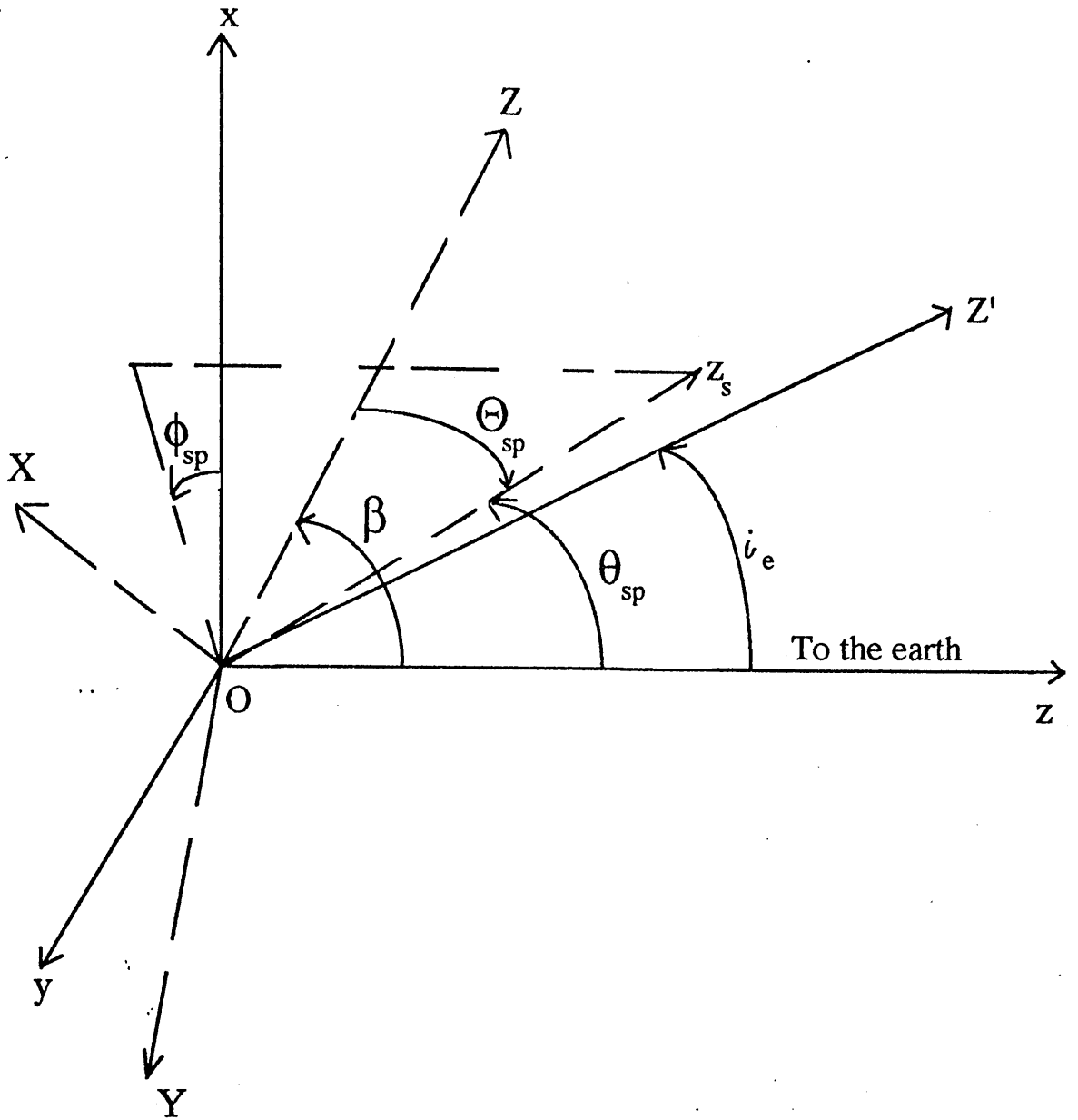
Fig. 4-2. The four coordinate systems, where
Oz_s-axis is the normal to the spot's area, OZ-axis is
the rotation axis of the star, OZ'-axis is the
rotational symmetric axis of the envelope, and Oz-axis
is the observer direction.

radiation at the Earth (distance D) as :

$$\left.\begin{matrix} F_{sc} \\ z^* \end{matrix}\right\} = \frac{1}{2 \ k^2 \ D^2} \ \iiint \ n(r,\theta,\phi) \ F'(r,\theta,\phi) \ r^2$$

$$\times \ \begin{cases} (i_1 + i_2) \\ (i_1 - i_2) \exp(-2i\phi) \end{cases} \qquad dr \ \sin\theta \ d\theta \ d\phi \quad (4\text{-}1)$$

with the same definitions as for Eq. (2-1).

For a star with spots $F'(r,\theta,\phi)$ describes the flux of both the star and the spot, and can be given in the form :

$$F'(r,\theta,\phi) = \frac{I_*}{r^2} + F(r,\theta,\phi) \qquad\qquad (4\text{-}2)$$

The function $F(r,\theta,\phi)$ in Eq. (4-2) describes the radiative properties of the spot (compared to the star) in the observer's frame, but we should naturally describe F in the spot coordinate system (r,θ_s,ϕ_s). Providing that F is a smooth function, we may express it in terms of spherical harmonics, viz :

$$F(r,\theta_s,\phi_s) = \sum_{\ell=0}^{\infty} \ \sum_{m=-\ell}^{m=\ell} F_{\ell m}(r) \ Y_{\ell m}(\theta_s,\phi_s) \qquad (4\text{-}3)$$

Using the rotation matrices described by Messiah (1962) to convert from the spot's frame (θ_s,ϕ_s) to the observer's frame (θ,ϕ)), we obtain the flux as a function of θ and ϕ :

$$F(r,\theta,\phi) = \sum_{\ell=0}^{\infty} \sum_{m=-\ell}^{m=\ell} F_{\ell m}(r) \sum_{n=-\ell}^{n=\ell} R_{nm}^{(\ell)}(\alpha,\beta,\gamma) \; Y_{\ell n}(\theta,\phi) \qquad (4-4)$$

For the particle density distribution n, we can in general express n in the observer frame as :

$$n(r,\theta,\phi) = \sum_{\ell'=0}^{\infty} \sum_{m'=-\ell'}^{m'=\ell'} n_{\ell' m'}(r) \; Y_{\ell' m'}(\theta,\phi) \qquad (4-5)$$

The $Y_{\ell m}(\theta,\phi)$ in Eqs. (4-4 and 4-5) are the spherical harmonics (see Sec. 2-2 and Sec. 3-2, see also Appendix D).

We can express the scattering function factors as :

$$1+\cos^2\theta = \frac{4}{3}\left[\sqrt{4\pi}\; Y_{00} + \sqrt{\frac{\pi}{5}}\; Y_{20}(\theta,\phi)\right] \qquad (4-6)$$

and ,

$$\sin^2\theta \; \exp(-2i\phi) = 4\sqrt{\frac{2\pi}{15}}\; Y_{22}^*(\theta,\phi) \qquad (4-7)$$

By substituting the above expressions in the integrals contained in Eq. (4-1), and using the properties of spherical harmonics, F_{sc} and Z^* can be written as:

$$F_{sc} = \frac{\sigma}{4\pi D^2}\left\{ \sqrt{4\pi}\, N_{00} + \sqrt{\frac{\pi}{5}}\, N_{20} + \sum_{\ell\, m\, n} R_{nm}^{\ell}(\alpha,\beta,\gamma) \sum_{\ell'\, m'} \right.$$

$$\left. \times \left[\sqrt{4\pi}\, C_{\ell\ell'\, nm'}^{00} + \sqrt{\frac{\pi}{5}}\, C_{\ell\ell'\, nm'}^{20}\right] S_{\ell\ell'\, mm'} \right\} \qquad (4-8)$$

and

$$Z^* = \frac{3}{4\pi} \frac{\sigma}{D^2} \sqrt{\frac{2\pi}{15}} \left\{ N_{22} + \right.$$

$$\left. \sum_{\ell \, m \, n} R^{\ell}_{nm}(\alpha,\beta,\gamma) \sum_{\ell' \, m'} C^{22}_{\ell\ell' \, nm'} \, S_{\ell\ell' \, mm'} \right\} \qquad (4\text{-}9)$$

where $C^{LM}_{\ell\ell' \, mm}$ are Clebsh-Gordon coefficients , arising from the products of two spherical harmonics , with the properties given in Sec. 3-2 (*cf.* Messiah 1962).

$$S_{\ell\ell' \, mm'} = \int_0^{\infty} F_{\ell m}(r) \quad n_{\ell' \, m'}(r) \; r^2 \; dr \qquad (4\text{-}10)$$

where,

$$F_{\ell m}(r) = \int_{-1}^{1} \int_0^{2\pi} F(r,\theta s,\phi s) \; Y^*_{\ell m}(\theta s,\phi s) \quad d\cos\theta s \; d\phi s \qquad (4\text{-}11)$$

,

$$n_{\ell' \, m'}(r) = \int_{-1}^{1} \int_0^{2\pi} n(r,\theta',\phi') \; Y^*_{\ell' \, m'}(\theta',\phi') \quad d\cos\theta' \, d\phi' \qquad (4\text{-}12)$$

and,

$$N_{\ell' \, m'} = I_* \int_0^{\infty} n_{\ell' \, m'}(r) \quad dr \qquad (4\text{-}13)$$

Eqs. (4-11 to 4-13) describe the effects of each function (F and n) in the appropriate spot and envelope frame (*cf.* Simmons 1982).

Now we can study the effects of anisotropy in both the flux F and the density distribution function n separately, showing how their interplay produces polarization. Next we will define F for the case of spots.

§4.3. THE PROJECTED AREA OF A SPOT:

The above expressions are general for any flux function and density distribution function and so can describe the case of a star with a spot. We can define F in the spot frame as:

$$F(r,\theta s,\phi s) = \frac{I_*}{r^2} \zeta \; \mathfrak{A}_{sp}(\theta s,\phi s) \qquad (4\text{-}14)$$

where ζ is a ratio of the extra brightness due to the presence of the spot to the total stellar flux, which can approximated safely by :

$$\zeta = \frac{T_{sp}^4 - T_*^4}{\pi \; T_*^4} \qquad (4\text{-}15)$$

with T_{sp} the spot temperature and T_* is the photosphere temperature. $\mathfrak{A}_{sp}(\theta s,\phi s)$ is the spot's projected area as seen in the direction $(\theta s,\phi s)$ of the scatterer. This area depends on the angle θs between the normal to the spot surface and the scattering particle only (i.e. independent of ϕs), this angle θs is also a latitude of a scattering particle. For simplicity we will express $\mathfrak{A}_{sp}$ for two cases (*see* Fig 4-3a&b), the first when the whole spot is observable in the direction $(\theta s,\phi s)$ (i.e. $|\theta s| \leq \pi/2-\psi$, where ψ is the spot angular reduce). Then the projected area will be :

$$\mathfrak{A}_{sp1}(\theta s,\psi) = \pi \; r_*^2 \; \sin^2\psi \; \cos\theta s \qquad (4\text{-}16a)$$

where $r_{sp} = r_\star \sin \psi$ (4-16b)

The second case is when the spot starts to disappear at the stellar limb $(\pi/2-\psi \leq |\theta_s| \leq \pi/2+\psi)$. To calculate the projected area of the spot, we have to calculate three areas, (1) the total projected area of the spot at that position, (2) the area of the spot (cross hatched in Figs. 4-3a&b) which is hidden behind the star $\mathfrak{A}_{hid}$, this area to be subtracted from the previous area, (3) the area of the sector of the stellar limb which is seen by the observer as a part of the disappearing spot (shaded in Figs. 4-3a&b). This area $\mathfrak{A}_{limb}$ clearly should be added to the total area of the projected spot. First we will calculate the projected area of the hidden segment of the spot, which has an angle at the spot center θ_{sg} given by :

$$\theta_{sg} = \cos^{-1}(\cot \theta_s \; \cot \psi)$$ (4-17a)

with θ_{sg} in radians The projected area of the hidden segment of the spot is:

$$\mathfrak{A}_{hid} = r_\star^2 \sin^2 \psi \; \cos \theta_s \; (\theta_{sg} - \sin \theta_{sg} \; \cos \theta_{sg})$$ (4-17b)

The contribution of the limb of the star is given by a segment seen by the observer to have an angle at the star center of $\theta_{sg\star}$ given by:

$$\theta_{sg\star} = \cos^{-1}\left(\frac{\cos \psi}{\sin \theta_s} \right)$$ (4-17c)

(again $\theta_{sg\star}$ in radian). Next we can calculate the
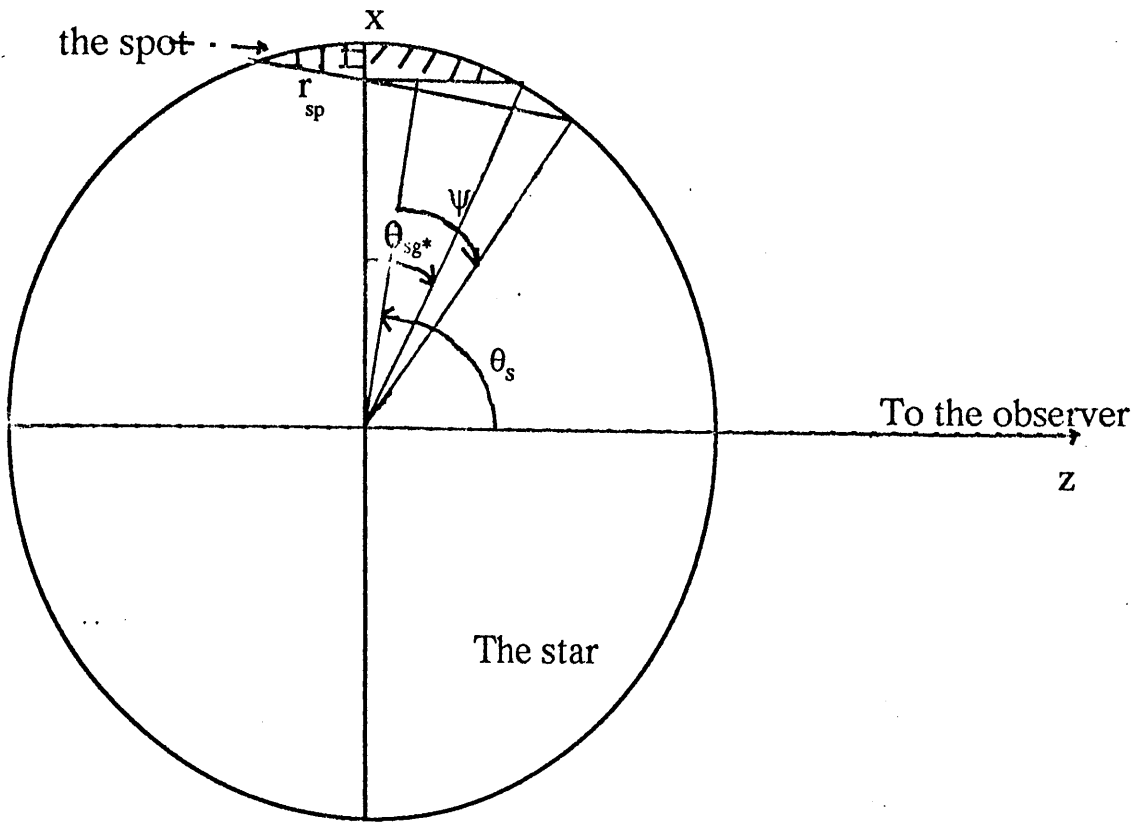
Fig. 4-3a. The star as seen from OX-direction, where the observer in the OZ-direction (for simplicity). We see the spot cross section, as comprising three areas, 1) the part of the spot which will hide behind the star (cross hatched), 2) the projection of the rest of the spot's area (white), and 3) the segment of the limb of the star which will observed by the observer as a part from the spot with the same properties of the spot (shaded).
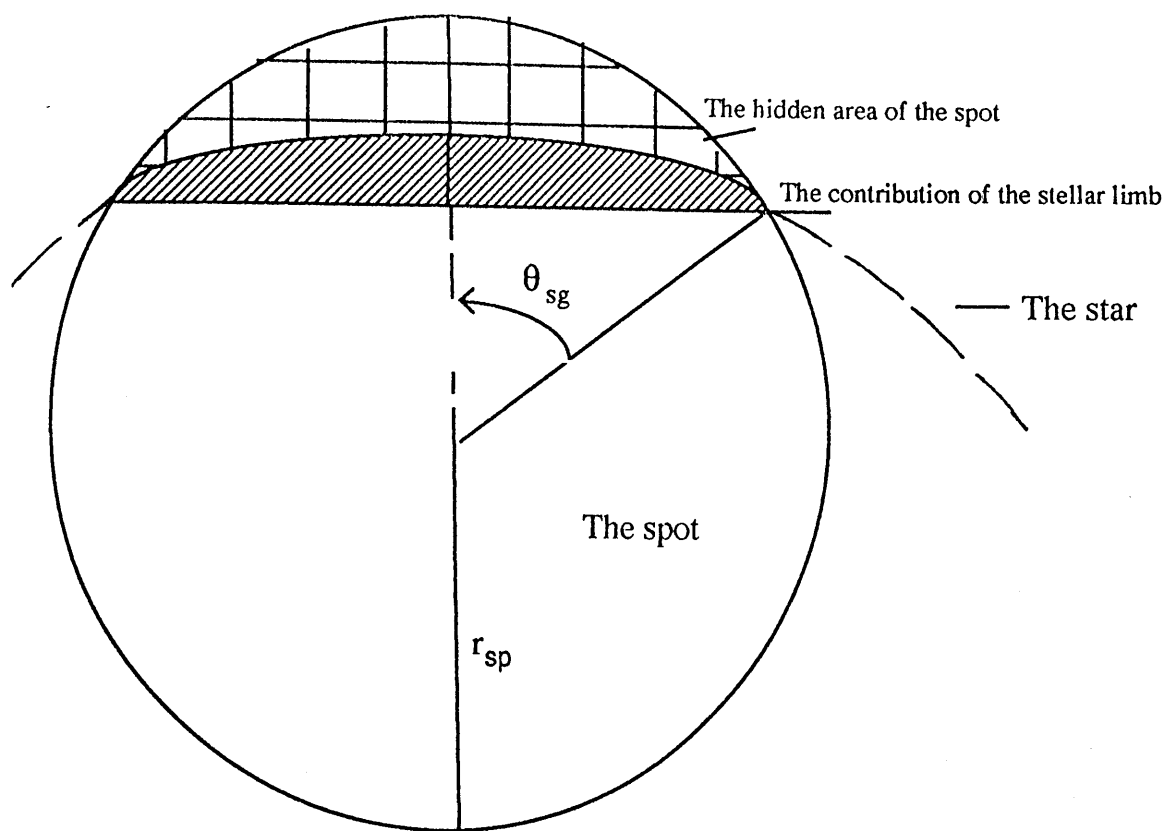
Fig. 4-3b. The spot face on with its three areas, and the angle θ_{sg}.

segment of the stellar limb observed as part of the disappearing spot as:

$$\mathfrak{A}_{lmb} = r_*^2 \left(\theta_{sg*} - \frac{\sin \theta_{sg*}}{\cos \theta_{sg*}} \right) \qquad (4\text{-}17d)$$

So the projected area of the spot when it has started to disappear until it is totally hidden (i.e. $\pi/2 - \psi \leq |\theta_s| \leq \pi/2 + \psi$) will be:

$$\mathfrak{A}_{sp2}(\theta_s, \psi) = \pi\, r_*^2\, \sin^2\psi\, \cos\theta_s - \mathfrak{A}_{hid} + \mathfrak{A}_{lmb} \qquad (4\text{-}17e)$$

Thus the spot projected area will be :

$$\mathfrak{A}_{sp}(\theta_s, \psi) = \begin{cases} \mathfrak{A}_{sp1}(\theta_s, \psi) & 0 \leq |\theta_s| \leq \pi/2 - \psi \\ \mathfrak{A}_{sp2}(\theta_s, \psi) & \pi/2 - \psi \leq |\theta_s| \leq \pi/2 + \psi \\ 0 & |\theta_s| \geq \pi/2 + \psi \end{cases} \qquad (4\text{-}18)$$

Since there is no dependence of ϕ_s, the spherical harmonics in Eqs. (4-11) will have m=0. So we can rewrite Eq. (4-11) as :

$$F_{\ell 0}(r) = \frac{I_*}{r^2} \zeta \left(\int_0^{\pi/2-\psi} \int_0^{2\pi} \mathfrak{A}_{sp1}(\theta_s, \psi)\ Y^*_{\ell 0}(\theta_s, \phi_s) \ + \right.$$
$$\left. \int_{\pi/2-\psi}^{\pi/2+\psi} \int_0^{2\pi} \mathfrak{A}_{sp2}(\theta_s, \psi)\ Y^*_{\ell 0}(\theta_s, \phi_s) \right) \sin\theta_s\, d\theta_s\, d\phi_s$$
$$(4\text{-}19)$$

Here we will again use the ellipsoidal circumstellar envelope model of Simmons 1982 (see Sec. 3-3), with an inclination angle i_e between the axis of symmetry Z'-axis of the envelope (the polar axis) and the line of sight, and an azimuthal angle ϕ_e (see Fig. 4-2). We then have :

$$n_{\ell,m'}(r) = 2\pi \ (R_1 - R_2) \ n_0 \ K_{\ell'} \ Y_{\ell,m'}(i_e, \phi_e) \qquad (4\text{-}20)$$

where we define :

$$n(r, \theta', \Phi)' = \begin{cases} n_0 & \text{when} \quad r_2(\mu) \le r \le r_1(\mu) \\ 0 & \text{otherwise} \end{cases} \qquad (4\text{-}21a)$$

Here n_0 is the number of particles within the column bounded by r_1 and r_2, where :

$$r_{1',2}(\mu) = \frac{R_{1,2}}{\sqrt{1 + (A_r^2 - 1) \ \mu^2}} \qquad (4\text{-}21b)$$

and $\quad \mu = \cos(\zeta) \qquad (4\text{-}21c)$

R_1 and R_2 are the outer and inner equatorial axis length , and A_r is the ratio of the length of the equatorial axis to the polar axis. The angle ζ is the angle between the radius vector and the axis of symmetry, which is related to our frames by the addition theorem of spherical harmonics (this explains the appearance of $Y_{\ell,m'}(i_e, \phi_e)$ in Eq. (4-20), see Simmons 1982, Sec. 3-3, and Jackson 1975). Finally $K_{\ell'}$ is given by:

$$K_{\ell'} = \int_{-1}^{1} \frac{P_{\ell'}(\mu)}{\sqrt{1 + (A_r^2 - 1) \ \mu^2}} \ d\mu \qquad (4\text{-}22)$$

Inserting Eqs. (4-19 to 4-22) in Eq. (4-10), we obtain :

$$S_{\ell\ell'0m'} = 2\pi \ I_* \ (R_1 - R_2) \ n_0 \ f_{\ell 0} \ K_{\ell'} \ Y_{\ell,m'}(i_e, \phi_e) \qquad (4\text{-}23a)$$

where,

$$f_{\ell 0} = \zeta \left(\int_0^{\pi/2-\psi} \int_0^{2\pi} \mathfrak{U}_{sp1}(\theta_s,\psi) \; Y_{\ell 0}^*(\theta_s,\phi_s) \; + \right.$$

$$\left. \int_{\pi/2-\psi}^{\pi/2+\psi} \int_0^{2\pi} \mathfrak{U}_{sp2}(\theta_s,\psi) \; Y_{\ell 0}^*(\theta_s,\phi_s) \right) \sin\theta_s \; d\theta_s \; d\phi_s$$

$$(4-23b)$$

Now the factors $f_{\ell 0}$ are functions of the spot's size and position only (i.e. of ψ and θ_s). Moreover, the factors K_ℓ, are (as in Sec. 3-3) functions of the envelope shape and size only (i.e. of A_r). The dependence of the polarization on these two factors is affected by whether the two functions enhance or offset one another.

From the properties of Euler angles, we can choose α as ϕ_s, which measures the rotational position of the star relative to the observer (see Fig. 4-2), β as the latitude of the spot θ_{sp} in the observer frame (the angle between the normal to the spot area and the line of sight Oz-axis). This angle is given by :

$$\cos\theta_{sp} = \cos i_s \; \cos\Theta_{sp} + \sin i_s \; \sin\Theta_{sp} \; \cos\Phi_s \quad (4-24)$$

where i_s is the inclination of the star, Θ_{sp} the latitude of the spot in the stellar frame and Φ_s the rotation angle of the star in the stellar frame (i.e. of the spot, since we deal with spherical stars), and finally we choose $\gamma = 0$.

To normalize the scattered flux and Stokes parameters, we have to divide them by the total flux

received F_{tot}, which comprises the combination of the scattered flux F_{sc} plus the direct flux from the star and spot. This latter component is a combination of the flux of the star and of the temperature difference due to the spot ($F_{dir*}+F_{dirsp}$) which is given by I_*/D^2 [1 $+\zeta\, \mathfrak{A}_{sp}(\theta_{sp},\psi)]$, where $\mathfrak{A}_{sp}$ here is the projected area of the spot seen from the Earth for $\theta_s = \theta_{sp}$, with the dependence on ϕ_s through θ_{sp}. The angular size of the spot ψ is independent of the frame. So we have to divide by F_{tot}, which is given by I_*/D^2 F_{norm}, and the latter is the normalization factor :

$$F_{norm} = 1 + \zeta\, \mathfrak{A}_{sp}(i_s,\phi_s) + (D^2/I_*)\, F_{sc} \qquad (4-25)$$

Then the general expressions for the normalized scattered flux and Stokes parameters (F_{scn} and Z_n^*, respectively) are :

$$F_{scn} = \frac{\tau}{4\pi\, F_{norm}} \left\{ \sqrt{4\,\pi}\, K_0 Y_{00}(i_e,\phi_e) + \sqrt{\frac{\pi}{5}}\, K_2\, Y_{20}(i_e,\phi_e) + \right.$$

$$+ \sum_{\ell\, n} R_{n0}^{\ell}(\phi_s,\theta_{sp},0)\, f_{\ell 0} \sum_{\ell'\, m'} K_{\ell'}\, Y_{\ell',m'}(i_e,\theta_e)$$

$$\left. \times \left[\sqrt{4\,\pi}\, C_{\ell\ell',nm'}^{00} + \sqrt{\frac{\pi}{5}}\, C_{\ell\ell',nm'}^{20} \right] \right\} \qquad (4-26)$$

and

$$Z^\star = \frac{3}{4\pi} \frac{\tau}{F_{norm}} \sqrt{\frac{2}{15}\pi} \left\{ K_2 Y_{22}(ie, \theta e) + \right.$$

$$\left. \sum_{\ell}\sum_{n} R_{n0}^{\ell}(\phi s, \theta s p, 0)\ f_{\ell 0} \sum_{\ell'}\sum_{m'} C_{\ell\ell'nm'}^{22}\ K_{\ell'}\ Y_{\ell'm'}(ie, \phi e) \right\}$$

$$(4-27)$$

where τ is the average envelope optical depth, equal to $(\sigma\ 2\pi\ (R_1-R_2)\ n_0\ )$, see Simmons (1982). However, the summation in Eqs. (4-26) and (4-27) will be similar to the summation in Eqs. (3-14a) and (3-14b), respectively.

The degree of polarization $p = |Z_n^\star| = |Z_n|$, and the polarization direction is given by $\phi_P = \frac{1}{2}$ arg Z.

Due to the symmetry of $f_{\ell 0}$ and $K_{\ell'}$, they are non-zero only for ℓ and ℓ' even. The convergence of $K_{\ell'}$ is discussed in Sec. 3-4 (see also Simmons 1982), which shows that summation up to $\ell'=2$ only is an acceptable approximation. In the case of $f_{\ell 0}$ all the harmonics of $\ell > 2$ for $f_{\ell 0}$ are important for $\psi > 45°$ (see Fig. 4-4). So for a physical spot size (i.e $\psi \le 30°$) an approximation to $\ell = 2$ is acceptable. So for $\ell = \ell' = 2$, F_{scn}, and Stokes' parameters will be given as :

$$F_{scn} = \frac{\tau}{4\pi\ F_{norm}} \left[\sqrt{4\ \pi}\ K_0 Y_{00}(ie,\phi e) + \sqrt{\frac{\pi}{5}}\ K_2\ Y_{20}(ie,\phi e)\ + \right.$$

$$\sqrt{4\ \pi} \left\{ \quad S_0^{22\ 2-2}\ C_{22\ 2-2}^{00} \quad + \right.$$

$$S_0^{22\ 1-1}\ C_{22\ 1-1}^{00} + \qquad S_0^{22\ 00}\ C_{22\ 00}^{00}\ +$$

$$S_0^{22\ -11}\ C_{22\ -11}^{00} + \qquad S_0^{22\ -22}\ C_{22\ -22}^{00} +$$

$$\left. S_0^{00\ 00}\ C_{00\ 00}^{00} \right\} \ + \ \sqrt{\frac{\pi}{5}}\ \left\{ S_0^{02\ 00}\ C_{02\ 00}^{20} \quad + \right.$$

$$S_0^{22\ 2-2}\ C_{22\ 2-2}^{20} + \qquad S_0^{22\ 1-1}\ C_{22\ 1-1}^{20} +$$

$$S_0^{22\ 00}\ C_{22\ 00}^{20}\ + \qquad S_0^{22\ -11}\ C_{22\ -11}^{20} +$$

$$\left. \left. S_0^{22\ -22}\ C_{22\ -22}^{20} + \qquad S_0^{20\ 00}\ C_{20\ 00}^{20} \right\} \right]$$

$$(4-28)$$

and

$$Z^* = \frac{3\ \tau}{4\pi\ F_{norm}}\ \sqrt{\frac{2\ \pi}{15}}\ \left\{ K_2\ Y_{22}(ie,\theta e)\ +\ S_0^{02\ 02}\quad C_{02\ 02}^{22} + \right.$$

$$S_0^{22\ 20}\quad C_{22\ 20}^{22}\ +\ S_0^{22\ 11}\ C_{22\ 11}^{22}\quad +$$

$$\left. S_0^{22\ 02}\quad C_{22\ 02}^{22}\ +\ S_0^{20\ 20}\ C_{20\ 20}^{22}\quad \right\}$$

$$(4-29)$$

where,

$$S_{m=0}^{\ell\ell'\ nm'} = R_{n0}^{\ell}(\phi s,\theta sp,0)\ f_{\ell 0}\ K_{\ell'}\ Y_{\ell',m'}(ie,\theta e)$$

$$(4-30)$$

§4.4. DISCUSSION:

In general the polarization increases as the spot (e.g. hot spot) size (ψ) increases, reaching a maximum at $\psi=45°$, the polarization variation with ψ is similar to f_{20} variation with ψ in Fig. 4-4. For larger spots $f_{\ell 0}$ of $\ell > 2$ have to be considered (see Fig. 4-4).

In the following discussion we will consider spot sizes up to $\psi=30°$, which allows the approximation of ℓ and $\ell' \leq 2$. Next we will discuss the effect of the temperature difference ΔT and the spot location θ_{sp} on the polarization, then calculate the qu-loci for fixed envelopes (spherical and non-spherical with different i_e's), rotating envelopes (with different speeds), and finally for time variable spots and for stars with more than one spot.

The polarization from hot spots has the opposite sign to that from cool spots. Also the polarization from the former is larger for the same $|\Delta T|$ because the fractional change in brightness is greater. Fig. 4-5 shows the polarization variation with ΔT for light scattering by a spherical envelope from a fixed star with an equatorial spot of size $\psi=15°$ located on the limb of star (i.e. $\theta_{sp}=0°$ and $\phi_s=90°$). To show some examples of polarization variations, we choose $i_s=45°$

150
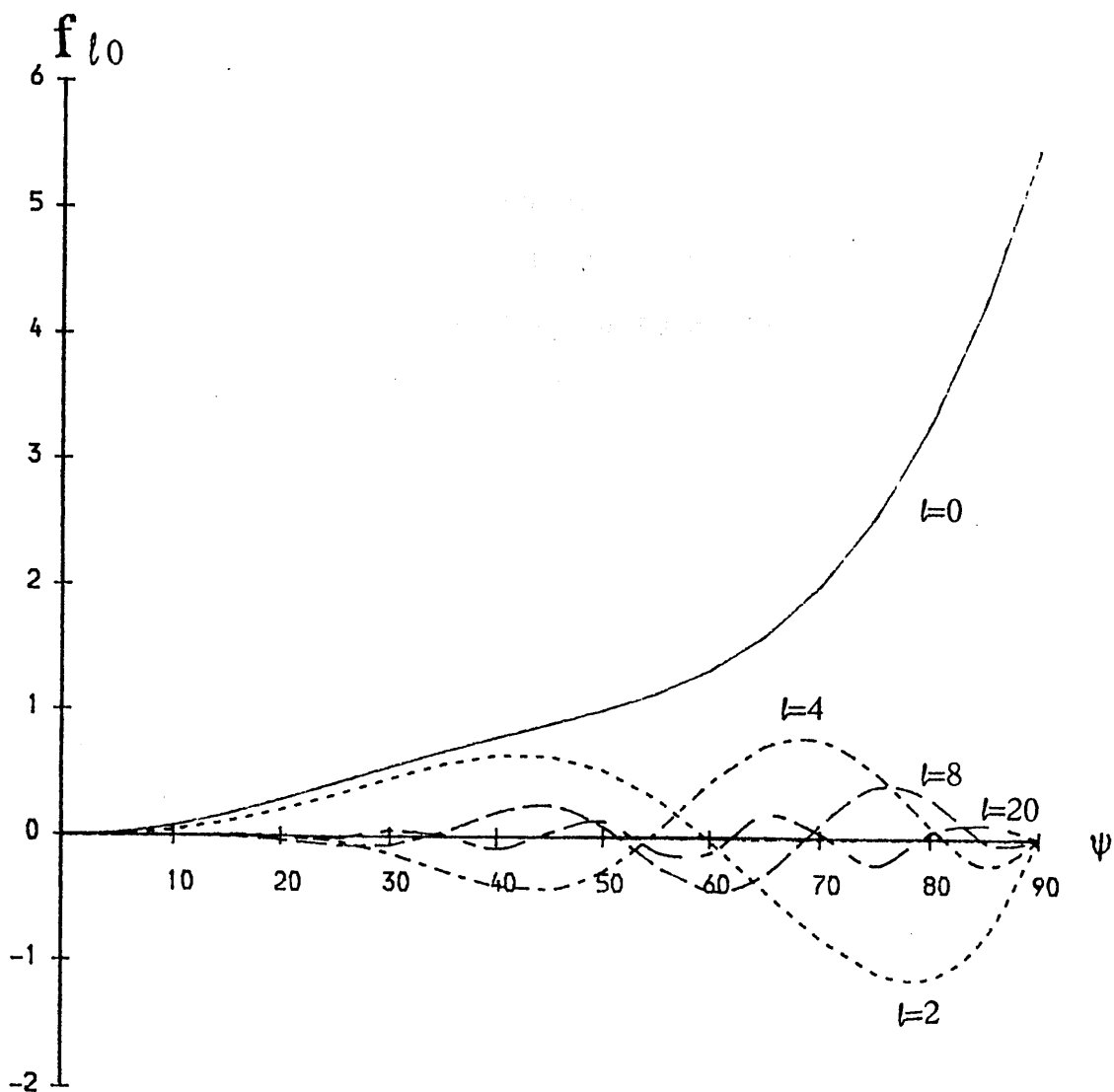
Fig. 4-4. The values of $f_{\ell 0}$ for different spherical harmonics as the spot's size ψ increases.

(the case of $i_s=0°$ will be discussed later). The total added flux F_{add}, is here a combination of the scattered flux and the direct flux of the spot due to the ΔT ($F_{add} = F_{tot}-1$) increasing up to about 25% of F_{tot} as as ΔT increases, while the normalized scattered flux F_{scn} is constant with a value of about 0.9% of F_{tot}.

For the same values as above, but with fixed ΔT of -1000 K (cool spot), Fig. 4-6 shows the variation of polarization p with θ_{sp}, which takes its maximum value, when the spot is at the equator, of -0.02%. The F_{add} has a variation like the variation of p with a maximum of 15.5% of F_{tot}, but F_{scn} is constant at about 0.9% of F_{tot}.

Of course, when $i_s=0°$ and $\phi_s=90°$, the polarization will have the same value as θ_{sp} varies, the only changes will occur in the polarization position angle. On the another hand, when $i_s=0°$ and $\phi_s=0°$ (the spot on the line of sight) there will be no polarization at all, due to polarization cancellations. Such polarization variation is equivalent to that expected from a cloud of electrons (or general cloud of scatterers) rotating about the stellar equator, as in the results of Brown *et al.* (1978) (*see also* Clarke & McGale 1986).

In the following we will study the qu-loci for
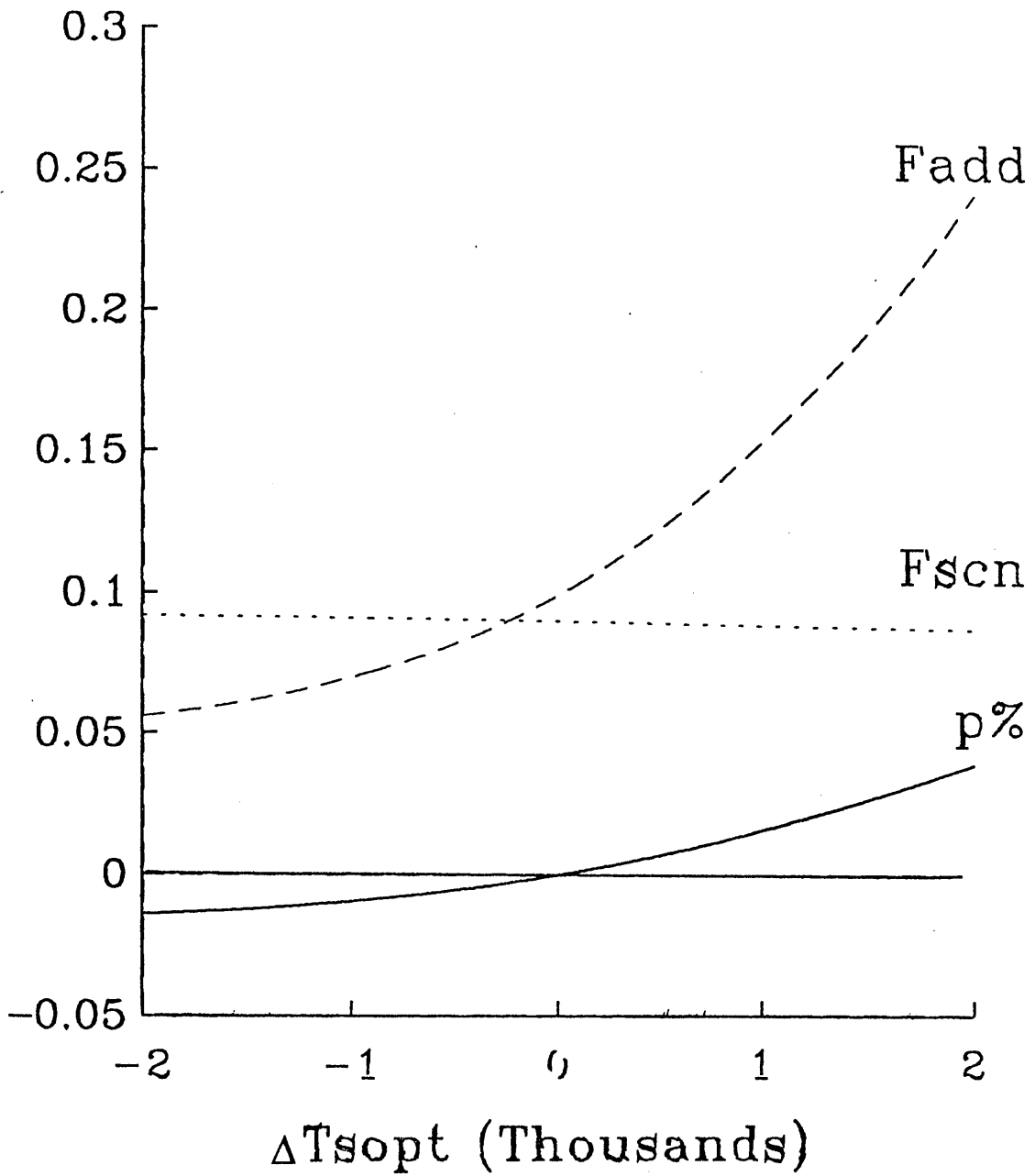
Fig. 4-5. The polarization p%, Fscn, and Fadd as function of ΔT (the temperature different between the star and the spot).
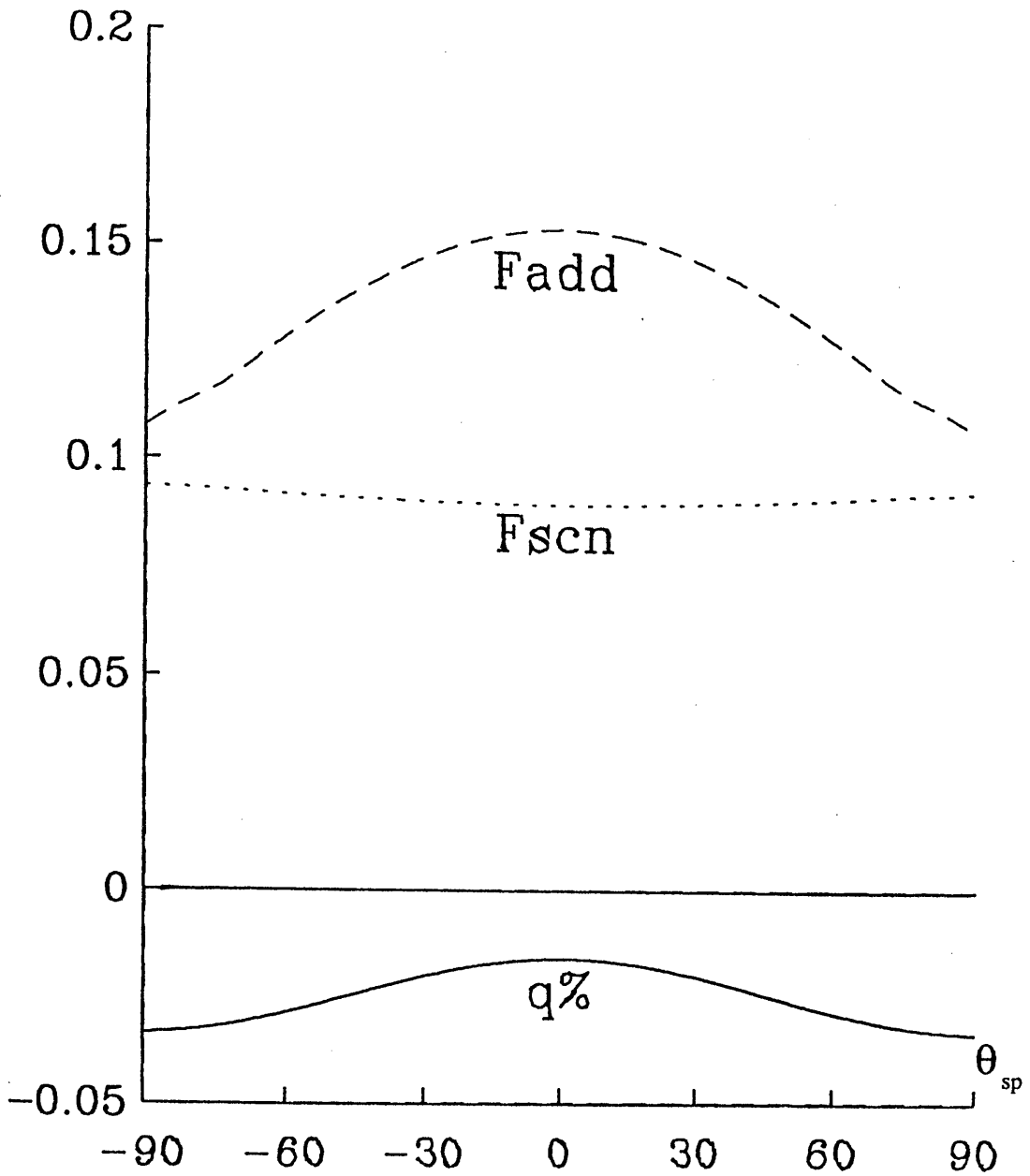
Fig. 4-6. The polarization p%, Fscn, and Fadd as
function of θsp (the location of the spot on the star)

154

different rotating stellar systems, concentrating on hot spots for illustration (Almost the same results will arise for cool spots but with a negative sign). First, to show the polarization expected due to the spot only, we assume a fixed spherical envelope with a rotating star having a spot of $\psi=15°$ and $\Delta T=1000$ K at $\theta_{sp}=30°$, for various stellar inclinations i_s (see Fig. 4-7). The polarizations are smaller than .04% and the qu-loci show double loops.

A non-spherical envelope is expected to affect the polarization value by enhancing or offsetting the effect of the spot, depending on the shape of the projected envelope as seen by the observer. Such envelopes can have different axial inclinations i_e from that of the star i_s, due to (e.g.) the magnetic pole is different that the stellar rotation pole. To show this effect we will calculate qu-loci for different fixed envelopes of $A_r=3$ and inclinations i_e. For $i_e=0°$ results will be the same as those for a spherical envelope, because the observer will see a circular projection of this envelope. For $i_e=45°$ the polarization value increases in the q direction to about $-.35\%$, keeping almost the same pattern as in Fig. 4-7 (see Fig. 4-8). For $i_e=90°$ the polarization increases to double that of the $i_e=45°$ case for q only, affecting the qu-locus as shown in Fig. 4-9.

Envelope rotation reduces the complicated qu-loci to circles in the case of a co-rotating envelope of $i_e=i_s+90°$ (see Fig. 4-10). Here the polarization is constant and has a value of about 0.6% for $i_s=0°$ and $i_e=90°$ and a value of about 0.03% at $i_s=90°$ and $i_e=0°$, but the position angle changes as the star rotates. In such stellar systems the envelope may rotate slower than the star. This effect increases the polarization by a small amount as shown in Fig. 4-11, for a system with the above values of $\psi=15°$ and $\Delta T=1000$ K at $\theta_{sp}= 30°$ and $A_r=3$, but with the star rotating four times faster than the envelope.

§4.4.1. NONUNIFORM SPOTS:

The model also allows us to describe a dark spot with umbra and penumbra (or a bright spot with inner area hotter than the outer). To illustrate this we will take the case of a nonuniform dark spot, which has two areas. The inner area has size $\psi=10°$ and $\Delta T=-500$ K, the outer area has a size $\psi=15°$ and $\Delta T=-1500$ K, and both are at $\theta_{sp}=30°$. With scattering on a co-rotating envelope of $A_r=3$ and $i_e=i_s+90°$, resulting polarization will increase as the stellar inclination increases, producing a circular qu-loci with radius degree of polarization 0.66% for $i_s= 0°$, 0.5% for $i_s=30°$, 0.18% for $i_s=60°$, and 0.02% for $i_s=90°$ (Fig. 4-12). The

qu-loci produced by this nonuniform spot look similar to those produced by a uniform spot because the nonuniform spot should be much larger with higher ΔT (i.e nonphysical spot, see Sec 4.1) to differ from a uniform spot.

The model also allows us to describe spots with time varying size, location, and ΔT (such as solar spots have). In the case of the sun the variation in polarization will be small, because the spots are small compared to the star. To show this effect we will assume a star with a spot growing from $\psi=5^\circ$ to $\psi=15^\circ$, rising and falling between $\theta_{sp}=0^\circ$ and $\theta_{sp}=30^\circ$, and getting hotter and cooler from $\Delta T=500$ K to $\Delta T=1500$ K, with a variation period of one fifth of the stellar rotation period. None of the above variations will increase the mean degree of polarization, but they affect the shape of the qu-loci as seen in Fig. 4-13.

Finally, we can use this model to calculate the polarization from more than one spot and for any shape of spot by representing it by a sum of circles, and also any variation of size; location; and ΔT. Fig. 4-14 plots the qu-loci for a rotating envelope of $A_r=3$ and $i_e=i_s+90^\circ$, with a star of five spots with the following characteristics:

spot no. 1- has $\psi=15^\circ$, $\theta_{sp}=30^\circ$, $\Delta T=1000$ k, and $\Phi_{sp}=0^\circ$.
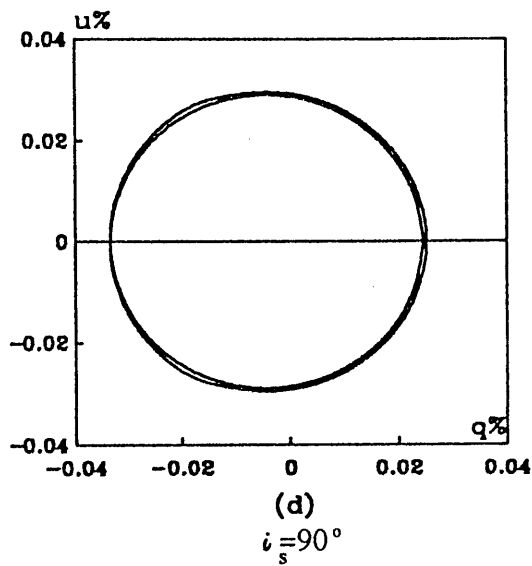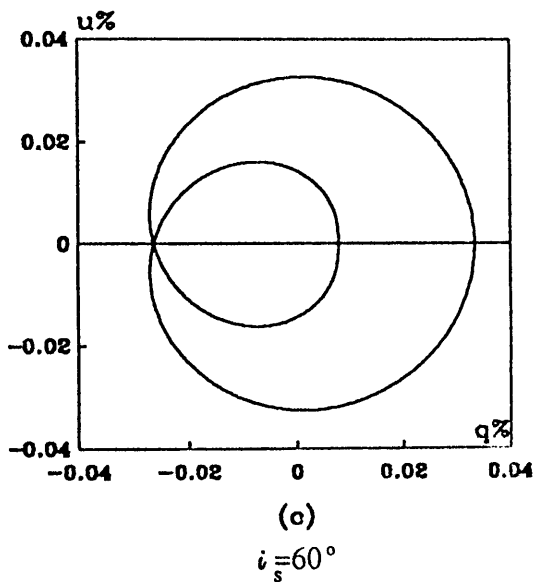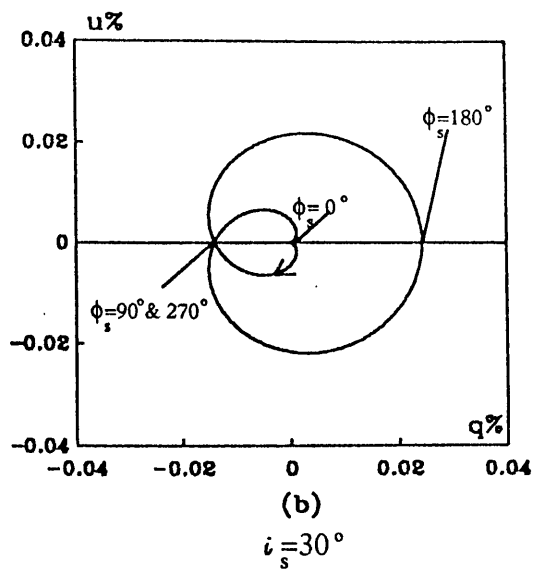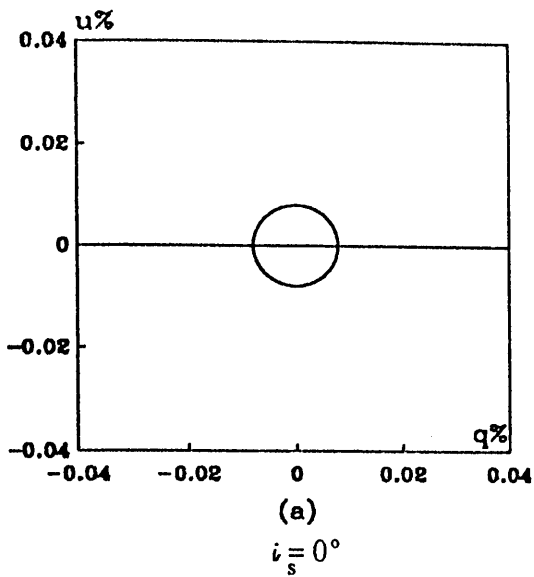
Fig. 4-7. The qu-plane for a rotating star within a fixed spherical envelope, the star having a spot of $\psi=15°$ and $\Delta T=1000$ K at $\theta_{sp}= 30°$, for various stellar inclinations i_s. (a) $i_s= 0°$, (b) $i_s=30°$, (c) $i_s=60°$, and (d) $i_s=90°$.
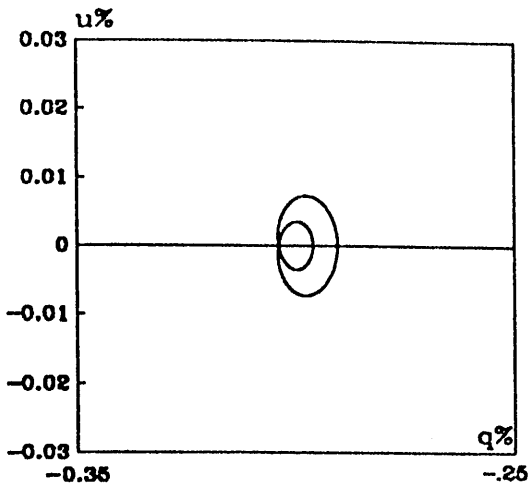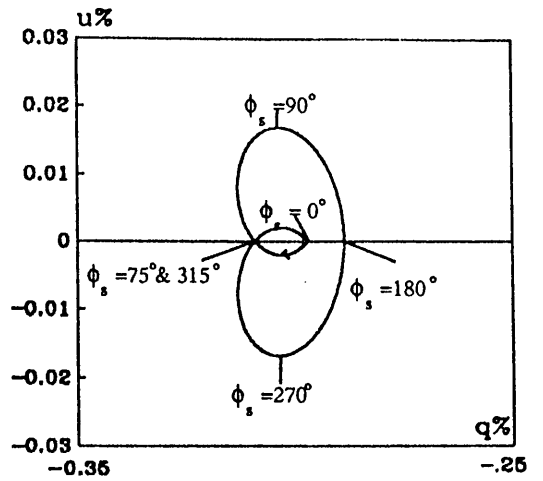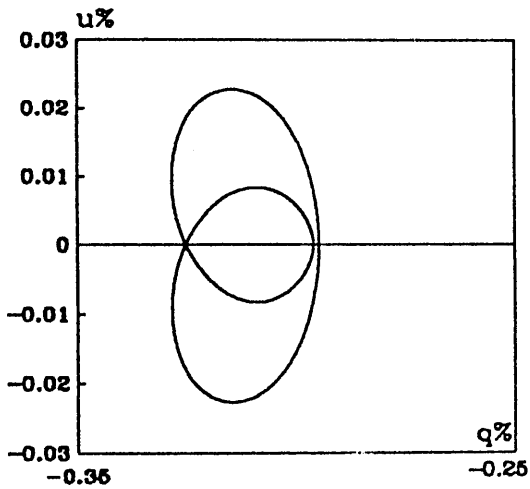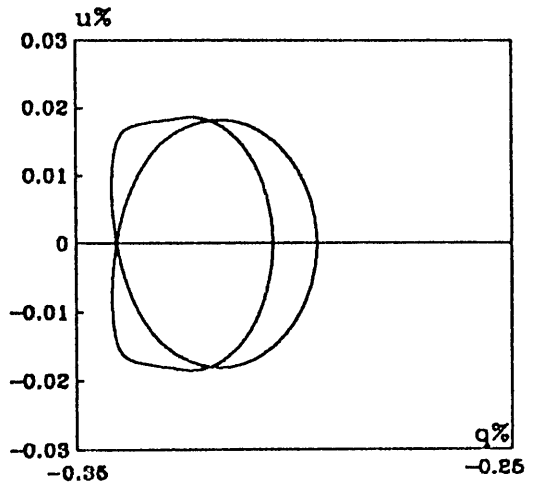
Fig. 4-8. The qu-plane for a rotating star within an ellipsoidal envelope of $A_r=3$ and $i_e=45°$. The star has a spot of $\psi=15°$ and $\Delta T=1000$ K at $\theta_{sp}= 30°$, for various stellar inclinations i_s. (a) $i_s= 0°$, (b) $i_s=30°$, (c) $i_s=60°$, and (d) $i_s=90°$.
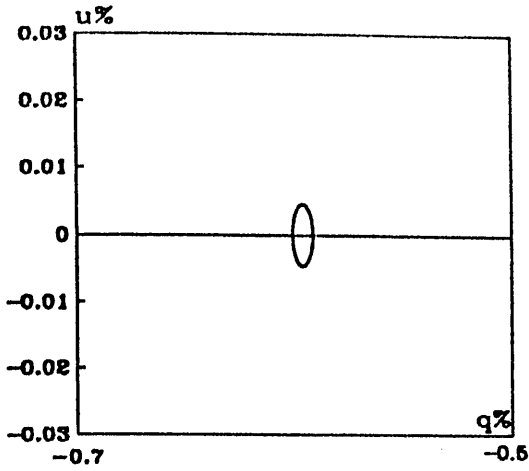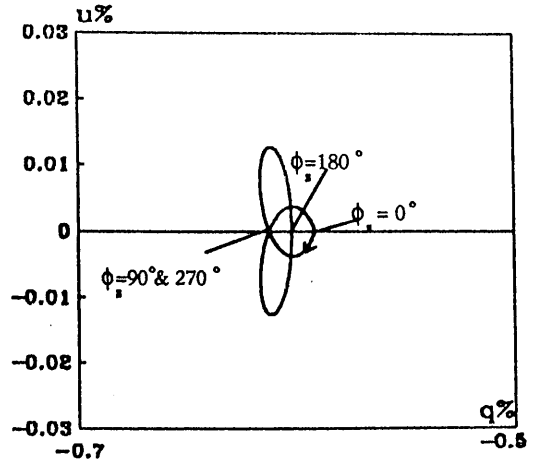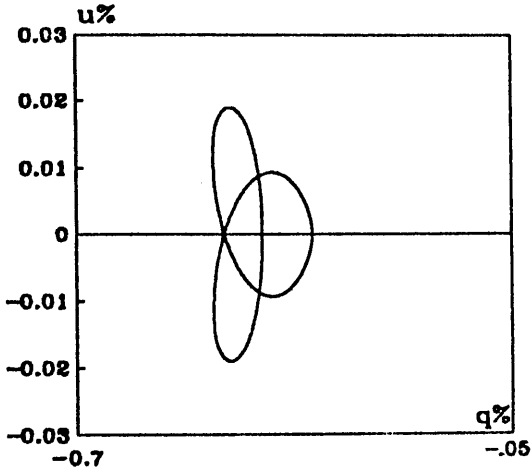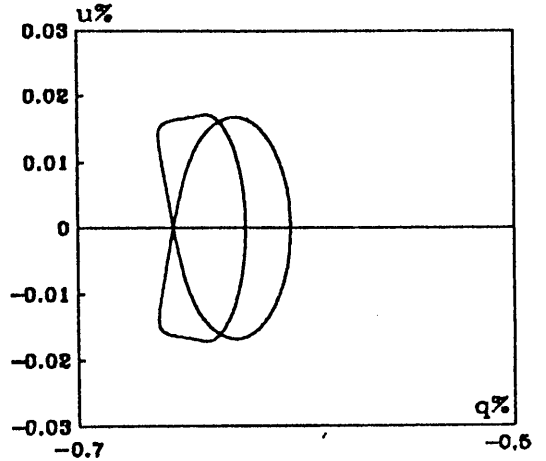
Fig. 4-9. The qu-plane for a rotating star within an ellipsoidal envelope of $A_r=3$ and $i_e=90°$. The star has a spot of $\psi=15°$ and $\Delta T=1000$ K at $\theta_{sp}= 30°$, for various stellar inclinations i_s. (a) $i_s= 0°$, (b) $i_s=30°$, (c) $i_s=60°$, and (d) $i_s=90°$.
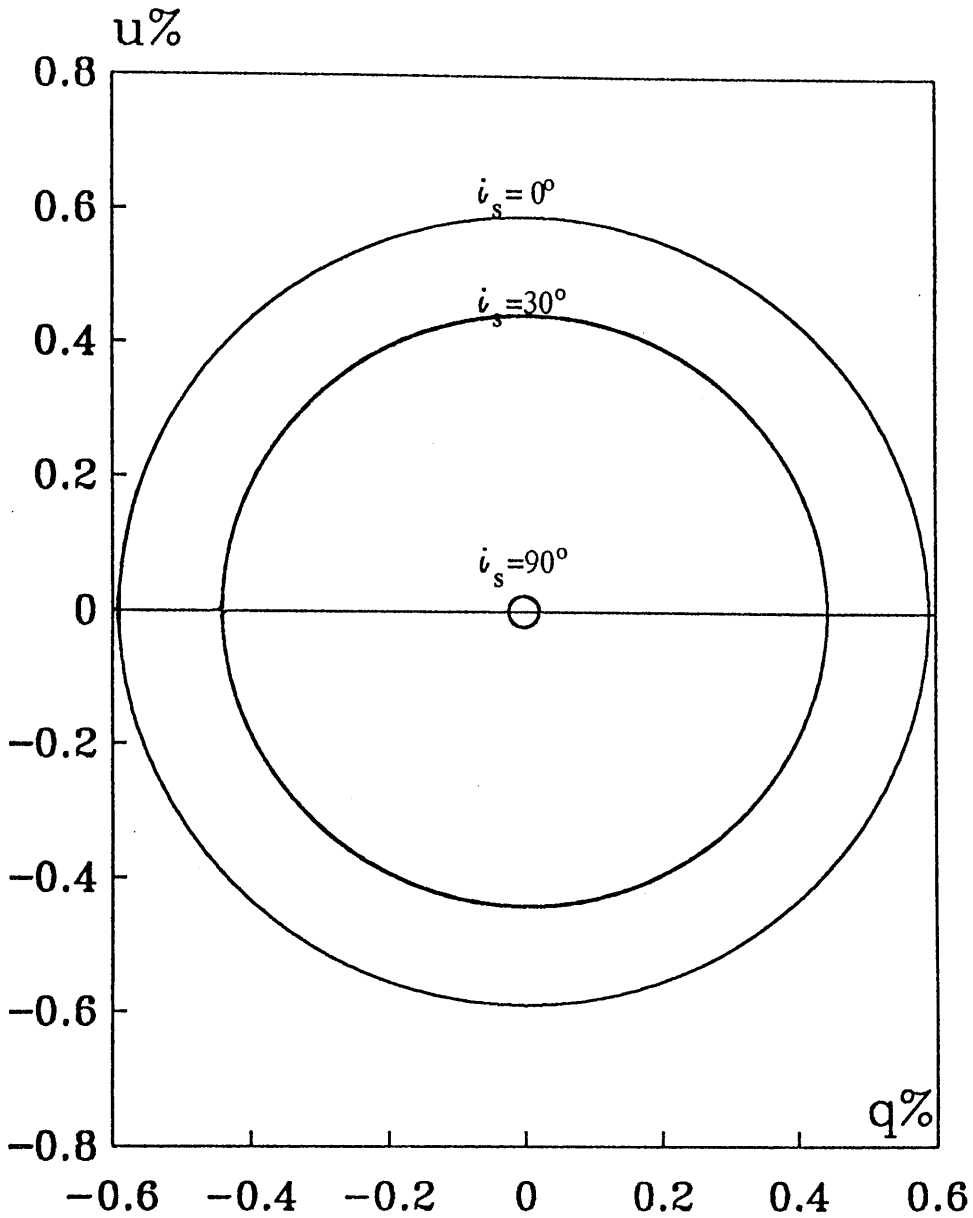
Fig. 4-10. The qu-plane for a rotating star within a co-rotating ellipsoidal envelope of $A_r=3$ and $i_e=i_s+90°$, the star having a spot of $\psi=15°$ and $\Delta T=1000$ K at $\theta_{sp}=30°$, for various stellar inclinations i_s $0°,30°,90°$.
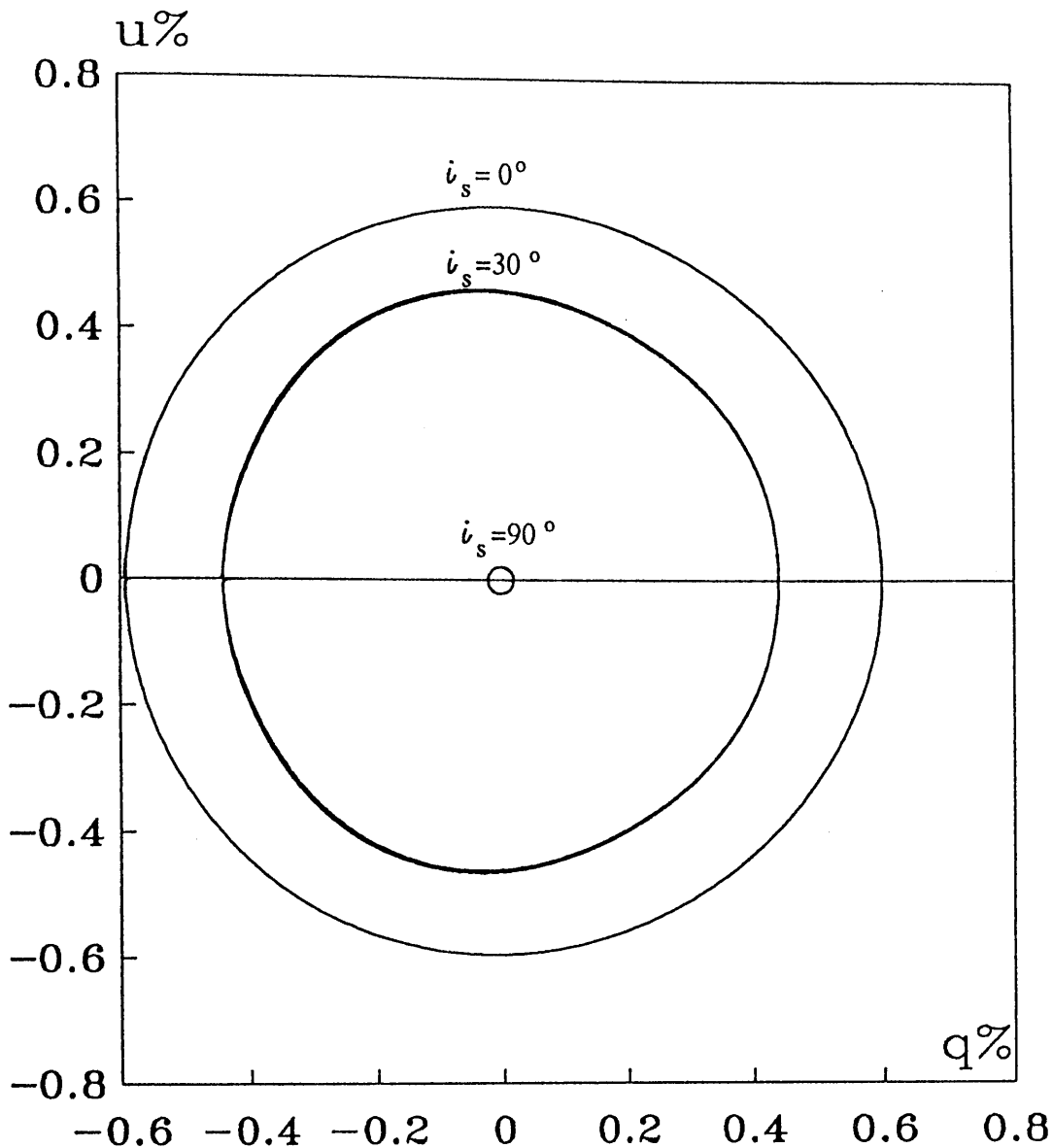
Fig. 4-11. The qu-plane for a rotating star within a slowly rotating envelope (completing a quarter rotation for each stellar rotation) of $A_r=3$ and $i_e=i_s+90°$. The star has a spot of $\psi=15°$ and $\Delta T=1000$ K at $\theta_{sp}=30°$, for various stellar inclinations i_s $0°,30°,90°$.
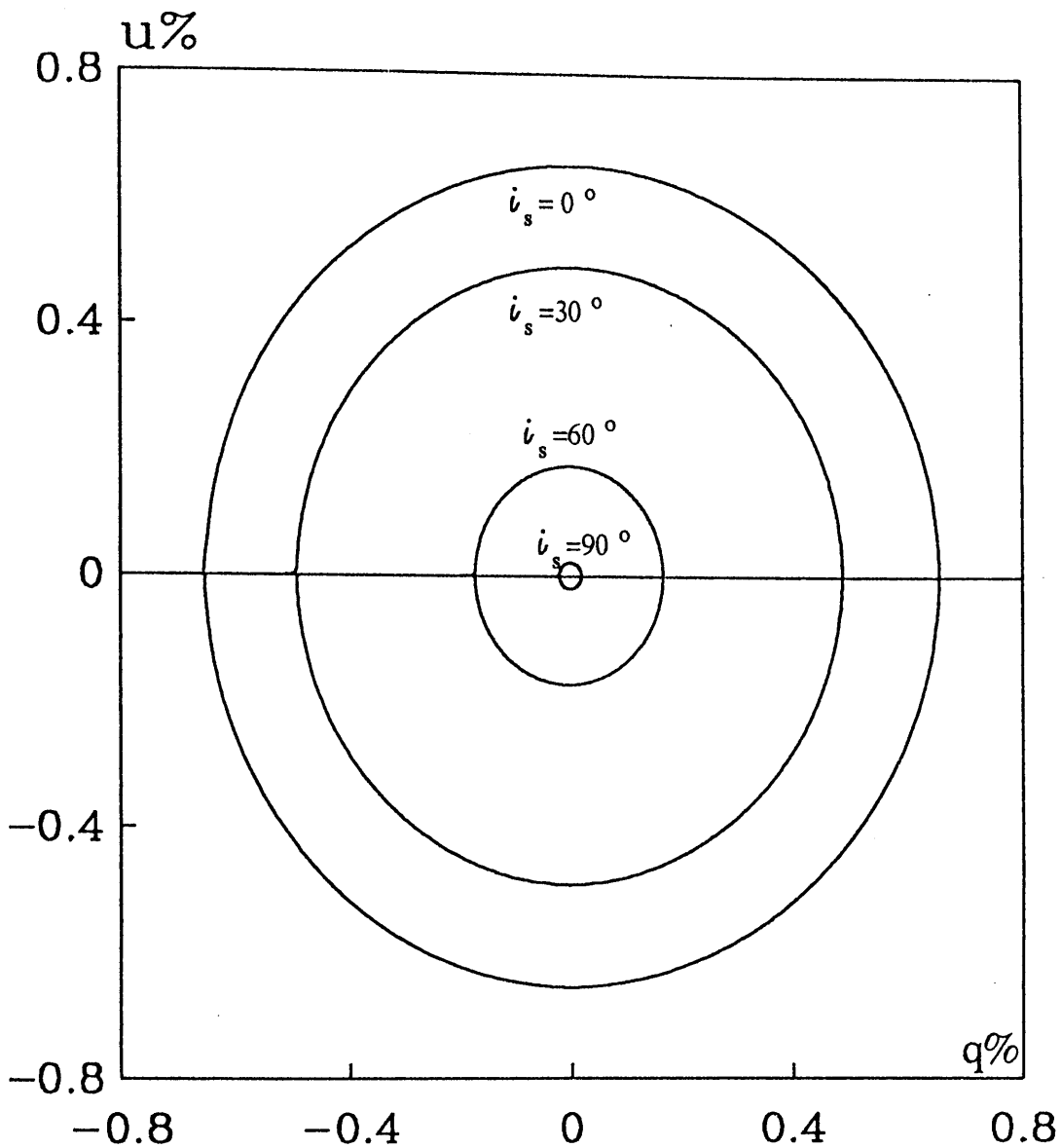
Fig. 4-12. The qu-plane for a rotating star within an envelope of $A_r=3$ and $i_e=i_s+90°$, the star having a dark spot with umbra and penumbra. The umbra has a size of $\psi=10°$ and $\Delta T =-500$ K, while the penumbra has a size of $\psi=15°$ and $\Delta T =-1500$ K, both being at $\theta_{sp}=30°$. For various stellar inclinations i_s $0°,30°,60°$, and $90°$.
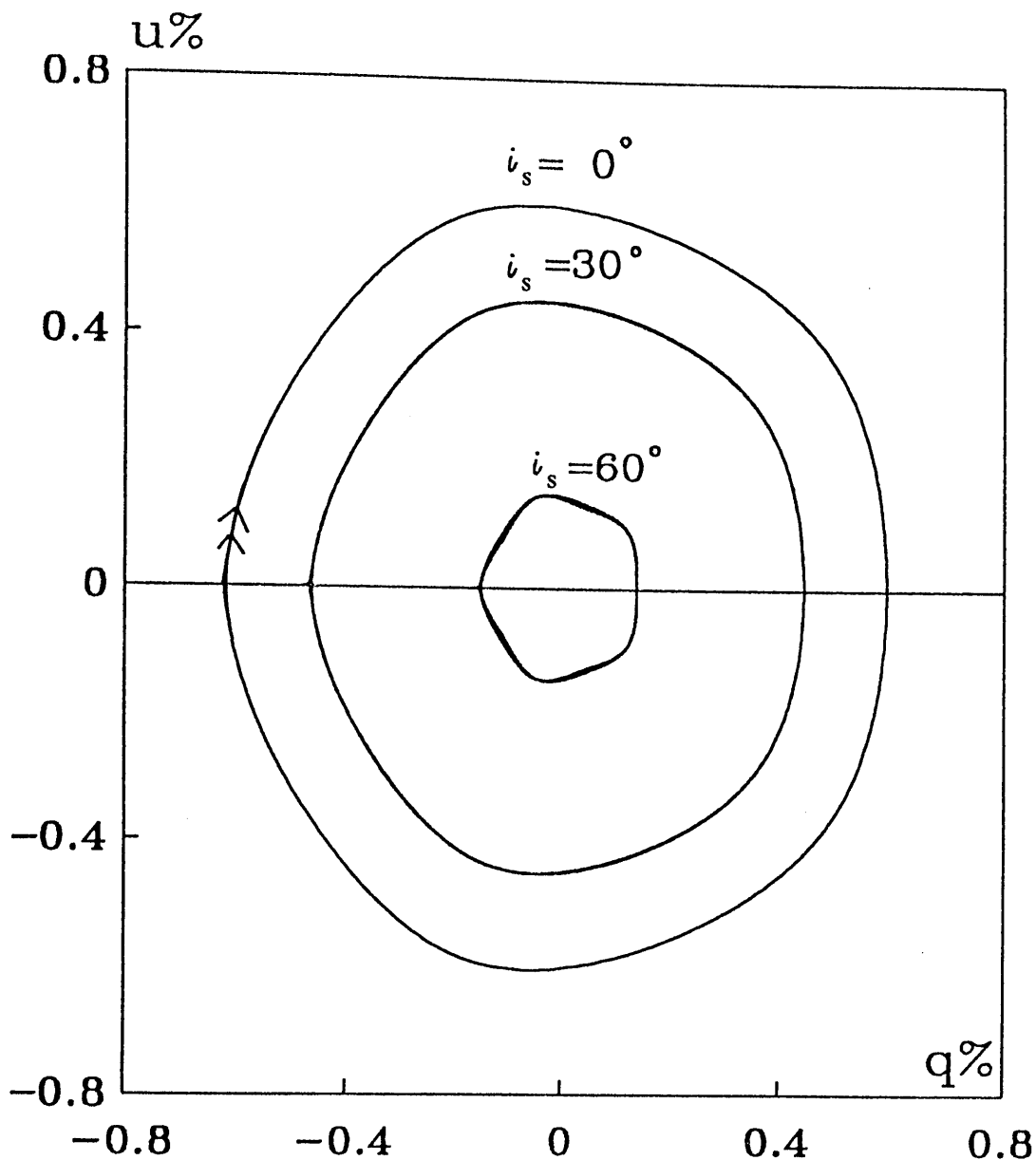
Fig. 4-13. The qu-plane for a rotating star within an envelope of $A_r=3$ and $i_e=i_s+90°$. The star has a spot growing from $\psi=5°$ to $\psi=15°$, rising and falling between $\theta_{sp}=0°$ and $\theta_{sp}=30°$, and getting hotter and cooler from $\Delta T=500$ K to $\Delta T=1500$ K, with a variation period of one fifth of the stellar rotation period. Various stellar inclinations i_s $0°,30°,60°$, and $90°$ are shown.
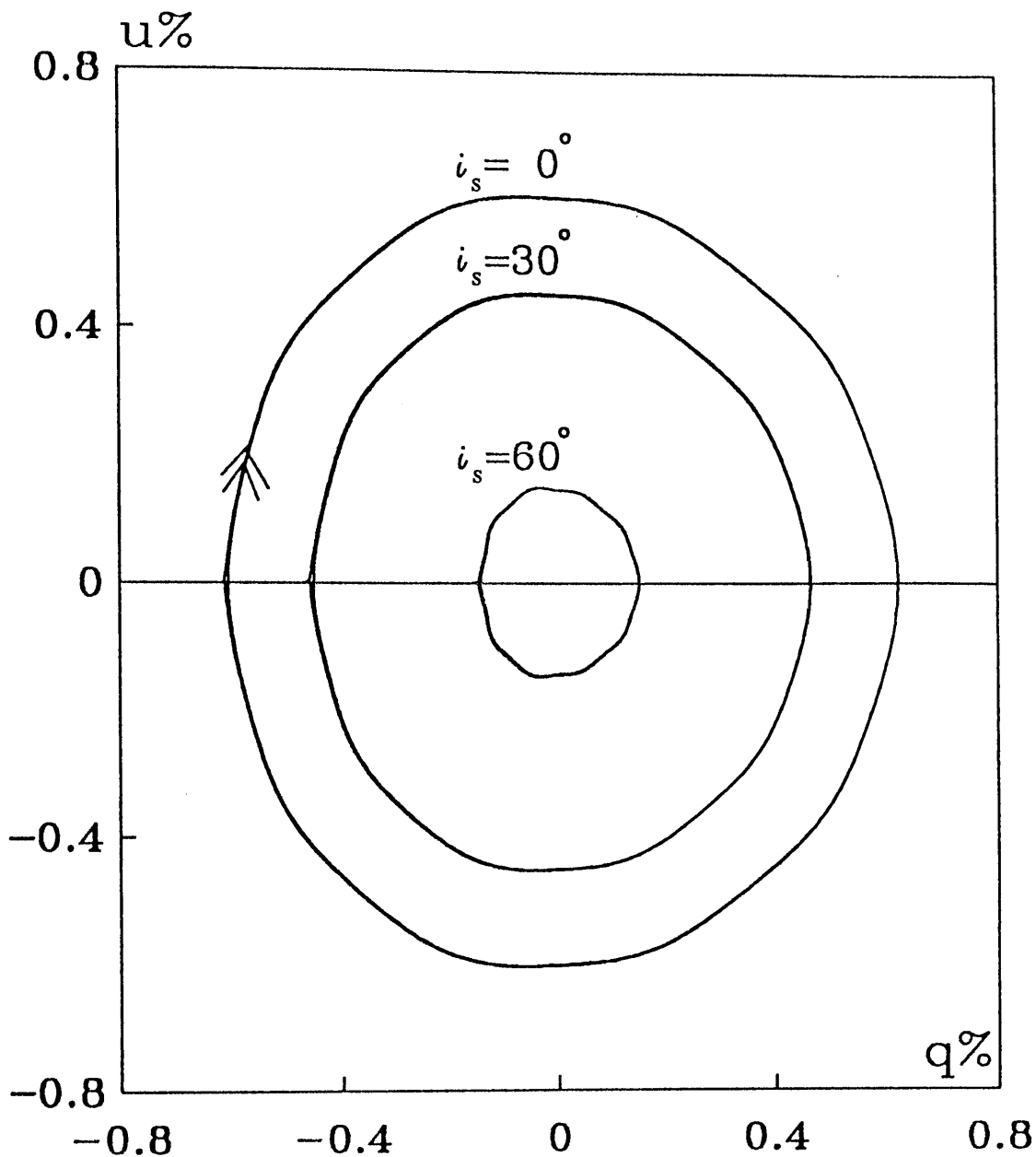
Fig. 4-14. The qu-plane for a rotating star within an envelope of $A_r=3$ and $i_e=i_s+90°$. The star has five spots as described in the text. Various stellar inclinations i_s $0°, 30°, 60°$, and $90°$ are shown.

spot no. 2- has $\psi=15°$, $\theta_{sp}=10°$, $\Delta T=-1200$ k, and $\Phi_{sp}=90°$.

spot no. 3- has oscillation between $\psi=5°$ and $\psi=15°$ ten times per rotation period Π_r (for a stellar rotation period Π_r of one day, the oscillation velocity is about 20 km/sec. This is much slower than Alfvén velocity of 220 km/sec for stars of solar corona and magnetic field of one gauss, Zirin 1988), $\theta_{sp}=0°$, $\Delta T=-800$ k, and $\Phi_{sp}=90°$.

spot no. 4-has oscillation between $\psi=5°$ and $\psi=10°$ every $2\Pi_r$ (so the oscillation velocity is about 2km/sec), and θ_{sp} varies from $0°$ to $60°$ every $2\Pi_r$ (the velocity of θ_{sp} variation is about 20 km/sec), $\Delta T=500$ k, and $\Phi_{sp}=120°$.

spot no. 5- has ψ varying between $0°$ and $5°$ every $1/3$ Π_r (then the velocity is about 0.3 km/sec), and θ_{sp} varying from $0°$ to $5°$ three times per Π_r (with a velocity of about 0.3 km/sec), $\Delta T=1000$ k, and $\Phi_{sp}=-45°$.

Although one might expect a resulting complicated qu-locus, this is not the case because summation of all these spots results in some cancellation and smoothing, so that almost circular qu-loci result for small i_s, and p decreases as i_s increase and qu-loci have some complication.

Generally, spots needed to be large to show an observable polarization, high resolution observations should be used to detect nonuniform spots specially if the spots are not bright enough. The main aspect of the

qu-loci produced by a spot is the lobes (see Figs. 4-7 to 4-9) which occur for fixed envelope, and are reduced for rotating envelopes (Figs. 4-10 to 4-13). For high quality and long observations, such lobes are expected for stars with spots, then this model can be used as a source function indicator in the data inversion problem (see e.g. Craig and Brown 1986).

Summary :

Using our general model of an anisotropic point light source surrounded by an arbitrary shape envelope , we calculate the polarization due to photospheric non-uniformity in the form of spots. Expressions are derived for the variation in projected area of a spot as it rotates with the star, including spot disappearance over the stellar limb.

The results show that, for a physical spot of angular extent up to $30°$, a description up to the second spherical harmonic is an acceptable approximation. In general the polarization from this kind of anisotropy is much smaller than the polarization from that due to non-sphericity of stars.

Evidently, there is a relation between the polarization produced by an anisotropic star due to a

spot surrounded by isotropic envelope, and the polarization of light from an isotropic star scattered by a cloud.

This model enables calculation of the polarization arising from multiple spots, hot and cool spots, cool spots with umbra and penumbra, or for hot spots with non-uniform temperature. Complicated spots which vary in size, temperature, and location with time, and generally, spots of any shape can be represented by a sum of circles. Such complicated shapes can be mapped by the spectroscopic technique as done for the spot of HR 1099 (Fig. 4-15, *cf.* Bopp 1987).

As expected the effect of hot spots on the Stokes' parameters are found to have the opposite sign from those of cool spots, so that a combination of hot and cool spots could explain the zero polarization for some spotted stars. The presence of many spots can also reduce the degree of the polarization by cancellation, depending on the temperature of the spots, their size, and location.
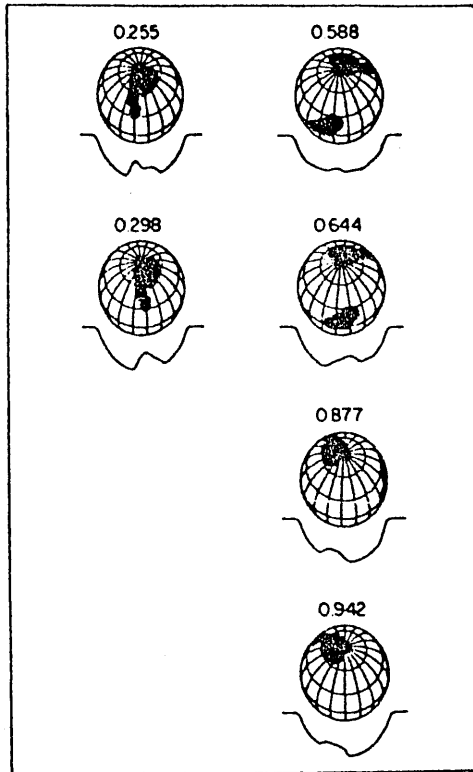
Fig. 4-15. Doppler map of HR 1099 derived from the
Doppler Imaged absorption line profiles (from Bopp
1987).

CHAPTER FIVE

5. CONCLUSIONS AND FUTURE WORK

CONTENTS :

§5.1. Conclusions:

In this work a model for anisotropic point light source within an arbitrary shape envelope was presented, by assuming either Thomson or Rayleigh scattering.

The mathematical analysis made full use of the properties of the spherical harmonics, and can be easily generalized to more complicated cases than those discussed here.

Using the first few spherical harmonics, used in this model, an acceptable approximation is shown. The results of the model indicated that the properties of the polarization are independent of specific assumptions for the source and form of anisotropy of the star or of the origin and form of the envelope shape. That is, the anisotropy of the star and envelope properties can be reduced to the products of multipole contributions. Consequently whether the anisotropy is specifically due to an ellipsoidal star or to a star with spots is not the intrinsically important factor. Because the first few terms of the spherical harmonics for any function (whether complicated or simple) will reduce to the same product of multipole components, one will obtain similar polarization properties. This can be particularly

important for the envelope, since the multipoles of the envelope K_ℓ, depends only on ℓ', so a wider choice of the particles' distribution function will be available, where for the anisotropy of the star, of the multipoles $f_{\ell m}$, the dependance on both ℓ and m, limited the stellar anisotropic functions choice.

A similarity between the polarization produced by an anisotropic star surrounded by an isotropic envelope only, and that of scattered light of an isotropic star surrounded by arbitrary shape (anisotropic) envelope only has been discovered. Chapter Two showed that there is a similarity between the polarization from a non-spherical star within a spherical envelope (present work), and the polarization from an arbitrarily shaped envelope illuminated by a spherical point source star (Brown and McLean 1977). Chapter Four showed a similarity between the polarization from a star with a spot within a spherical envelope, and the polarization from a spherical point source star with a localised cloud of scatterers (Brown *et al.* 1978).

The model was applied to three special cases :
1 - Ellipsoidal star within spherical envelope.
2 - Ellipsoidal star within ellipsoidal envelope.
3 - Star with spots within ellipsoidal envelope.

§5.1.1. APPLICATION TO ELLIPSOIDAL STARS ONLY:

Application of the model to an ellipsoidal star (in Sec. 2.3 and 2.4) showed that a maximum polarization of 20% with a total observed flux equal to the scattered flux, can be expected for any optical depth τ. This extreme occurs for a disk like star with zero thickness viewed edge on. The maximum of the polarization for a needle shape star depends on τ, but it is much smaller than that of the disk shape, although the normalized scattered flux is approaching unity. The calculations for rotating non-spherical stars showed that qu-plane loci are represented by elliptical patterns, which agrees with observational results for RV Tauri Stars (*see* Serkowski 1970). The multi-mode character of non-radially oscillating stars, can be explained by an oscillation in one or more of the star's axis with $\omega \neq 1$. The degrees of polarization expected by the anisotropic radiation model are within the range of observational results (see Sec. 1.3).

§5.1.2. APPLICATION TO ELLIPSOIDAL STARS WITHIN

ELLIPSOIDAL ENVELOPES:

The application of the general model to an ellipsoidal star within an ellipsoidal envelope (Sec.

3.3 and 3.4) showed that the maximum polarization can be up to 35% of the total light, occurring for disk like stars with zero thickness viewed edge on (i.e. perpendicular to the line of sight) and surrounded by a disk of particles perpendicular to the disk of the star, so the direct light will be the light of the stellar disk edge, where the scattered light is coming from the surface of the stellar disk (see Fig. 5-1a). When the disk like envelope became parallel to the disk like star a reduction in the polarization to -11% of the total light would occur, here both the direct light and the scattered light is produced by the edge of the disk like star, which will reduce the polarization. The negative sign is due to the polarization being at 90° from that of a perpendicular disk like envelope (see Fig. 5-1b). The scattered flux in both cases approaches unity. These values are independent of the optical depth τ.

For any non-spherical star, the maximum polarization would be expected when the largest axis of the star is perpendicular to the equatorial plane of the envelope, since the geometrically oblate star is prolate in photometry (see e.g. for the extreme case Figs. 5-1, and the theoretical polarimetric results in Sec. 3.4). In general the polarization is dependent on the angle between i_s and i_e, combined with the effect of the projected areas of the star and of the envelope toward

The disk like envelope

The scattered light

The surface of
the stellar disk,
which radiates
most of the
radiation

The direct light =0

To the Earth

The edge of the
stellar disk, almost no radiation
is produced by such edges.

The polarization direction
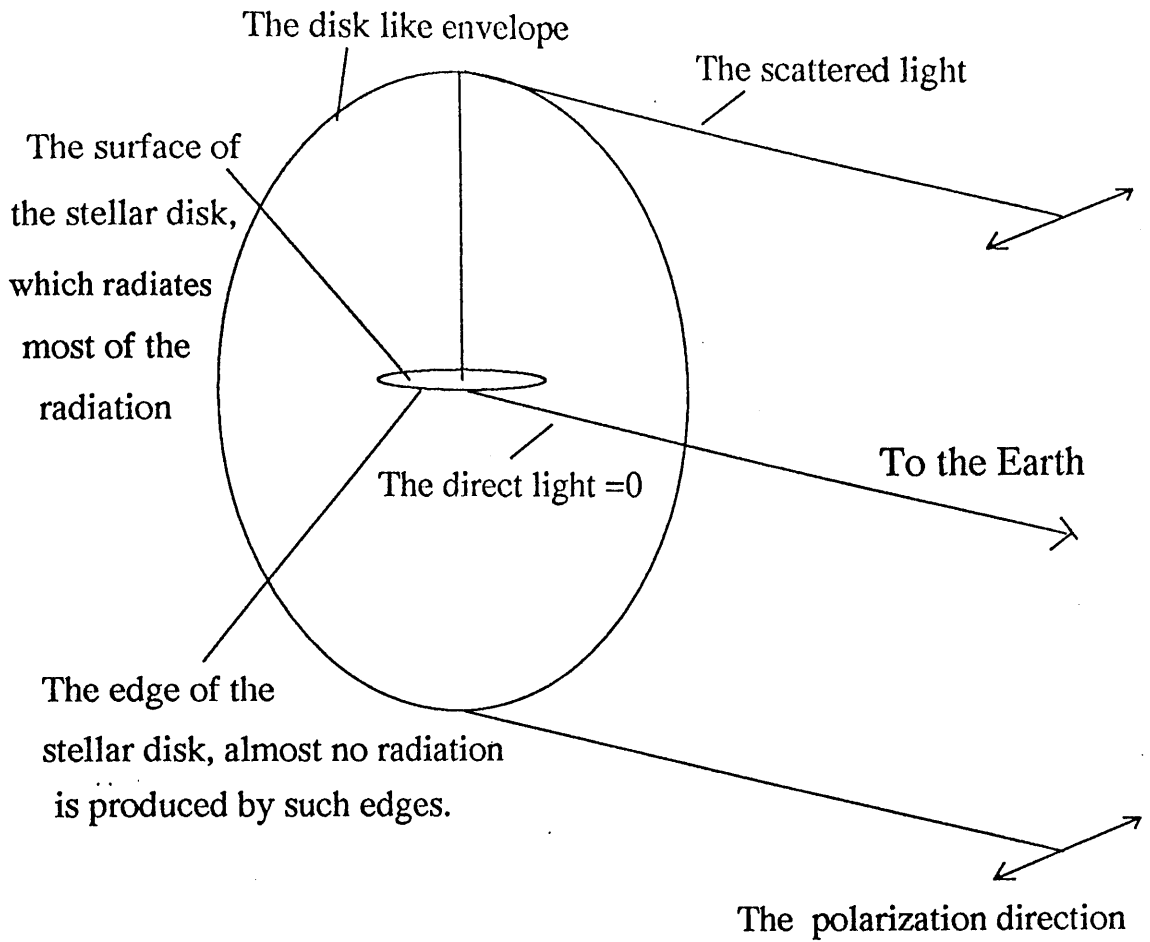
Fig. 5-1 a. The extreme case of disk like star (of
zero thickness) viewed edge on and surrounded by a
perpendicular disk of particles.

The disk like envelope

The surface of the stellar disk,
there is no direct light seen from it,
and no scattered light either.

The scattered light,
which scattered from
the edge of the stellar
disk.

The direct
light from the
edge of the disk
like star, is = 0.

The polarization direction

To the Earth
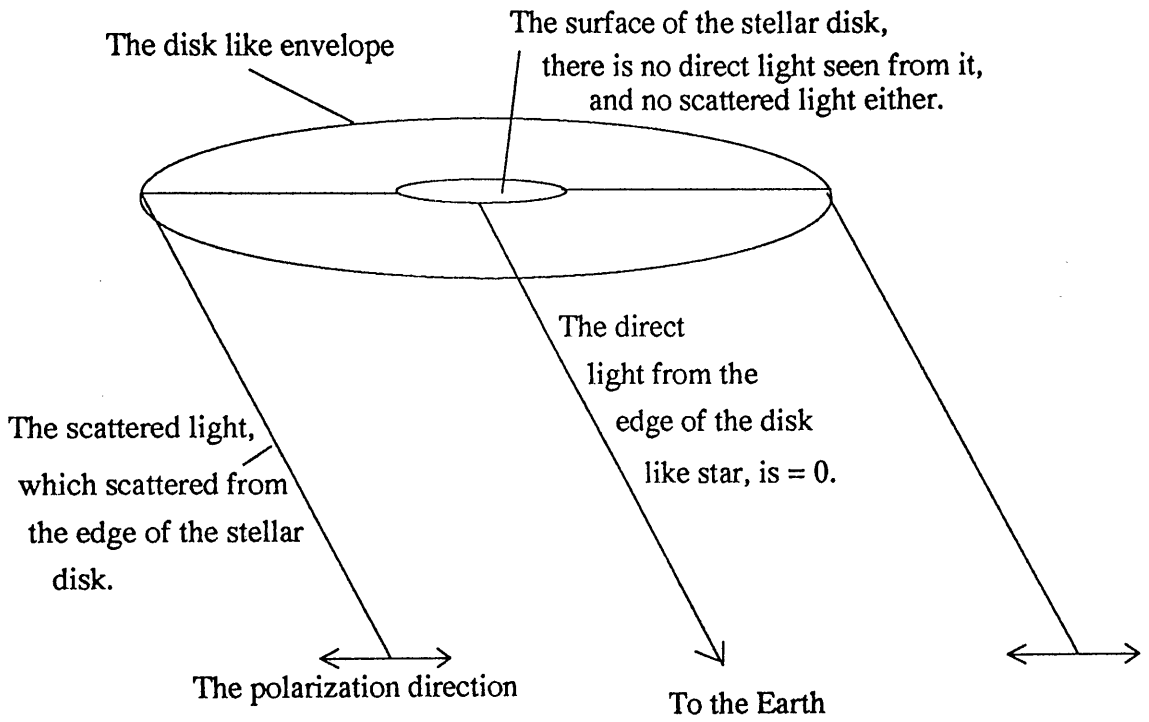
Fig. 5-1 b. The extreme case of disk like star (of zero thickness) viewed edge on and surrounded by a parallel disk of particles.

the observer. The qu-plane loci are still ellipses for fixed envelopes with a rotating star, but are complicated for a rotating envelope and rotating star.

The normalized scattered flux is not affected much by assuming an ellipsoidal envelope instead of a spherical one. This is expected since the scattered flux depends more on the mechanism which produces the scattering (e.g. *Mie* scattering) rather than on the detailed distribution function of the particles (see Sec. 1.1.1).

§5.1.3. APPLICATION TO STARS WITH SPOTS WITHIN AN ELLIPSOIDAL ENVELOPE:

In Eqs. (4-18) the first expressions have been derived to calculate the variation of the projected area of a spot as a star rotates, and the shape of the spot as it disappears at the limb. These expressions show that a considerable area of the spot still has an effect even when the center of the spot is on the limb (where previous workers assumed that the spot is totally hidden). Using these expressions in our general formulation for an anisotropic star within an arbitrarily shaped envelope, developed in chapters Two and Three, we calculated the polarization produced by spots.

By assuming $\tau=0.1$, we find the polarization from a spherical envelope and a star with one spot of size $\psi=15°$ is very small (0.03%) compared to the polarization produced by a star having quite small distortions from sphericity. That is because any phenomena on the stellar surface has to be very big and bright, to show an observable degree of polarization from the whole star, while small distortions from sphericity (i.e. $\simeq 0.05$) are big enough to produce observable polarization effects.

This spot model can also describe more than one spot, of any shape, with umbra and penumbra, and with the spot properties varying. Some of the these possibilities are used above to calculate the polarization. Relatively complicated qu-loci resulting from such spot variations have been found. Though the variations are small due to their effects being integrated over the rotating envelope, they still contribute to the observed polarization variations.

Some solar type stars are expected to have spots, but they show no polarization. This can be explained in terms of our model by having two (or more) comparable hot and cool spots with similar $|\Delta T|$. It can also arise for two hot or two cool spots with same θ_{sp} and ΔT but

having $\Delta\Phi_{sp}=\pi/2$, since in these positions the spots produce polarizations of opposite signs.

Of course, although this work goes quite far beyond previous work, the model still has limitations, which should be covered by future work.

§5.2 FUTURE WORK :

This is science:- whenever you think that you have answered a question, many other questions appear!. Our model is no exception and suggests future work mainly in two fields :
1 - Application to observational data.
2 - Development of the model.

§5.2.1. APPLICATIONS :

It is interesting to apply our model to pulsating stars such as RV Tauri, β Cep., to binaries such as Cygnus X-1, and to stars with spot such as α Ori.

An expression can be derived from Eqs. (3-26), and (3-27a&b) to determine the inclination of a stellar system like those developed for binaries by Brown *et al.* (1978), Rudy and Kemp (1978) and Simmons (1983). Also, we think the model will be useful in fitting data from

some X-ray binaries such as Cygnus X-1. But there will be two difficulties: 1- In our model there are two inclinations one for the rotation axis of the star, and the second for the axis of the symmetry of the envelope. 2 - The effect of tidal deformation polarization, where there is no straightforward method to remove it from the observation (Dolan 1992).

The application of the star with spots can be used to explain almost anything in the way of polarization variation by proper choice of spots' life time, size, temperature, and location on a rotating star, as is the case in photometry (Vogt 1981), e.g. by choosing short life time for a spot compared to the stellar rotation period, a sudden polarization will occur, so a number of such spots will show a very complicated qu-loci. The effects of limb darkening and wavelength dependency can be included to study their effects on stars such as α Ori.

Galaxies also show a very high polarization (p ~ 10% to 30% , Coleman and Shields 1990 and Draper *et al.* 1991).Since the galaxies are very distorted light sources, they would be good candidates for treatment as disk like sources of light, especially as they produce observed degrees of polarization within our model's expectations.

Although our model is a polarimetric model, it also predicts the direct flux and the scattered flux, which can be useful in photometric studies.

§5.2.2. Development of the model :

In the above section improvements to our model have been suggested for observational data fitting.

As far as the model is concerned, it will be important to calculate the effects of the finite size of an anisotropic star, in another words, the depolarization factor of our model (see Cassinelli *et al.* 1987, and Brown *et al.* 1989). Also calculation of the effects of scatterer occultation by finite stars should be done (see Milgrom 1979, Brown and Fox 1989, and Fox 1991).

The model as it is can be applied to multi anisotropic light sources, non-spherical stars with spots, and to more complicated envelope shapes, or all the above together.

Moreover, there will be an interesting statistical modelling, for the probability of having a polarization degree and a position angle (or q and u), due to a spot

of independent parameters of life time, size ψ, ΔT, and location (θ_{sp},ϕ_s), for given stellar and envelope inclinations.

Finally, it is interesting to have a model for the most general case of the polarization from an arbitrary scattering mechanism for the light of an anisotropic light source scattered by an arbitrary shape envelope, which will be a combination of the work of Simmons (1982) and Shawl (1975), and our model.

APPENDICES

CONTENTS :

Appendix A

The analysis of Serkowski's data of U Mon

Serkowski made his observations of U Mon in the *UBV* spectral region, using the 24-inch rotatable telescope of Siding Spring Observatory (Serkowski 1970). Integrations of 20 sec. were made in yellow and blue; 40 sec. integrations were made in the ultraviolet, as listed in Table A.1. The observations for which the mean error of percentage polarization is larger than ±0.08% in the yellow or blue or larger than ±0.15% in the ultraviolet are denoted in Table A.1 by colons.

Most of the photometric observation of U Mon since 1873 until the observations by Preston *et al.*(1963) indicated a mean period of light variations of 92.26 days. The minima reported by Serkowski (1970) deviate, however, quite considerably from these elements, which show that the period between the time of observation by Preston *et al.* (1963) and Serkowski's observation was 91.3 days (Serkowski 1970).

In our analysis of Serkowski's data, first we calculated the q and u values for the polarimetric data of U Mon reported by Serkowski (see Table A.1). Then we referred them to their center by subtracting from each

TABLE A.1.

POLARIMETRIC OBSERVATIONS OF U MON.

JD 24...	Phase	V	B-V	U-B	Percentage Polarization p^V	p^B	p^U	Position Angle θ^V	θ^B	θ^U
U Monocerotis (HD 59693) $l^{II} = 226°$, $b^{II} = +4°$										
39822	0ᵖ05	5.97	0.90	0.66	2.38	2.57	2.58	6°2	4°2	3°5
39834	.18	5.55	0.97	0.73	1.59	1.54	1.20	0.1	178.5	176.4
39878	.66	5.58	0.94	0.70	1.92	1.84	1.78	7.1	5.8	3.0
39880	.68	5.58	1.00	0.83	1.89	2.03	1.71	7.4	6.4	10.9
39884	.73	5.63	1.09	1.01	1.93	2.16	2.37	7.8	9.5	12.3
39886	.75	5.72	1.13	1.08	1.93	2.13	2.38	8.9	10.2	12.0
39890	.79	5.84	...	...	2.08	2.23	2.58	8.2	10.6	16.6
39906	.97	6.93	1.00	0.74	2.91	3.01:	3.03	3.3	3.3:	6.8
39909	.00	6.9:	0.90	0.70	3.04:	3.19:	2.98:	5.1:	4.9:	2.4:
39912	.03	6.63	0.88	0.71	2.83	2.90	3.26	7.1	7.9	7.7
39919	.11	...	...	...	...	2.30	...	...	9.8	...
39925	.17	...	...	...	...	1.80	...	...	12.1	...
39926	.18	...	...	...	1.83	1.85	...	10.8	12.2	...
39934	.27	5.60	1.03	0.96	1.70	1.60	1.50	11.2	9.7	8.0
39939	.33	5.84	1.05	0.97	1.78	1.75	1.25	9.2	5.5	8.8
39948	.42	...	...	...	1.73	1.54:	1.44	8.3	9.9:	1.0
39950	.45	6.14	1.15	0.92	1.52	1.55	1.47	9.4	6.9	3.5
39952	.47	6.14	1.12	0.87	1.49	1.44	1.30	10.4	8.3	10.0
39954	.49	6.19	1.06	0.82	1.56	1.46	1.21	11.6	9.6	4.7
39967	.63	...	...	...	1.55:	1.48	1.58	12.9:	13.3	8.2
39968	.64	5.61	0.86	0.60	1.60	1.47	1.38	14.7	14.2	11.6
39983	.80	5.75	1.24	1.31	1.82 —	1.93	1.66	11.3	9.7	15.5
39997	.96	...	...	...	...	2.41:	...	...	9.2:	...
40011	.11	6.11	0.90	...	3.10	2.81	...	14.9	14.1	...
40012	.12	5.95	0.95	0.57:	...	2.61	2.66	...	14.1	9.9
40014	.14	5.76	0.96	0.66	2.36	2.34	2.05:	13.9	13.0	12.5:
40016	.16	5.61:	1.02:	...	...	2.14	...	...	12.9	...
40110	.19	5.53	0.94	...	...	1.27	...	...	15.9	...
40115	.24	5.37	0.88	0.73:	1.27	1.06	0.62	13.2	16.4	23.3
40124	.34	5.64	1.02	0.88:	1.17	0.96	0.64	10.5	10.3	7.0
40137	.48	6.15	1.08	0.78:	0.99	0.82	0.56	9.8	12.1	31.6
40140	.51	6.15	1.01	0.71:	1.11	0.94	0.51	12.9	16.4	36.2
40142	.53	6.14	0.95	0.56:	1.27	1.12	0.73	12.1	15.1	21.8
40150	.62	...	...	...	...	1.24:	...	...	9.7:	...
40158	.71	...	...	...	...	1.35	...	...	15.0	...
40163	.76	5.8:	...	...	...	1.51	...	...	14.2	...
40200	.16	5.87	1.04	0.81	1.76	1.81	1.96	11.8	13.9	19.4
40202	.18	5.76	1.10	0.87	1.66·	1.61	1.76	12.7	14.3	21.8
40209	.26	...	...	...	1.55	1.42	...	14.0	15.3	...
40238	.58	...	...	...	1.12	1.13	1.21	10.3	14.4	23.9
40264	.86	6.03	1.21	1.31	2.23	2.60	2.82	6.3	5.8	6.2
40268	.90	6.03	1.21	1.21	2.43	2.58	2.60	5.4	5.5	8.7
40277	.00	6.66	1.19	0.96	2.29:	2.29	2.27:	3.4:	5.1	8.6:
40280	.03	6.76	1.15	0.96	1.92:	2.03	2.15:	4.2:	5.6	8.2:
40283	.07	6.52	1.06	0.83	1.58	1.58	1.91:	6.1	9.7	5.8:
40300	.25	5.64	1.03	0.84	1.73	1.86	1.74	4.1	2.4	1.9
40303	.28	5.72	1.08	0.97	1.71	1.85	1.65:	2.8	2.5	3.1:
40330	.58	...	...	...	...	1.22	1.23	...	24.3	24.2
40348	.77	5.87	1.11	...	...	2.02	...	...	178.9	...
40375	.07	5.9:	...	...	...	1.48:	...	...	13.9:	...
40390	0.23	5.7:	...	...	1.36:	1.28	...	8.0:	4.9	...

value their average). By neglecting the high error observations we were left with 34 values in the U band, 45 values in the B band, and 33 values in the V band.

Applying Fourier analysis described by Cuypers (1987) to q and u, with frequencies (ν's) started from as low as 0.002 per day (i.e. of (1/ν) 500 days), with an increment of 5.9×10^{-5} per day, up to a frequency of 0.036 per day (i.e. down to about 28 days period), we did not find any indication of period of about 92 days in the u direction. This may be because the values of u were small compared to q and so the relative noise was high in this direction. In the q direction the results were interesting – we found a different period for each band. For the U band we obtained two comparable periods, of 97.13 days, and of 93.04 (see Fig. A-1). There was no indication for the photometric periods (92.26 days or 91.3) occuring in the U band Fourier analysis. In the B band there are again two comparable periods , of 96.92 days, and of 91.75 days (see Fig. A-2).The latter period is between the two above photometric periods. We obtained clearly one period of 92.23 days in the V band (see Fig. A-3), which is almost the period of Preston et $al.$ (1963) -not of Serkowski as expected. This period diference may be due to errors caused by the noise of the data, or the fewer number of polarimetric data compared to the photometric data.

The changes of U Mon in polarimetry and photometry with the phase of the light variation are shown in Fig. 1-6. A quick application of Fourier analysis to the polarizations (p) data of U Mon without referring p to their center, shows almost the same results as for q above. This indicates that the polarization is affected by the rotation so we can obtain the stellar rotation period direct from the polarimetric data in the *V* band. However, more analysis of Serkowski's data is needed to find whether there is a pulsating period different from the rotation period, especially if the pulsation are strong in *U* or *B* bands. On the other hand, more polarimetric and photometric observations are needed to define the envelope shape and the pulsation size of RV Tauri stars. Preston *et al.* (1963) show a difference in phase shift between the light curves in *V* and in *B-V* band, which may explain why we did not find the same period in *B* and *U* regions.
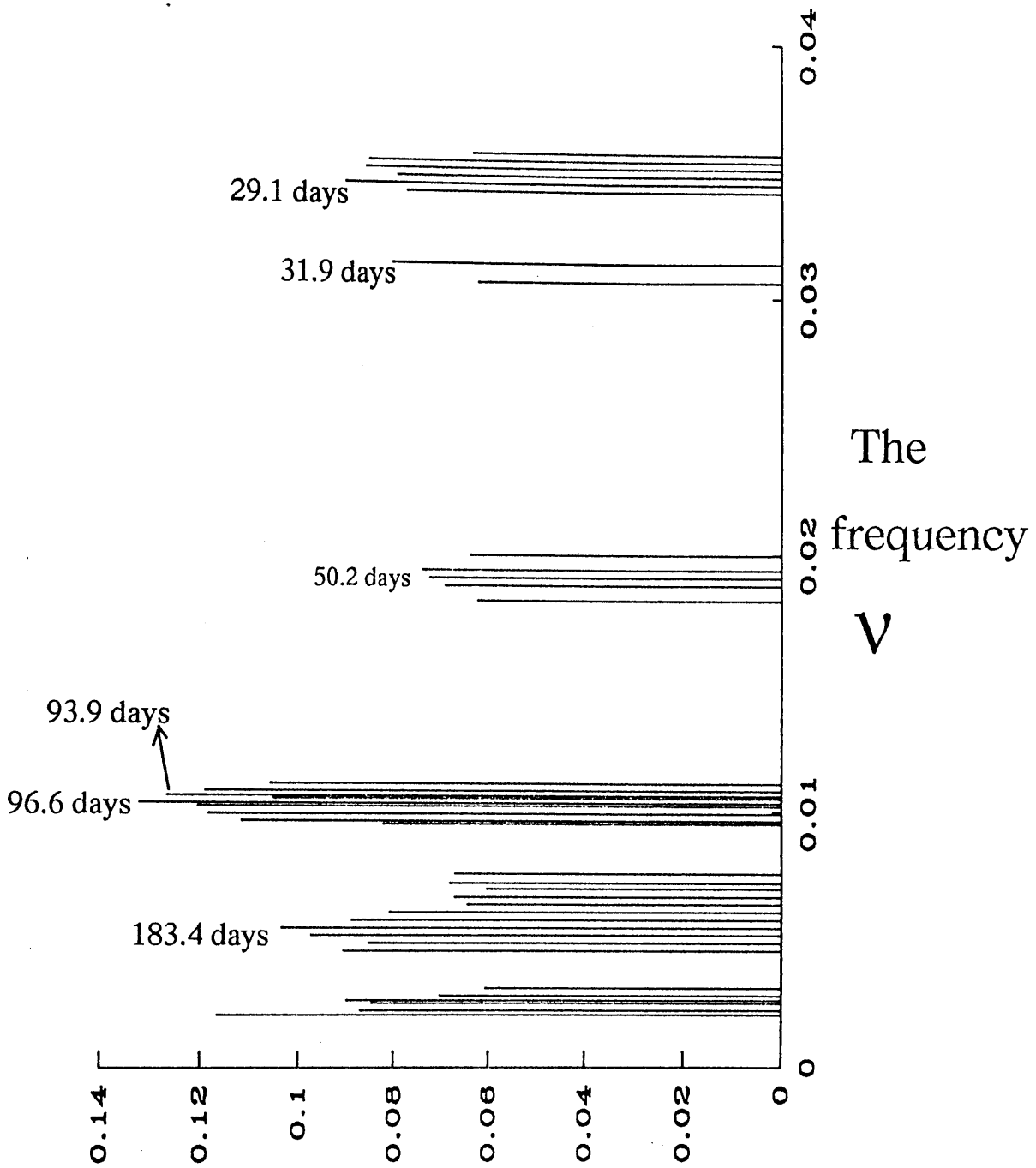
The Fourier analysis Amplitude

Fig. A-1. The amplitude of Fourier analysis for q-direction of Serkowski's data versus frequencies (ν's) in the U band.
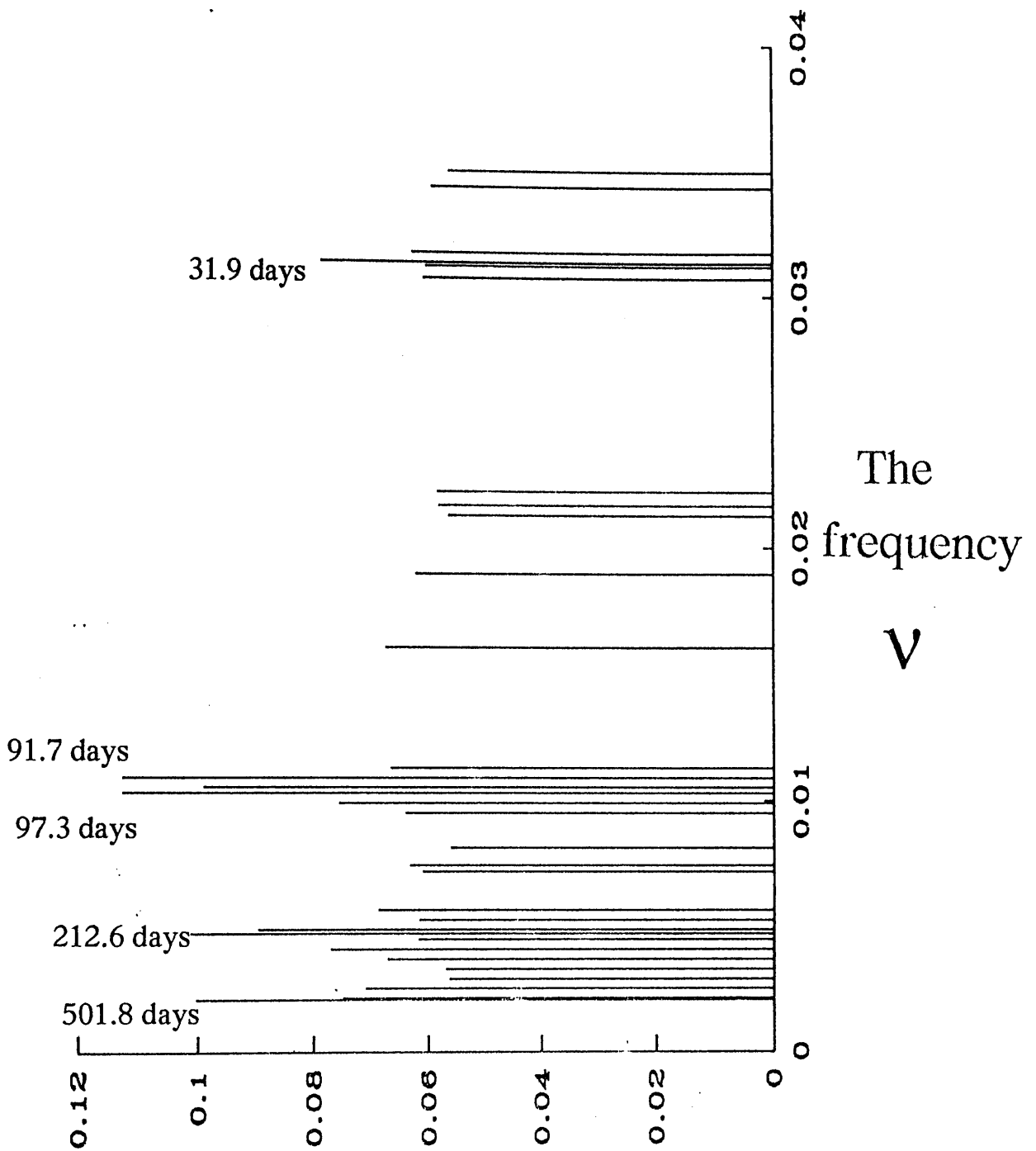
The Fourier analysis amplitude

Fig. A-2. The amplitude of Fourier analysis for q-direction of Serkowski's data versus frequencies (ν's) in the B band.
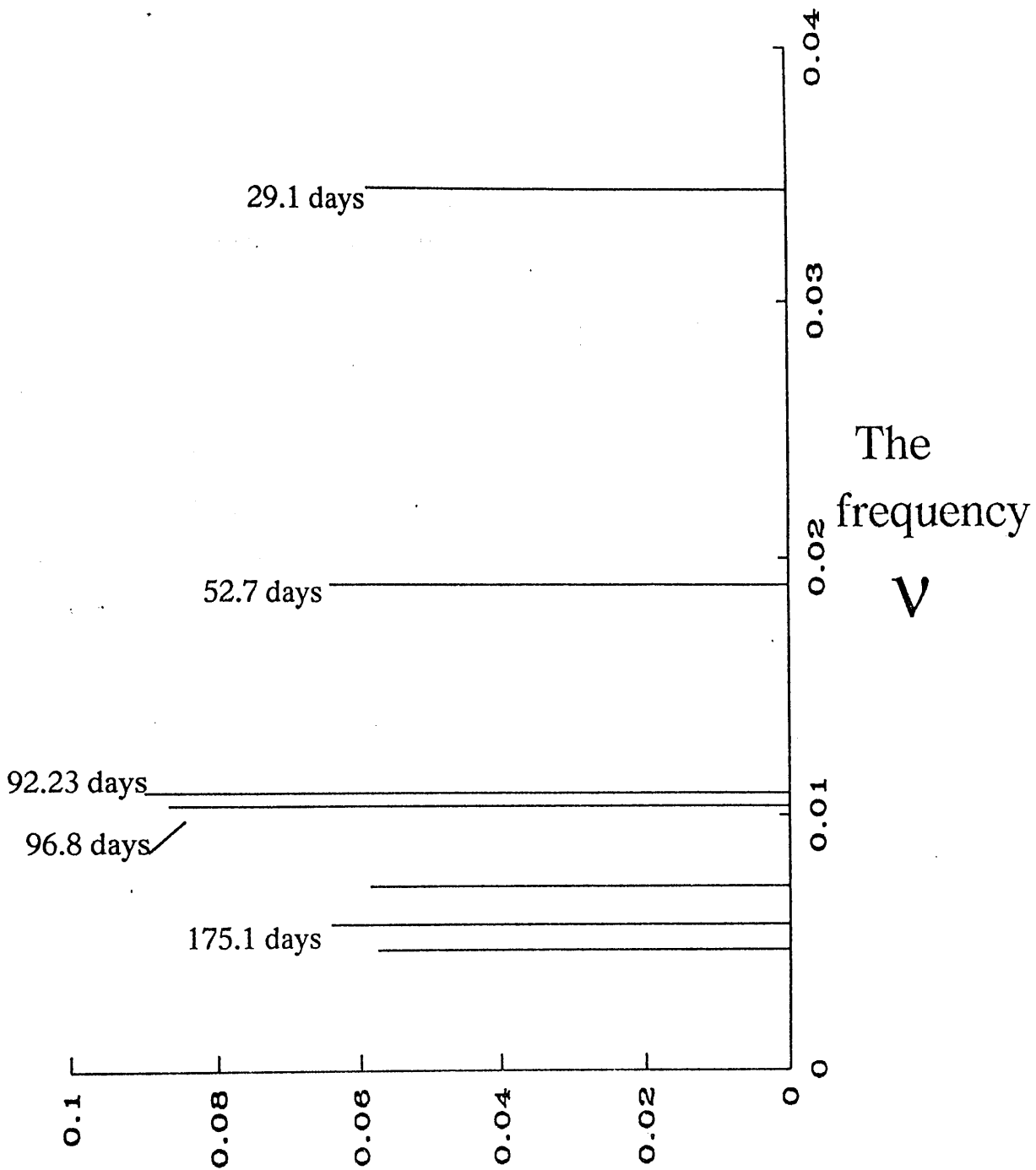
The Fourier analysis amplitude

Fig. A-3. The amplitude of Fourier analysis for q-direction of Serkowski's data versus frequencies (ν's) in the V band.

APPENDIX B

Mathematical proof for the projected area
of an ellipsoid

The projection of an ellipsoid along any line of sight, will have an elliptical cross section of true area R, but the observer will see only the projection of that cross section (denoted by R_P), which we want to calculate. To simplify the problem we will define two frames (see Fig. B-1a&b). In 'real' frame one the ellipsoid equation will be :

$$\frac{x^2}{a^2} + \frac{y^2}{b^2} + \frac{z^2}{c^2} = 1 \qquad\qquad (B-1a)$$

Transformation from frame one to frame two is defined by:

$$x = a\,x' \quad , \quad y = b\,y' \quad , \quad z = c\,z' \qquad\qquad (B-1b)$$

so the ellipsoid in frame one will be a sphere in frame two, given by :

$$x'^2 + y'^2 + z'^2 = 1 \qquad\qquad (B-1c)$$

In frame two, R' will be the cross section (and since we deal here with sphere due to the transformation, the line of sight will be normal to R', and R' a circle of area π), i.e. the normal to area R_P' will make an angle ξ with the line of sight, so R_P' given by :

R_p

$\overline{L}$

z

$\overline{M}$

$\neg y$

x

R

(a)

Frame one

$\overline{M'}$

$\overline{L}$

z'

R'_p

$\neg y'$

x'

R'

(b)

Frame two

192
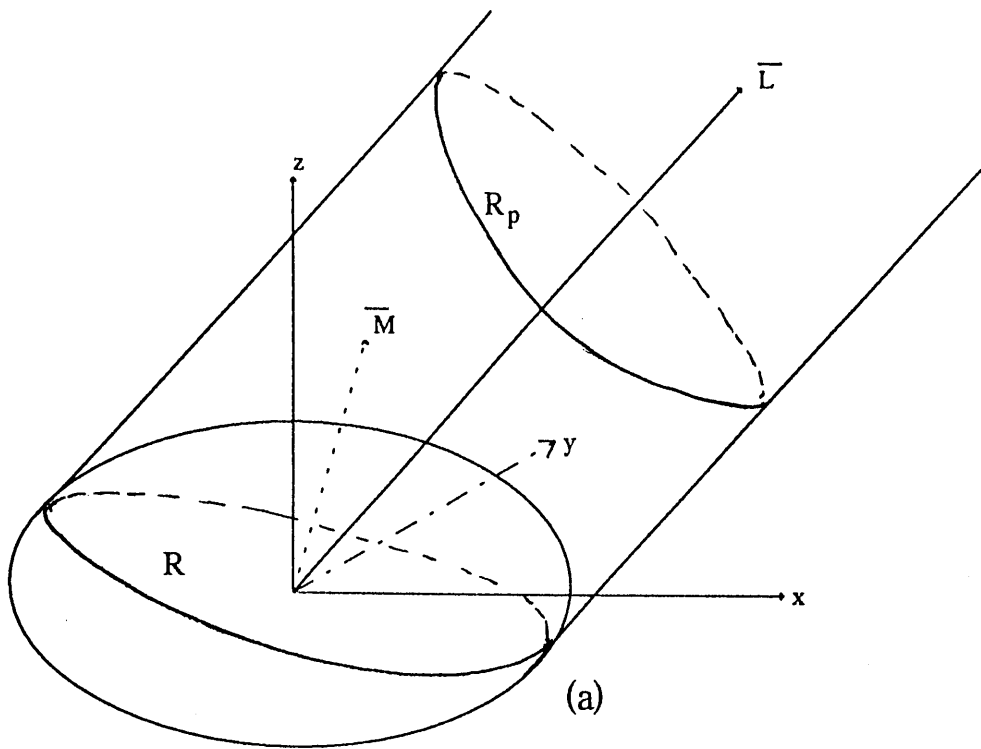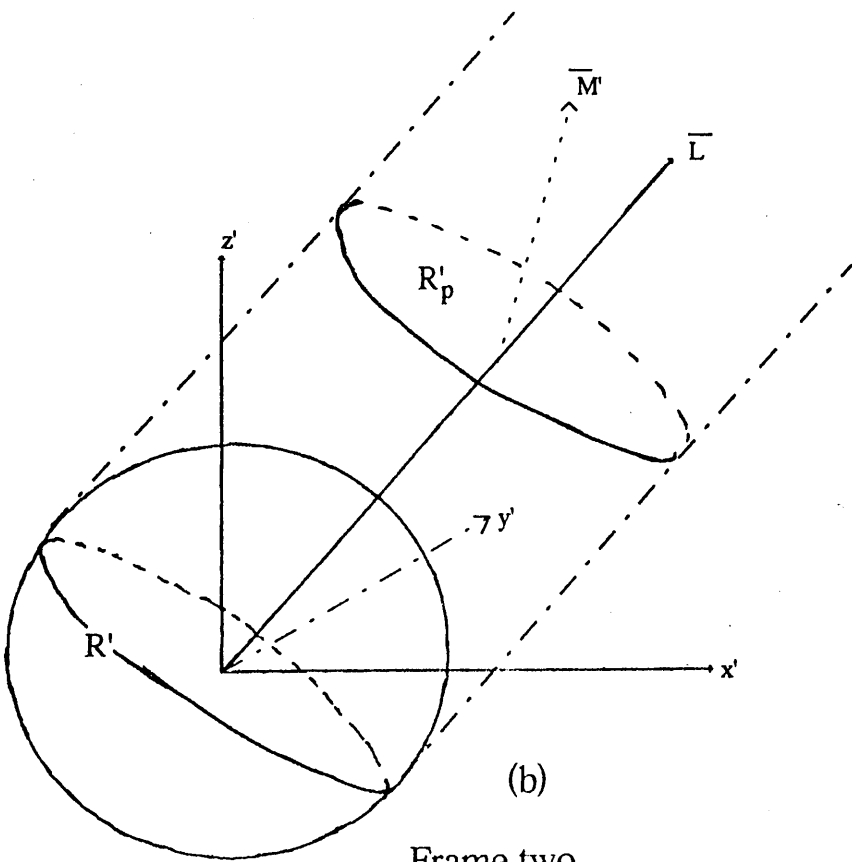
Fig. B-1. a) Frame one which contains the ellipsoid and where $\overline{L}$ is the direction of the line of the sight. $\overline{M}$ is the normal to the cross section R. b) Frame two, which is the transformation of frame one.

$$R_p' = R' \sec \xi = \pi \sec \xi \qquad \text{(B-2)}$$

The line of sight in frame two has direction cosines such that, since the normal to R' is given :

$$\ell\, x' + m\, y' + n\, z' = 0 \qquad \text{(B-3a)}$$

so the direction cosines will be :

$$(\lambda 1, \mu 1, \nu 1) = \frac{\left(\dfrac{\ell}{a}, \dfrac{m}{b}, \dfrac{n}{c} \right)}{\left[\dfrac{\ell^2}{a^2} + \dfrac{m^2}{b^2} + \dfrac{n^2}{c^2} \right]^{1/2}} \qquad \text{(B-3b)}$$

where ℓ, m, and n are unit vectors in the directions x, y, and z, respectively. The plane R_p which has the normal :

$$\ell\, x + m\, y + n\, z = 0 \qquad \text{(B-4a)}$$

and transforms to R_p' which has the normal :

$$\ell\, a\, x' + m\, b\, y' + n\, c\, z' = 0 \qquad \text{(B-4b)}$$

with corresponding direction cosines :

$$(\lambda 2, \mu 2, \nu 2) = \frac{(\ell\, a, m\, b, n\, c)}{[\ell^2 a^2 + m^2 b^2 + n^2 c^2]^{1/2}} \qquad \text{(B-5)}$$

so the angle ξ will given as :

$$\cos \xi = \mid (\lambda 1, \mu 1, \nu 1) \odot (\lambda 2, \mu 2, \nu 2) \mid \qquad \text{(B-6a)}$$

so that R_p' in frame two will be :

$$R_p' = \pi \left[(\ell^2 a^2 + m^2 b^2 + n^2 c^2) \left[\frac{\ell^2}{a^2} + \frac{m^2}{b^2} + \frac{n^2}{c^2} \right] \right]^{1/2} \qquad \text{(B-6b)}$$

To transform this back to frame one, it is easier to go via a plane in which the area transformation is known, e.g. the z'=0 and z=0 planes, noting that normal projected area of R_p' onto z'=0 transforms into normal

projected area of R_P onto z=0.

The projected area R_P' onto Ox'y' $(R_P'^{(z)})$ will be :

$$R_P'^{(z)} = R_P' [(\lambda_2,\mu_2,\nu_2) \odot (0,0,1)] \qquad (B-7)$$

or

$$R_P'^{(z)} = \pi c n \left[\frac{\ell^2}{a^2} + \frac{m^2}{b^2} + \frac{n^2}{c^2} \right]^{1/2} \qquad (B-8a)$$

So we can obtain $R_P^{(z)}$ easily as :

$$R_P^{(z)} = R_P'^{(z)} \times a b \qquad (B-8b)$$

but R_P is given as :

$$R_P = R_P^{(z)} / [(\ell,m,n) \odot (0,0,1)] \qquad (B-9a)$$

So the projected area of an ellipsoidal seen from any direction will be :

$$R_P = \pi abc \left[\frac{\ell^2}{a^2} + \frac{m^2}{b^2} + \frac{n^2}{c^2} \right]^{1/2} \qquad (b-9b)$$

or

$$R_P = \pi \left| \sqrt{(b c \ell)^2 + (a c m)^2 + (a b n)^2} \right| \qquad (B-10)$$

where $(\ell,m,n) = (\cos\Phi \sin\theta , \sin\Phi \sin\theta , \cos\theta)$ are the direction cosines of the line of sight.

Appendix C

Numerical Values of the Expressions Used in the Model

Here we will present values of the integral $f_{\ell m}$ for ellipsoids of different values of their a, b, and c-axis, in four tables as :

1- For c-axis varying from 0 to 100, with a=b=1

2- For c-axis varying from 0 to 1, with b=c and a=1

3- For b-axis varying from 0 to 1, with a=c=1

4- For b-axis varying from 0 to 1, with a=b and c=1

and one table taken from Simmons (1982) for the values of the integral K_ℓ for different Ar (the ratio of equatorial to polar axes).

TABLE C.1.

The c-axis variation of $f_{\ell m}$ with a=b=1

c	f_{00}	f_{20}	f_{22}
0.00	5.56651	3.11483	0.00000
0.01	5.57074	3.11056	0.00000
0.02	5.57843	3.10336	0.00000
0.03	5.58934	3.09349	0.00000
0.04	5.60321	3.08123	0.00000
0.05	5.61974	3.06691	0.00000
0.06	5.63873	3.05074	0.00000
0.07	5.65999	3.03292	0.00000
0.08	5.68335	3.01364	0.00000
0.09	5.70868	2.99304	0.00000
0.10	5.73584	2.97125	0.00000
0.11	5.76474	2.94837	0.00000
0.12	5.79527	2.92450	0.00000
0.13	5.82735	2.89973	0.00000
0.14	5.86090	2.87413	0.00000
0.15	5.89585	2.84776	0.00000
0.20	6.08946	2.70649	0.00000
0.30	6.55273	2.39234	0.00000
0.40	7.09139	2.05606	0.00000
0.50	7.68526	1.71069	0.00000
0.60	8.32117	1.36300	0.00000
0.70	8.99005	1.01659	0.00000
0.80	9.68531	0.67340	0.00000
0.90	10.40209	0.33439	0.00000
1.00	11.13666	0.00000	0.00000
2.00	19.03477	-3.11279	0.00000
3.00	27.37885	-5.95018	0.00000
4.00	35.88998	-8.64780	0.00000
5.00	44.48195	-11.26805	0.00000
6.00	53.11923	-13.84146	0.00000
7.00	61.78444	-16.38450	0.00000
8.00	70.46810	-18.90673	0.00000
9.00	79.16457	-21.41413	0.00000
10.0	87.87031	-23.91057	0.00000
20.0	175.14396	-48.60955	0.00000
30.0	262.54305	-73.14852	0.00000
40.0	349.97543	-97.64342	0.00000
50.0	437.42147	-122.11998	0.00000
60.0	524.87442	-146.58717	0.00000
70.0	612.33137	-171.04892	0.00000
80.0	699.79083	-195.50724	0.00000
90.0	787.25196	-219.96326	0.00000
100.	874.71428	-244.41765	0.00000

TABLE C.2.

The c-axis variation of $f_{\ell m}$ with b=c and a=1

c	f_{00}	f_{20}	f_{22}
0.000	0.000	0.000	0.000
0.010	0.088	0.012	−0.015
0.020	0.175	0.024	−0.030
0.030	0.263	0.037	−0.045
0.040	0.350	0.049	−0.060
0.050	0.438	0.061	−0.074
0.060	0.526	0.073	−0.089
0.070	0.614	0.085	−0.104
0.080	0.702	0.096	−0.118
0.090	0.790	0.108	−0.132
0.100	0.879	0.120	−0.146
0.150	1.325	0.175	−0.215
0.200	1.779	0.225	−0.276
0.300	2.718	0.309	−0.378
0.400	3.708	0.364	−0.446
0.500	4.759	0.389	−0.477
0.600	5.877	0.381	−0.466
0.700	7.070	0.338	−0.414
0.800	8.341	0.261	−0.320
0.900	9.696	0.148	−0.182
1.000	11.137	0.000	0.000

TABLE C.3.

The b-axis variation of $f_{\ell m}$ with a=c=1

b	f_{00}	f_{20}	f_{22}
0.000	5.567	-1.555	-1.904
0.010	5.574	-1.555	-1.904
0.020	5.580	-1.553	-1.900
0.030	5.591	-1.547	-1.894
0.040	5.604	-1.541	-1.887
0.050	5.621	-1.534	-1.878
0.060	5.639	-1.526	-1.868
0.070	5.660	-1.517	-1.857
0.080	5.684	-1.507	-1.846
0.090	5.709	-1.497	-1.833
0.100	5.736	-1.486	-1.820
0.150	5.896	-1.424	-1.744
0.200	6.089	-1.353	-1.657
0.300	6.553	-1.196	-1.465
0.400	7.091	-1.028	-1.259
0.500	7.685	-0.855	-1.048
0.600	8.321	-0.681	-0.835
0.700	8.990	-0.508	-0.623
0.800	9.685	-0.337	-0.412
0.900	10.402	-0.167	-0.205
1.000	11.137	0.000	0.000

TABLE C.4.

The b-axis variation of $f_{\ell m}$ with a=b and c=1

b	f_{00}	f_{20}	f_{22}
0.000	0.000	0.000	0.000
0.010	0.088	-0.024	0.000
0.020	0.175	-0.049	0.000
0.030	0.263	-0.073	0.000
0.040	0.350	-0.097	0.000
0.050	0.438	-0.122	0.000
0.060	0.526	-0.146	0.000
0.070	0.614	-0.169	0.000
0.080	0.702	-0.193	0.000
0.090	0.790	-0.216	0.000
0.100	0.879	-0.239	0.000
0.150	1.325	-0.350	0.000
0.200	1.779	-0.451	0.000
0.300	2.718	-0.617	0.000
0.400	3.708	-0.729	0.000
0.500	4.759	-0.778	0.000
0.600	5.877	-0.762	0.000
0.700	7.070	-0.677	0.000
0.800	8.341	-0.522	0.000
0.900	9.696	-0.296	0.000
1.000	11.137	0.000	0.000

TABLE C.5.

The integral K_ℓ for different Ar (from Simmons 1982)

ℓ	2	4	6	8	10
Ar					
1	0	0	0	0	0
2	0.054	0.0077	0.0016	0.0004	0.0001
3	0.069	0.015	0.0046	0.0016	0.0006
4	0.072	0.019	0.0069	0.003	0.0014
5	0.071	0.021	0.0086	0.0041	0.0021
6	0.069	0.022	0.0097	0.005	0.0027
7	0.067	0.022	0.07	0.0056	0.0032
8	0.064	0.022	0.011	0.006	0.0036
9	0.062	0.022	0.011	0.0064	0.0039
10	0.059	0.021	0.011	0.0066	0.0042
20	0.043	0.017	0.01	0.0067	0.0047

Appendix D

Spherical harmonics, rotation matrices,

and Clebsh-Gordon coefficients

D.1. The spherical harmonics we used thoughout this thesis are generally given in this form (as in Sec. 2.2) :

$$Y_{\ell n}(\theta,\phi) = \alpha(\ell,n) \ P_\ell^n(\cos\theta) \ \exp(in\phi) \qquad (D-1a)$$

$$\text{with} \quad \alpha(\ell,n) = \sqrt{\frac{(2\ell+1)}{4\pi}\frac{(\ell-n)!}{(\ell+n)!}} \qquad (D-1b)$$

and

$$P_\ell^n(x) = (-1)^n \ (1-x^2)^{n/2} \ \frac{d^n}{dx^n} \ P_\ell(x) \qquad (D-1c)$$

where the $P_\ell(x)$ are Legendre polynomials. The explicit expressions for the spherical harmonics used in this thesis are (*cf.* Jackson 1975) :

$$Y_{00}(\theta,\phi) = \sqrt{\frac{1}{4\pi}} \qquad (D-2a)$$

$$Y_{20}(\theta,\phi) = \sqrt{\frac{5}{16\pi}} \ (3\cos^2\theta - 1) \qquad (D-2b)$$

and,

$$Y_{22}(\theta,\phi) = \sqrt{\frac{15}{32\pi}} \ \sin^2\theta \ \exp(2i\phi) \qquad (D-2c)$$

D.2. The rotational matrices are given as (see Sec. 2.2) :

$$R_{nm}^{(\ell)}(\alpha, \beta, \gamma) = \exp(-i \, n \, \alpha) \; r_{nm}^{(\ell)}(\beta) \; \exp(-i \, m \, \gamma) \qquad \text{(D-3a)}$$

and $r_{nm}^{(\ell)}(\beta)$ are defined by the Wigner formula :

$$r_{nm}^{(\ell)}(\beta) = \sum_{t} (-1)^t \sqrt{\frac{(\ell+n)! \; (i-n)! \; (\ell+m)! \; (\ell-m)!}{(\ell+n-t)! \; (\ell-m-t)! \; t! \; (t-n+m)!}}$$

$$\times \; [\cos(\tfrac{1}{2}\beta)]^{2\ell+n-m-2t} \; [\sin(\tfrac{1}{2}\beta)]^{2t-n+m} \qquad \text{(D-3b)}$$

where t is an integer value for which the factorials have meaning ,i.e. for which the arguments of the factorials are positive or zero . The number of terms in this sum is $1+\eta$, where η is the smallest of the four numbers $\ell \pm n$ and $\ell \pm m$ (*cf.* Messiah, 1961).

The element $r_{nm}^{\ell}(\beta)$ of the rotation matrices R_{nm}^{ℓ} has the following symmetry properties :

$$r_{nm}^{\ell}(\beta) = r_{mn}^{\ell}(-\beta) = (-1)^{n-m} \; r_{-n \; -m}^{\ell}(\beta) \qquad \text{(D-3c)}$$

Then the values of $r_{nm}^{\ell}(\beta)$ which are used in the model are :

$$r_{00}^{2}(\beta) = \frac{1}{2} \, (\, 3 \cos^2 \beta -1 \,) \qquad \text{(D-4a)}$$

$$r_{02}^{2}(\beta) = r_{20}^{2}(\beta) = r_{0-2}^{2}(\beta) = r_{-20}^{2}(\beta) = \sqrt{\frac{3}{8}} \; \sin^2 \beta \qquad \text{(C-4b)}$$

$$r_{22}^{2}(\beta) = r_{-2 \; -2}^{2}(\beta) = \frac{1}{4} \, (\cos^2 \beta + 2 \cos \beta + 1) \qquad \text{(D-4c)}$$

and,

$$r_{-22}^{2}(\beta) = r_{2 \; -2}^{2}(\beta) = \frac{1}{4} \, (\cos^2 \beta - 2 \cos \beta + 1) \qquad \text{(D-4d)}$$

D.3.

The Clebsh-Gordon coefficients $c^{LM}_{\ell\ell' mm'}$ arise from the products of two spherical harmonics (see Sec. 3.2), and are given by (*cf.* Messiah 1962) :

$$c^{LM}_{\ell\ell' nm'} = (-1)^M \sqrt{\frac{(2\ell+1)(2\ell'+1)(2L+1)}{4\pi}} \begin{pmatrix} \ell & \ell' & L \\ 0 & 0 & 0 \end{pmatrix} \begin{pmatrix} \ell & \ell' & L \\ n & m' & M \end{pmatrix} \quad (D\text{-}5)$$

where,

$$\begin{pmatrix} a & b & c \\ \alpha & \beta & \gamma \end{pmatrix} = (-1)^{a-b-\gamma} \sqrt{\Delta(abc)}$$

$$\times \sqrt{(a+\alpha)!\ (a-\alpha)!\ (b+\beta)!\ (b-\beta)!\ (c+\gamma)!\ (c-\gamma)!}$$

$$\times \left\{ \sum_t (-1)^t \left[t!\ (c-b+t+\alpha)!\ (c-a+t-\beta)! \right.\right.$$

$$\left.\left. \times (a+b-c-t)!\ (a-t-\alpha)!\ (b-t-\beta)! \right] \right\}$$

$$(D\text{-}6)$$

this expression called the *Racah formula*, which is non-zero under the following two conditions :

(1) $\alpha + \beta + \gamma = 0$ (D-7a)

and,

(2) $|a - b| \leq c \leq a + b$ (D-7b)

and with,

$$\Delta(abc) = \frac{(a+b-c)!\ (b+c-a)!\ (c+a-b)!}{(a+b+c+1)!} \quad (D\text{-}7c)$$

The number t in Racah formula has the same interpretation as in Appendix D.2, but with η the smallest of the nine numbers $a\pm\alpha$, $b\pm\beta$, $c\pm\gamma$, $a+b-c$, $b+c-a$, and $c+a-b$ (*cf.* Messiah, 1961).

Special cases of the Racah formula occur when $\alpha=\beta=\gamma=0$. It is then zero for odd $(a+b+c)$, while for even

(a+b+c)=2p, the Racah formula is given by :

$$\begin{pmatrix} a & b & c \\ \alpha & \beta & \gamma \end{pmatrix} = (-1)^P \sqrt{\Delta(abc)} \ \frac{p!}{(p-a)! \ (p-b)! \ (p-c)!} \qquad (D-8)$$

Then we can show the Clebsh-Gordon coefficients, that were used in the model for $\ell \& \ell' \leq 2$ and L=M=0; L=2 and M=0; and L=M=2 as :

TABLE D.1.

The values of $C^{00}_{\ell\ell',\,mm'}$, empty boxes are zero for cases not satisfying the conditions in (D-7 a and b)

ℓ, ℓ' m , m'	2 , 2	1 , 1	0 , 0
2 , -2	$\sqrt{\frac{1}{4\pi}}$		
1 , -1	$\sqrt{\frac{-1}{4\pi}}$	$\sqrt{\frac{-1}{4\pi}}$	
0 , 0	$\sqrt{\frac{1}{4\pi}}$	$\sqrt{\frac{1}{4\pi}}$	$\sqrt{\frac{1}{4\pi}}$
-1 , 1	$\sqrt{\frac{-1}{4\pi}}$	$\sqrt{\frac{-1}{4\pi}}$	
-2 , 2	$\sqrt{\frac{1}{4\pi}}$		

TABLE D.2.

The values of $C^{20}_{\ell\ell',mm'}$, empty boxes are zero

for cases not satisfying the conditions in (D-7 a and b)

m,m' \ ℓ,ℓ'	2 , 0	2 , 1	2 , 2	1 , 1	1 , 2	0 , 2
2 , -2			$\sqrt{\frac{-1}{4\pi}}\,\frac{12}{7}\sqrt{5}$			
1 , -1		0	$\sqrt{\frac{-1}{4\pi}}\,\frac{12}{7}\sqrt{5}$	$\sqrt{\frac{1}{4\pi}}\sqrt{\frac{4}{5}}$	0	
0 , 0	$\sqrt{\frac{1}{4\pi}}$	0	$\sqrt{\frac{1}{4\pi}}\,\frac{12}{7}\sqrt{5}$	$\sqrt{\frac{1}{4\pi}}\sqrt{\frac{2}{5}}$	0	$\sqrt{\frac{1}{4\pi}}$
-1 , 1		0	$\sqrt{\frac{-1}{4\pi}}\,\frac{12}{7}\sqrt{5}$	$\sqrt{\frac{1}{4\pi}}\sqrt{\frac{4}{5}}$	0	
-2 , 2			$\sqrt{\frac{-1}{4\pi}}\,\frac{12}{7}\sqrt{5}$			

and,

TABLE D.3.

The values of $C^{22}_{\ell\ell',mm'}$, empty boxes are zero

for cases not satisfying the conditions in (D-7 a and b)

m,m' \ ℓ,ℓ'	2 , 0	2 , 1	2 , 2	1 , 1	1 , 2	0 , 2
2 , 0	$\sqrt{\frac{1}{4\pi}}$	0	$\sqrt{\frac{-1}{4\pi}}\sqrt{\frac{20}{49}}$			
1 , 1		0	$\sqrt{\frac{1}{4\pi}}\sqrt{\frac{30}{49}}$	$\sqrt{\frac{1}{4\pi}}$	0	
0 , 2			$\sqrt{\frac{-1}{4\pi}}\sqrt{\frac{20}{49}}$		0	$\sqrt{\frac{1}{4\pi}}$

REFERENCES :

Angel, J.R.P., 1974, " *Planets, Stars and Nebulae Studied with Photopolarimetry* ", Ed. T. Gehrels, University of Arizona Press, p. 54

Aspin, C., Simmons, J.F.L., Brown, J.C., 1981, MNRAS 194, 283

Becker, S.A., 1987, *Stellar Pulsation*, Ed. A.N. Cox, W.m. Sparks & S.G. Starrfield, Los Alamos, New Mexico, 16

Bochkarev, N.G., Karitskaya, E.A., Shakura, N.I., 1979, Sv A 23, 8

Böhm-Vitense, E., 1989, *Stellar astrophysics*, Vol. 1, Cambridge University press, p. 117

Bopp, B.W., 1987, Vistas in Astronomy 30, 53

Bopp, B.W., Evans, D.S., 1973, MNRAS 164, 343

Bowell, E., Zellner, B., 1974, " *Planets, Stars and Nebulae Studied with Photopolarimetry* ", Ed. T. Gehrels, University of Arizona Press, p. 381

Brown, J.C., McLean, I.S., 1977, A&A 57, 141

Brown, J.C., McLean, I.S., Emslie, A.G., 1978, A&A 68, 415

Brown, J.C., Carlaw, V.A., Cassinelli, J.P., 1989, ApJ 344, 341.

Brown, J.C., Fox, G.K., 1989, ApJ 347, 468

Capps, R.W., Coyne, G.V., Dyck, H.M., 1973, ApJ 184, 173

Cassinelli, J.P., Haisch, B.M., 1974,ApJ 188, 101

Cassinelli, J.P., Nordsieck,K.H., Murison,M.A.,1987,
    ApJ 317, 290

Chandrasekhar, S., 1946a, ApJ 103, 351

Chandrasekhar, S., 1946b, ApJ 104, 110

Chandrasekhar, S., 1947, ApJ 105, 424

Chandrasekhar, S., 1963, ApJ 138, 1182

Clarke, D., 1986, A&A 161, 412

Clarke, D., McGale, P.A., 1986, A&A 169, 251

Clarke, D., McGale, P.A., 1987, A&A 178, 294

Coffen, D.L., Hansen, J.E., 1974, " *Planets, Stars and
    Nebulae Studied with Photopolarimetry* ", Ed. T.
    Gehrels, University of Arizona Press, p. 518

Coleman, H.H., Shields, G.A., 1990,ApJ 363, p. 415

Collins, G.W.II., 1970, ApJ 159, 583

Collins, G.W.II., Buerger, P.F., 1974, " *Planets, Stars
    and Nebulae Studied with Photopolarimetry* ", Ed.
    T. Gehrels, University of Arizona Press, p. 663

Coulson, K.L., Dave, J.V., Sekera, Z., 1960, " *Tables
    related to radiation emerging from a planetary
    atmosphere with Rayleigh scattering* ", Berkeley
    & Los Angeles, Univ. Calif. Press

Craig, I.J.D., Brown, J.C., 1986, " *Inverse problems in
    astronomy* ", Adam Hilger Ltd., 10

Cuypers, J., 1987, Astronomisch Instituut Katholieke
    Universiteit Leuven, Belgium No. 3

Doherty, L.R., 1986, ApJ 307, 261

Dolan, J.F., 1992, ApJ 384, 249

Dolan, J.F., Tapia, S. 1984, A&A 139, 249

Draper, p., Rolph, C., Scarrott, M., Tadhunter, C., Lawrence, A., McMahon, R., 1991, *Gemini* 34, 14

Dyck, H.M., Jennings, M.C., 1971, AJ 76, 431

Dyck, H.M., Forrest, W.J.,Gillett, F.C., Stein, W.A., Gehrz, R.D., Woolf, N.J., Shawl, S.J., 1971, ApJ 165, 57

Fekel, F.C., 1983, AJ 268, 274

Friend, D.F., Cassinelli, J.P., 1986, ApJ 306, 215.

Fox, G.K., Brown, J.C., 1991, ApJ 375, 300

Fox, G.K., 1991, ApJ 379, 663

Gehrels, T., 1974, " *Planets, Stars and Nebulae Studied with Photopolarimetry* ", Ed. T. Gehrels, University of Arizona Press, p. 3

Gehrz, R.D., 1971, *Bull. Am. Astron. Soc.* 3, 454

Gehrz, R.D., Woolf, N.J., 1970, ApJ 161, L213

Gnedin, Yu.N., Silant'ev, N.A., Shibanov, Yu.A., 1976, Sv A 20, 530

Grigoryan, K. A., 1958, Soob. Byurakan Obs., 25, 45.

Haisch, B.M., Cassinelli, J.P., 1976, ApJ 208, 253

Henson, G.D., Kemp, J.C., Kraus, D.J., 1985, *Publication of the Astronomical Soc. of the Pacific* 97, 1192

Jackson, J.D., 1975, *Classical Electrodynamics* 2nd edn. J. Wiley & Son, New York .

Karovska, M., Nisenson, P., Papaliolios C., 1992, Sky & Telescope 83, 130.

Kemp, J.C., 1974, " *Planets, Stars and Nebulae Studied with Photopolarimetry* ", Ed. T. Gehrels, University of Arizona Press, p. 607

Kemp, J.C., Wolstencroft, R.D., 1972, ApJ 176, L115

Kruszewski, A., 1974, " *Planets, Stars and Nebulae Studied with Photopolarimetry* ", Ed. T. Gehrels, University of Arizona Press, p. 845

Kruszewski, A., Gehrels, T., Serkowski, K., 1968, A J 73 , 677.

Lefèvre, J., 1992, A&A 254, 274

Messiah, A., 1962, *Quantum Mechanics* V II, North-holland publishing company, Amsterdam, p. 1053

Milgrom, M., 1978, A&A 65, L1

Odell, A.P., 1981, ApJ 246, L77

Ostriker, J.P., Bodenheimer, P., 1968, ApJ 151, 1089

Papaloizou, J.C.B.,Whelan, J.A.J., 1973, MNRAS 164, 1

Pieters, C.E., 1974, " *Planets, Stars and Nebulae Studied with Photopolarimetry* ", Ed. T. Gehrels, University of Arizona Press, p. 405

Preston, G.W., ApJ 140, 173

Preston, G.W., Krzeminski, W., Smak, J., Williams, J.A., ApJ 137, 401

Raveendran, A.V., Kameswara Rao, N., 1988, A&A 192, p. 259

Raveendran, A.V., Kameswara Rao, N., Anandaram, M.N., 1989, MNRAS 240, 823

Rudy, R.J., Kemp, J.C., 1978, ApJ 221, 200

Schwarz, H.E., 1984, Ph. D. Thesis, *Spectropolarimetry of cool giants and supergiants*, University of Glasgow.

Schwarz, H.E., Clarke, D., 1984, A&A 132, 370

Schwarzschild, M., 1975, ApJ 195, 137

Serkowski, K., 1966, ApJ 144, 857

Serkowski, K., 1970, ApJ 160, 1107

Serkowski, K., 1971, *Kitt Peak Obs. Contr.* 554, 107

Shakhovskoi, N.M., 1962, SvA 6, 587

Shakhovskoi, N.M., 1965, SvA 8, 833

Shawl, S. J., 1972, Ph.D. dissertation, University of Texas at Austin.

Shawl, S.J., 1974, " *Planets, Stars and Nebulae Studied with Photopolarimetry* ", Ed. T. Gehrels, University of Arizona Press, p. 821

Shawl, S. J., 1975, ApJ 80, 595.

Shu, F.H., 1982, *The physical universe, An Introduction to Astronomy*, University Science Books, Mill Valley, California, p. 244

Simmons,J.F.L., 1982, MNRAS 200, 91

Simmons,J.F.L., 1983, MNRAS 205, 153

Simmons,J.F.L., Aspin, C., Brown, J.C., 1982, MNRAS 189, 45

Stamford, P.A., Watson, R.D., 1980, Acta Astron 30, 193

Tassoul, J.L., 1978, *Theory of Rotating Stars*, Princeton University Press, Princeton, New Jersey, U.S.A..

Tinbergen, J., Greenberg, J.M., Jager, C. de., 1981, A&A

95, 215

Unno, W., Osaki, Y., Ando, H., Shibahashi, H, 1979,
    Nonradial Oscillations of Stars, University of
    Tokyo press, p. 38

van de Hulst, H.C., 1957, " *Light Scattering by Small
    Particles* ", Wiley & Son, New York

Vogt, S.S., 1980, ApJ 240, 567

Vogt, S.S., 1981, ApJ 250, 327

Wilson, R., Baldwin, J., Warner, P., Buscher, D., 1991,
    Gemini 34, 20

Zellner, B., 1971, AJ 76, 651

Zirin, H., 1988, *Astrophysics of the Sun*, Cambridge
    University Press, p. 48 & 375